12-16-2020

Regulation Of Cardiovascular Homeostasis By Autophagy

Jing Mu
Georgia State University

REGULATION OF CARDIOVASCULAR HOMEOSTASIS BY AUTOPHAGY

by

JING MU

Under the Direction of Ming-hui Zou, MD/PhD

ABSTRACT

Macroautophagy (hereafter autophagy) is a fundamental cellular process that removes unnecessary or dysfunctional components. It allows the orderly degradation and recycling of cellular components. Mitophagy refers to the selective removal of damaged mitochondria via autophagy pathway. In addition to utilizing core autophagic machinery components, mitophagy exploits a variety of molecules, such as PTEN-induced putative kinase protein 1 (PINK1) and Parkin, to identify and eliminate damaged or superfluous mitochondria. Dysregulation of autophagy and mitophagy contributes to a variety of human disorders, including cardiovascular diseases, such as atherosclerosis and diabetic cardiomyopathy. Vascular smooth muscle cells (VSMCs) are a major component of the vascular media, and are vital for maintaining vessel homeostasis. Migration of VSMCs from the media to intima occurs during the development of

atherosclerosis. Although alterations in autophagy activity have been reported in atherosclerosis, further investigation is required to delineate the mechanism by which autophagy regulates microtubule stability and cell migration. Diabetic cardiomyopathy, which develops in the absence of traditional risk factors, is a major cause of heart failure in Type 2 diabetic patients. Although multiple factors may collectively contribute to the development of diabetic cardiomyopathy, there is an urgent need to determine the role of autophagy in the development of diabetic cardiomyopathy.

This dissertation has explored the role of autophagy and mitophagy in regulating VSMCs migration as well as in the development of diabetic cardiomyopathy, using comprehensive physiological, pathophysiological, molecular, and genetic approaches. We show that activation of autophagy selectively degrades KAT2A/GCN5, a histone acetyltransferase that acetylates α-tubulin in VSMCs, leading to microtubule instability and promotion of VSMC migration. In diabetic heart, defective autophagy and PINK1/Parkin-mediated mitophagy are regulated by bromodomain-containing protein 4 (BRD4), a bromodomain and extra-terminal domain (BET) family of proteins. Administration of JQ1, one of the BET bromodomain inhibitors, restores PINK1/Parkin-mediated mitophagy and prevents high-fat-diet induced diabetic cardiomyopathy. Collectively, our work suggests that autophagy suppression in VSMCs is an important therapeutic target for atherosclerosis and that suppression of BRD4 may be a new therapeutic approach for diabetic cardiomyopathy.

INDEX WORDS: Autophagy, BRD4, Diabetic cardiomyopathy, JQ1, KAT2A/GCN5, Microtubule, Mitophagy, PINK1, VSMCs

REGULATION OF CARDIOVASCULAR HOMEOSTASIS BY AUTOPHAGY

by

JING MU

A Dissertation Submitted in Partial Fulfillment of the Requirements for the Degree of

Doctor of Philosophy

in the College of Arts and Sciences

Georgia State University

2020

REGULATION OF CARDIOVASCULAR HOMEOSTASIS BY AUTOPHAGY

by

JING MU

Committee Chair: Ming-hui Zou

Committee: Zhonglin Xie

Binghe Wang

Christopher Basler

Electronic Version Approved:

Office of Graduate Services

College of Arts and Sciences

Georgia State University

December 2020

DEDICATION

This dissertation is dedicated to my parents, Jianping Mu and Liqing Yao.

Your love always raises me up.

ACKNOWLEDGEMENTS

First and foremost, I would like to acknowledge my advisor, Dr. Ming-hui Zou, for accepting me as his advisee and offering me the chance to step in the word of science. I would like to thank him for the ongoing moral and academic guidance throughout my graduate career, which has been a bumpy yet meaningful journey. Without his guidance and help, I would not be where I am today.

I would also like to thank Dr. Zhonglin Xie, who is not only my committee member but also my mentor. Not only did he teach me all of the necessary laboratory techniques when I was a freshmen graduate student but also provide scientific and professional advice all the way through my graduate career. My great thanks also go to my committee members, Dr. Binghe Wang and Dr. Christopher Basler, for their time and insightful suggestion on my project. They improved my presentation skills and scientific thinking.

I would also like to thank some faculty members at GSU. Dr. Ming Luo and Dr. Jenny J. Yang provided their valuable advising when I took my qualifying examination. Dr. Jenny J. Yang and Dr. Tim Denning kindly wrote the reference letter when I applied for some research fellowship. Dr. Chunying Li always encouraged me and sharing valuable research seminar information.

I would also like to thank the colleagues and friends I met in Zou lab. Including but not limited to Dr. Qiulun Lv, Dr. Shengnan Wu, Dr. Qilong Wang, Dr. Ye Ding, Dr. Chenghui Yan, Dr. Huan Wang, Dr. Ramprasath Tharmarajan, Dr. Imoh Okon, Dr. Young-min Han, Zhaohua Cai, Hongmin Yao, Sean Michael Carr, Junqin An, Dr. Donghong Zhang, Dr. Xiaoxu Zheng, Dr. Zhixue Liu, Dr. Jian Li, Dr. Yunli Tian, Dr. Fujie Zhao, Yao Qu, Dr. Qiang Zhao, Dr. Changjiang Yu, Dr. Haingo Fransky Mitchell Hantelys, Dr. Sichong Ren, Dr. Yang Wu, Dr.

Venkata Naga Lakshmi Ramarao Sure, Dr. Lingxue Zhang, Dr. Ganesh Satyanarayana, Yin Wu, Ouyang Liu, Yanqiao Lu, Pratima Kumari. Thank you for your companionship for many years, and sharing your knowledge and happiness with me.

Special thanks to Mrs. Cindy Zhao, a wise and wonderful woman who is dedicated to serving the lab. She makes the best egg tart that one can ask for. I'm also grateful to Dr. Ping Song, Dr. Shaojin You, Kay Gilstrap, Fa'Tima Geeston, Izaura Garrison, Tammy Ku, Zeidy Rivera Morales, Yu Qiu. Without your contribution to the Center for Molecular and Translational Medicine, the lab couldn't function so smoothly and the working experience here couldn't be so great.

Dr. Weike Li joined me at the beginning of this journey and became a very special and irreplaceable piece of my life. Without his encouragement and inspiration, I'm not able to go through all the late nights and early mornings in the lab. Without his love and care, I'm not able to go through all the hard times in this journey. Thank you for everything you has done for me.

Last but not least, I would like to thank my parents, Jianping Mu and Liqing Yao, for their unconditional love and support. Thank you for raising me to be an independent thinker and a hard worker. Thank you for being the person who are always there to help so that I can pursue my dream without fears.

I do not have enough words to thank the people who helped me become who I am.

TABLE OF CONTENTS

LIST OF TABLES

LIST OF FIGURES

LIST OF ABBREVIATIONS

AGEs	advanced glycation end-products
ALP	autophagy–lysosomal pathway
AMPK	AMP-activated protein kinase
ATAT1	α-tubulin *N*-acetyltransferase 1
Atgs	autophagy-related genes
BAECs	bovine aortic ECs
Bcl2-L-13	Bcl-2-like protein 13
BECN1	Beclin 1
BET	bromodomain and extraterminal
BH	Bcl-2 homology domain
BNIP3	BCL2 and adenovirus E1B 19-kDa-interacting protein 3
BRD4	bromodomain-containing protein 4
BSA	bovine serum albumin
cAMP	cyclic adenosine monophosphate
ChIP-qPCR	chromatin immunoprecipitation coupled with real-time PCR
CQ	chloroquine
CryABR120G	αB-crystallin
E/A ratio	ratio of LV early filling and filling from atrial contraction
ECs	vascular endothelial cells
EF	ejection fraction
eNOS	endothelial nitric oxide synthase
FBS	fetal bovine serum
FOXO	forkhead box-containing protein O
FS	fractional shortening
FUNDC1	FUN14 domain containing 1
GST	glutathione S-transferase
HASMCs	human aortic smooth muscle cells
HBSS	Hank's buffered salt solution
HDAC6	histone deacetylase 6
HF	heart failure

HFD	high-fat diet
hMOF	human males absent on the first
HUVECs	human umbilical vein endothelial cells
H3K27ac	histone H3 lysine 27 acetylation
H4K16ac	histone H4 lysine 16 acetylation
IMM	inner mitochondria membrane
IP	immunoprecipitation
I/R	ischemia/reperfusion
IRS	insulin receptor substrate
IVRT	isovolumic relaxation time
KAT8	lysine acetyltransferase 8
KAT2A	lysine acetyltransferase 2A
αLA	α-lipoic acid
Lacta	lactacystin
LAMP1	lysosomal-associated membrane protein 1
LC3	microtubule associated protein 1 light chain 3
LIR	LC3-interacting region
LPS	lipopolysaccharides
LV	left ventricular
MEFs	mouse embryonic fibroblasts
MFN2	mitofusin 2
MI	myocardial infarction
mTOR	mammalian target of rapamycin
MTORC1	mTOR complex 1
MTORC2	mTOR complex 2
ND	normal diet
OCR	oxygen consumption rate
OMM	outer mitochondria membrane
oxLDL	oxidized low-density lipoprotein
PA	palmitate
PAS	phagophore assembly site

PDGF	platelet-derived growth factor
PE	phosphatidylethanolamine
PGC-1α	peroxisome proliferator-activated receptor γ coactivator-1α
PINK1	PTEN-induced putative kinase protein 1
PKA	protein kinase A
PKB	protein kinase B
PtdIns3K	phosphatidylinositol 3-kinase
RCR	respiratory control ratio
RER	respiratory exchange ratio
ROS	reactive oxygen species
SCG10	ervical ganglion 10
SIRT1	sirtuin 1
SIRT2	sirtuin 2
SQSTM1/p62	sequestosome 1
S6K1	ribosomal protein S6 kinase 1
TAC	transverse aortic constriction
TEM	transmission electron microscopy
Tfam	mitochondrial transcription factor A
TFEB	transcription factor EB
TIM23	translocase of the inner membrane 23
TSC	tuberous sclerosis complex
ULK1	unc-51-like kinase 1
UVRAG	UV radiation resistance associated protein
VDAC1	voltage-dependent anion channel 1
VEGFR2	vascular endothelial growth factor receptor 2
VPS	vacuolar protein sorting
VSMCs	vascular smooth muscle cells
vWF	von Willebrand factor
WIPI	WD-repeat domain phosphoinositide interacting protein
WT	wild-type

1 INTRODUCTION

1.1 Overview of autophagy

1.1.1 Molecular machinery of autophagy

Autophagy is an intracellular catabolic pathway in which long-lived proteins and organelles are delivered to lysosomes for degradation. There are three types of autophagy: macroautophagy, microautophagy, and chaperone-mediated autophagy. The term "autophagy" usually indicates macroautophagy (1). Autophagy consists of several sequential steps, including sequestration, transport to lysosomes, degradation, and utilization of degradation products.

Autophagy process is controlled by autophagy-related genes (Atgs). In mammalian cells, autophagy induction is controlled by the serine/threonine protein kinase ULK1 (unc-51-like kinase 1, a homologue of yeast Atg1) complex. Other subunits include Atg13, FIP200 (focal adhesion kinase family interacting protein of 200 kD) and Atg101 (2-4). Basal-level autophagy is very low under normal conditions. As the main nutrient-sensitive pathway, starvation stress generally activates AMP-activated protein kinase (AMPK) and inactivate MTORC1 (mTOR complex 1) pathways. AMPK and MTORC1 signals regulate complex of ULK1 and ATG13 activity by phosphorylation or dephosphorylation of ULK1 (5,6). The activated ULK1 complex translocates to the phagophore assembly site (PAS) and regulates the class III phosphatidylinositol 3-kinase (PtdIns3K) complex (7). The PtdIns3K complex consists of VPS34 (vacuolar protein sorting 34), as well as VPS15, Atg14L (Atg14-like), and Beclin-1. This complex is responsible for the production of the phospholipid phosphatidylinositol 3-phosphate (PI3P) at PAS. Activation of the PtdIns3K complex causes induction of autophagy, which involves formation of an isolation membrane to which the Atg proteins are recruited. The expansion of the isolation membrane is regulated by two ubiquitin-like protein conjugation

pathways, Atg12-Atg5 and the microtubule-associated protein light chain 3-phosphatidylethanolamine (LC3-PE). The E1 enzyme Atg7 and the E2 enzyme Atg10 sequentially conjugates Atg12 to the lysine residue in Atg5. Atg12-Atg5 then binds to Atg16 to form a complex essential for recruitment of LC3 and elongation of the membrane. On the other hand, Atg8 (LC3) is first converted to LC3-I by the cysteine protease Atg4. Atg8 is then activated by Atg7 (shared with Atg12) and finally conjugated to the amino group of the lipid PE via the E2 enzyme Atg3. LC3-PE translocates to the autophagosome membrane in an Atg12–Atg5–Atg16 complex-dependent manner. Atg8 (LC3) is widely used as a marker to monitor autophagy induction (8). When autophagosome formation is completed, it fuses with lysosomes to form autolysosomes where the inner membrane of the autophagosome and its contents are digested by lysosomal hydrolases (9) (**Fig. 1.1**).

1.1.2 Mitophagy as a selective form of autophagy

Although autophagy has been considered a nonspecific process that randomly sequesters cytoplasmic components and delivers to lysosome for degradation and recycling during nutrition deprivation, increasing evidence suggests that autophagy can also specifically recognize and target redundant or damaged organelles for elimination. For example, specifically degradation of peroxisomes (pexophagy) (10), mitochondria (mitophagy), endoplasmic reticulum (reticulophagy) (11), and ribosomes (ribophagy) (12).

The selective removal of damaged mitochondria via autophagy is referred to as mitophagy. Although mitochondria can be engulfed non-selectively together with other cytosolic component during general autophagy through the core machinery of autophagy, mitophagy exploits a variety of molecules to identify and eliminate damaged or superfluous mitochondria. In mammalian cells, mitophagy is defined as two basic types, PINK1/Parkin pathway-mediated

mitophagy and receptor-mediated mitophagy, according to how mitochondria is delivered to autophagosomes (**Fig. 1.2**).

1.1.2.1 PINK1/Parkin-mediated mitophagy

PINK1 (PTEN-induced putative kinase protein 1) is a serine/threonine kinase that locates in part on outer mitochondria membrane (OMM). In healthy mitochondria, PINK1 is imported to inner mitochondria membrane (IMM) and rapidly degraded by mitochondrial proteases. Upon loss of mitochondrial membrane potential, PINK1 accumulates on the surface of the mitochondria (13). Parkin locates in the cytosol and acts as an ubiquitin E3 ligase (14). The genes encoding PINK1 (15) and Parkin (16) were firstly found to be mutated in certain forms of autosomal recessive Parkinson's disease and related to mitochondrial quality control. To date, the most well-studied mitophagy pathway is the PINK1/Parkin-mediated, which activates mitophagy in an ubiquitination-dependent manner.

Mitochondrial damage causes PINK1 to accumulate on the mitochondrial surface and phosphorylate OMM proteins including MFN2 (mitofusin 2) (17). To maintain mitochondrial homeostasis, some E3 ligases, such as Mul1 (18) and March5 (19), constitutively ubiquitinate some OMM proteins. PINK1 can phosphorylate these preexisting ubiquitin molecules on mitochondria and then activate and recruit Parkin to further ubiquitinate OMM proteins (20). Ubiquitinated proteins then recruit LC3 through ubiquitin-binding adaptor, SQSTM1/p62 (sequestosome 1). The SQSTM1/p62 protein binds to ubiquitinated OMM proteins through its ubiquitin-associated domain and to LC3 on the phagophore through its LC3-interacting region (LIR) (21). Thus, the binding of SQSTM1/p62 to ubiquitinated mitochondrial proteins provides a molecular tether between cargo (mitochondria) and autophagosome (22).

1.1.2.2 Receptor-mediated mitophagy

Another type of mitophagy is receptor-mediated mitophagy that relies on various OMM proteins such as BNIP3 (BCL2 and adenovirus E1B 19-kDa-interacting protein 3), BNIP3-like (BNIP3L)/NIX, and FUN14 domain-containing protein 1 (FUNDC1) (23). These proteins contain LIR motifs that bind to LC3 on autophagosome membrane independent of ubiquitin and adaptor protein p62 (24). BNIP3L/NIX mediates removal of mitochondria through mitophagy during reticulocyte maturation (25,26), and in hypoxia-stimulated mammalian fibroblasts (27). Similarly, BNIP3 induces selective removal of the mitochondria in cardiac myocytes (28). In addition, BNIP3 and BNIP3L/NIX can directly activate autophagy by disrupting the interaction between Bcl2 and Beclin1 (29).

FUNDC1 is a conserved outer mitochondrial membrane protein that interacts with LC3 through LIR at its cytosol-exposed N-terminus. Similar to BNIP3 and BNIP3L/NIX, it is another mitophagic receptor that mediates mitophagy. FUNDC1 is maintained in an inactive state through phosphorylation on Tyr18 and Ser13 residues by SRC kinase and CK2 respectively. Inactivation of SRC kinase during hypoxia decreases phosphorylation of FUNDC1, which triggers mitophagy in HeLa cells (30). FUNDC1 can also be regulated by ULK1. Under hypoxia condition, ULK1 translocates to mitochondria and phosphorylates FUNDC1 at Ser17, which enhances FUNDC1 binding to LC3 in MEFs (mouse embryonic fibroblast) (31).

Bcl2-L-13 (Bcl-2-like protein 13) is an OMM protein that induces mitochondrial fragmentation and mitophagy in HEK293 cell. The BH domains of Bcl2-L-13 are important for the fragmentation of mitochondria, while the LIR facilitates its binding to LC3 and triggers mitophagy (32). Importantly, Bcl2-L-13 forms a complex with ULK1 and LC3B which is required for Bcl2-L-13-mediated mitophagy (33).

1.1.3 Regulation of autophagy

Autophagy is an essential process for protein degradation and organelle turnover, which is required for maintaining cellular homeostasis and survival (9). Disruption of this process results in abnormal cell growth or cell death, and leads to various diseases (34). Thus, the cell finely regulates autophagy by multiple molecules/pathways.

1.1.3.1 Regulation of autophagy by signaling pathways

1.1.3.1.1 Amino acid dependent regulation

It was known that excess amino acids repress autophagy, whereas amino acid starvation stimulates autophagy (35,36). Mammalian target of rapamycin (mTOR) is the primary sensor of amino acids and plays a role in the regulation of autophagy. mTOR is the catalytic subunit of two distinct protein complexes, known as mTOR Complex 1 (MTORC1) and 2 (MTORC2) with distinct composition and function. Amino acids can activate mTORC1 via Ras-related GTPases and the guanine-exchange factors. Since nutrient availability and cellular stress modulate MTORC1 activity, MTORC1 is a consistent inhibitor of autophagy. Thus inhibition of MTORC1 by rapamycin or Torin1 inactivates autophagy.

1.1.3.1.2 Insulin/growth factor dependent regulation

Insulin and insulin-like growth factors inhibit autophagy through activating MTORC1. Upon insulin binding, tyrosine residues of the insulin receptor will be auto-phosphorylated, which in turn recruit and phosphorylate IRS1 and IRS2 (insulin receptor substrate 1 and 2). As a consequence, class I PtdIns3K is recruited to IRS, which then recruits PDK1 (phosphoinositide-dependent protein kinase 1), leading to phosphorylation and activation of its downstream target PKB/Akt (protein kinase B). The activity of MTORC1 is inhibited by the heterodimer

TSC1/TSC2 (TSC, tuberous sclerosis complex). PKB/Akt phosphorylates TSC2 and inactivates TSC1/TSC2 complex, resulting in activation of MTORC1 (37-39).

1.1.3.1.3 Energy/glucose dependent regulation

Regulation of autophagy by the cellular energy level or glucose metabolism is also important. Although MTORC1 is activated in the presence of amino acids or insulin, it can be inhibited by the activation of AMPK when energy falls short (a decreasing ATP/AMP ratio). AMPK activation leads to phosphorylation and activation of the TSC1/TSC2 complex, which inhibits MTORC1 activity (40). In addition to its ability to inhibit MTORC1, AMPK also activates autophagy by direct phosphorylation of ULK1 (41).

The Ras/PKA (protein kinase A) signaling pathway plays an important role in glucose sensing. In the presence of glucose, PKA is activated by binding with cAMP (cyclic adenosine monophosphate). Constitutive activation of the Ras/PKA pathway suppresses autophagy induced by TOR inhibition (42). PKA suppressed autophagy through phosphorylation of Atg1 and Atg13, which prevents the localization of Atg13 to the PAS (43).

1.1.3.2 Transcriptional regulation of autophagy

1.1.3.2.1 FOXO family proteins

The regulation of autophagy involves not only the different signaling pathways, but also a coordinated transcriptional activation/suppression of the *Atgs* or related genes. The FOXO (forkhead box-containing protein O) subfamily transcription factors are the first identified transcriptional regulators related to the regulation of autophagy in the *Drosophila* larval fat body (44). Mammalian cells have four FOXO members, FOXO1, FOXO3, FOXO4, and FOXO6. The transcription-dependent mechanism regulating autophagy via FOXO3 was discovered in the studies of muscle atrophy (45,46). FOXOs are downstream targets of PKB/Akt. Phosphorylation

of FOXOs by PKB/Akt inhibits its translocation from cytoplasm to the nucleus, where FOXO3 directly binds to the promoters of autophagy-related genes such as *LC3B*, *Gabarapl1*, *atg12*, *Bnip3l,* and *Bnip3* to activate gene transcription.

1.1.3.2.2 TFEB

TFEB (transcription factor EB), a master regulator of the autophagy–lysosomal pathway (ALP), was discovered and characterized in 2009 (47). Under baseline conditions, TFEB is phosphorylated by MTORC1 and binds to the 14-3-3 family of proteins, which leads to its retention in the cytoplasm (48). However, MTORC1 inhibition under conditions of nutrient depletion (starvation) or rapamycin treatment results in dephosphorylation and nuclear translocation of TFEB (49,50), where it binds directly to the promoters of multiple autophagy-related genes, including *ATG4*, *ATG9B*, *MAP1LC3B*, *SQSTM1*, *UVRAG* (UV radiation resistance associated protein), and *WIPI* (WD-repeat domain phosphoinositide interacting protein), promoting the genes transcription. TFEB is also a master regulator of lysosomal biogenesis, since its overexpression can increase *Lamp1* gene expression in mouse liver (49).

1.1.3.2.3 ZKSCAN3 and BRD4

ZKSCAN3 (ZNF306) belongs to a family of zinc finger transcription factors with KRAB and SCAN domains. Unlike TFEB that positively regulates ALP genes expression, ZKSCAN3 functions as a transcription suppressor and serves as the counterpart of TFEB by transcriptionally upregulating the expression of genes related to autophagy and lysosome biogenesis. Silencing ZKSCAN3 by shRNA is sufficient to induce autophagy, whereas its overexpression can inhibit autophagy in bladder cancer cells. Conversely, starvation-induced autophagy, but not hypoxia- and ER stress-induced autophagy, can change its ZKSCAN3 mRNA level and promotes cytoplasmic localization, (51).

BRD4 (bromodomain containing 4) is a member of the bromodomain and extraterminal (BET) family. It is another transcriptional repressor of autophagy and lysosome genes expression via binding to the histone lysine methyltransferase EHMT2/G9a at the gene promoter region. Knocking down of BRD4 induces autophagy *in vitro* and *in vivo* in response to starvation- and rapamycin-induced autophagy. Under starvation conditions, AMPK and SIRT1 (sirtuin 1) can displace BRD4 from the promoters of Atgs and genes involved in lysosome function, thereby activating autophagy and maintaining cell survival (52).

1.2 Autophagy and mitophagy in cardiovascular diseases

1.2.1 Autophagy and mitophagy in different vascular cell types

Autophagy can be activated in vascular endothelial cells (ECs) in response to many pathophysiological stimuli, such as oxidized low-density lipoprotein (oxLDL) (53), lipopolysaccharides (LPS) (54), ROS (55), hypoxia (56), advanced glycation end-products (AGEs) (57), and C6-ceramide (58). PINK1/Parkin-mediated mitophagy can be activated by palmitic acid (PA) to protect mitochondrial integrity and EC function (59). Although the understanding of autophagy and mitophagy in ECs is mainly based on *in vitro* experiments using either human umbilical vein ECs (HUVECs) or bovine aortic ECs (BAECs), increasing evidence reveals that autophagy and mitophagy is an essential *in vivo* process mediating EC function. *Atg7* EC-specific knockout mice exhibit impaired synthesis and release of von Willebrand factor (vWF), while retaining normal vessel structure and capillary density (60). Recent studies indicate that autophagy or autophagy-dependent mitochondria clearance in ECs can regulate angiogenesis. By using EC-specific *TFEB* transgenic and knockout mice, Fan *et al.* demonstrate that TFEB positively regulates angiogenesis through activating AMPKα and autophagy (61). EC-specific *Atg5* deletion decreases pathological angiogenesis in a murine model of retinopathy

of prematurity by impairing mitochondrial respiratory activity, mitochondrial ROS production, and VEGFR2 (vascular endothelial growth factor receptor 2) phosphorylation (62). Autophagy increases shear stress-induced eNOS (endothelial nitric oxide synthase) expression. Suppression of autophagy leads to defective purinergic signaling to eNOS phosphorylation and NO production via PKCδ (63,64). EC-specific *ATG7* knockout mice attenuates thrombosis by down regulating the expression of tissue factors (TF), which are procoagulant molecules (65). Taken together, these findings indicate that the proper regulation of autophagy and mitophagy is critical in maintaining ECs survival and endothelial function such as angiogenesis, NO production, and thrombosis.

Vascular smooth muscle cells (VSMCs) are the major component of the vascular system. Autophagy can regulate VSMCs viability, proliferation, and phenotype switch. Similarly to the ECs autophagy, VSMCs autophagy can be stimulated by many vascular disease-related stimuli and serve as a prosurvival mechanism. For example, excessive free cholesterol in VSMCs activates autophagy and promotes cell survival by degradation of dysfunctional organelles such as mitochondria and endoplasmic reticulum (66). Autophagy can also be stimulated by oxidized lipids. Modest amounts of ox-LDL enhances autophagy and apoptosis, however, higher concentrations of ox-LDL induces high levels of apoptosis but suppresses autophagy (67). Moreover, PINK1/Parkin-mediated mitophagy can be activated in VSMCs to prevent oxLDL-induced cell death (68). Other pathophysiological stimuli, such as AGEs (69), hypoxia (70), and inflammatory cytokines (71) also stimulate autophagy in VSMCs. Autophagy is important in maintaining VSMCs viability, as VSMCs-specific *Atg7* knockout mice are more resistant to oxidative stress-induced cell death (72). Unlike many other mature cell types in the adult body, VSMCs do not terminally differentiate but retain a remarkable plasticity. Upon stimulation with

various stimuli, it can shift between a differentiated, contractile phenotype and a dedifferentiated, synthetic phenotype (73). Autophagy may play a role in this phenotype switching. Treatment of VSMCs with platelet-derived growth factor (PDGF) induces autophagy which results in decreased expression of contractile proteins and increased synthetic protein markers, thereby promoting a synthetic VSMCs phenotype. Pharmacological inhibition of autophagy by 3-methyladenine or spautin-1 stabilizes the contractile phenotype and prevents PDGF-induced VSMCs proliferation (74). Interestingly, *Atg7*-deficient VSMCs show increased collagen content and elevated migration potential, which provides a novel link between autophagy and VSMCs phenotype switching (72). A recent study uncovers a link between autophagy and VSMCs senescence, a process that irreversibly makes cells lost proliferation potential. *Atg7*-deficient VSMCs exhibit elevated p62 protein and mRNA levels, which induce p16/RB-mediated senescence and promote atherosclerosis (72).

1.2.2 Autophagy and mitophagy in the heart

The heart is rich in mitochondria and is susceptible to cellular damage caused by dysfunctional mitochondria. Therefore, general autophagy or mitophagy-mediated mitochondria clearance has been intensively studied by researchers in this field. Nakai and colleagues report that at the basal level, *Atg5* cardiomyocyte-specific knock out mice develop cardiac hypertrophy, left ventricular dilatation and contractile dysfunction (75). A more recent study indicates that genetic *Pink1* global knock out induces early left ventricular dysfunction and cardiac hypertrophy by increasing oxidative stress and impairing mitochondrial function (76). Nevertheless, *Beclin1+/-* and *Parkin* global knock out mice do not exhibit cardiac dysfunction (77,78). Moreover, *Mfn2* cardiac-specific knock out mice, a model of impaired mitochondria fusion, present accumulating abnormal mitochondria by interrupting PINK1/Parkin-mediated

mitophagy (17). These studies suggest that general autophagy and mitophagy play a vital role in maintaining normal cardiac structure and function.

Under cardiac stress conditions, activation of autophagy seems to have a protective effect. Suppression of autophagy is detrimental in *Beclin1*+/- mice subjected to chronic myocardial infarction (MI) and ischemia-reperfusion (I/R) (78). I/R-dependent activation of autophagy is associated with upregulation of multifunctional prosurvival molecule, Bcl-2-associated athanogene (79). In addition, the autophagic vacuoles are large and contain degraded mitochondria in the border zone, while the remote zone contains normal-sized autophagosomes (80). Intensive studies show that mitophagy also plays a protective role under cardiac stress conditions. *Parkin* knock out mice have reduced survival rates and develop larger infarcts after MI (77). Loss of *Pink1* increases the infarct size after I/R (81). Moreover, AMPKα2-induced PINK1 S495 phosphorylation activates mitophagy and prevents heart failure (HF) in patients and mouse model of transverse aortic constriction (TAC) (82). These studies suggest that PINK1/Parkin-mediated mitophagy is important in protecting cardiomyocytes against cardiac stress. Another study indicates that both *Bnip3* and *Nix* cardiac-specific knock outs accelerate cardiac hypertrophy and mitochondrial dysfunction in mice (83). FUNDC1, a mitophagic receptor, has been found to regulate mitochondrial homeostasis and protect the heart from I/R injury (84,85). Taken together, these studies suggest that autophagy and mitophagy are important in protecting the heart against various stresses.

1.2.3 Autophagy and mitophagy in atherosclerosis

Atherosclerosis is a chronic inflammatory disease which remains the leading cause of death in the developed world. It is characterized by the formation of lipid-containing plaques in large- and medium-sized arteries. There are three major types of cell in atherosclerotic plaques,

including VSMCs, ECs, and inflammatory cells (such as macrophages) (86,87). Rupture of plaques is the main cause of acute cardiovascular events. The mechanisms underlying plaque rupture may involve foam cell formation, endothelial dysfunction, VSMCs phenotype switching, and inflammation (88). During plaque formation, autophagy is stimulated in all three cell types of atherosclerotic plaques, as evidenced by transmission electron microscopy (TEM) analysis. It is suggested that atherosclerosis largely induces the formation of autophagosomes containing amorphous materials, which are rarely observed under normal conditions (89). These findings are also supported by western blot analysis of lysates from advanced human plaques, which indicate elevated levels of LC3-II (90).

Macrophages are known to play a pivotal role in atherosclerosis and macrophage autophagy is important in inhibiting the process of atherosclerosis. Macrophage autophagy is involved in the clearance of cholesterol deposits in vascular tissue at early stages. Reverse cholesterol transport is a pivotal pathway involved in the return of excess cholesterol from peripheral tissues to the liver for excretion in the bile (91). *Atg5*-deficient macrophages show reduced efflux of cholesterol. Increased protein levels of mTOR and phospho-mTOR are found in *Atg5*-deficient macrophage-derived foam cells. Inhibition of mTOR with siRNA suppresses foam cell formation, which indicate activation of autophagy promotes cholesterol efflux and inhibits the formation of atherosclerotic plaques (92). Macrophage autophagy also plays a protective role in the development of atherosclerosis. In macrophage-specific *Atg5* deletion $LDLR^{-/-}$ mice, autophagy deficiency enhanced the total necrotic area in advanced atherosclerotic plaques due to an increasing oxidative stress caused by augmented macrophage apoptosis (93). Autophagy deficiency is associated with NLRP3 inflammasome hyperactivation, which further promotes atherosclerosis progression (94). In addition, macrophage-specific *TFEB* transgenic

mice exhibit enhanced autophagy and reduced atherosclerosis by promoting aggrephagy of p62-enriched protein aggregates, blunting macrophage apoptosis, and reducing pro-inflammatory IL-1β levels (95). Taken together, these studies provide evidence that macrophage autophagy protects against atherosclerosis progression.

1.2.4 Autophagy and mitophagy in diabetic cardiomyopathy

Diabetes mellitus is a devastating disease, affecting 34.2 million people in the United States (10.5% of the population) and more than 347 million people worldwide (according to National Diabetes Statistics Report, 2020, Centers for Disease Control and Prevention). Type 2 diabetes is the most common form of diabetes, affecting 90% to 95% of all patients with diabetes. Diabetic cardiomyopathy develops in the absence of traditional risk factors, such as coronary artery disease, uncontrolled hypertension, significant valvular heart disease, and congenital heart disorders (96). The prevalence of cardiomyopathy increases from 3% to 12% in diabetic patients, which is a major cause of heart failure in patients with Type 2 diabetes (97). Multiple factors, such as hyperglycemia, insulin resistance, and increased fatty acids, may collectively contribute to the development of diabetic cardiomyopathy. Here, we will focus on the effect of autophagy and mitophagy on the development of diabetic cardiomyopathy.

Mitochondria are essential for energy production, but if damaged, they become a major source of reactive oxygen species (ROS) and pro-apoptotic factors. Increasing evidence suggests that damaged mitochondria leads to the increased sustainment of ROS which is a central event in the development of diabetic cardiomyopathy (98). Therefore, mitochondria quality control through autophagy and mitophagy is an important mechanism to maintain mitochondrial homeostasis and preserve cell viability. Xie *et al.* report that autophagy is suppressed in mouse hearts with type 1 diabetes, including OVE26 and STZ-induced diabetic mouse models, because

hyperglycemia inhibits AMPK. The suppression of autophagy contributes to the development of diabetic cardiomyopathy is supported by the evidence that metformin, an AMPK activator, can rescue autophagic activity, and concomitantly ameliorates diabetic cardiomyopathy (99,100). Another group shows that inhibited autophagy in STZ-induced diabetic mouse model is due to an increase in MTORC1 activity. However, they think this is an adaptive response to prevent excessive autophagic degradation of cellular components (101). In addition, Kobayashi *et al.* demonstrate that hyperglycemia induced suppression of autophagy is a beneficial adaptive response against high glucose toxicity in cultured cardiomyocytes (102).

Compare to type 1 diabetes, the results from type 2 diabetes are controversial due to different animal models and different criteria for autophagy. For example, activation of myocardial autophagy is associated with systemic insulin resistance in fructose-fed mice (103). Expression of autophagy marker LC3B-II and Beclin1 significantly increases in the specimens from diabetic and non-diabetic patients subjected to coronary artery bypass graft surgery, suggesting that autophagy is activated in type 2 diabetic heart (104). By contrast, high-fat diet (HFD)-fed mice exhibit inhibition of cardiac autophagy (105,106). Taken together, these results suggest that mitochondria quality control by autophagy/ mitophagy is important in protecting against diabetic cardiomyopathy.

1.3 Objectives

The goal of this dissertation is to identify the novel signaling regulations of autophagy and mitophagy pathways and investigate how these processes contribute to the development of cardiovascular diseases, which are the major cause of deaths world-wide. In this light, all the presented studies have been designed to be translational applicable in the context of cardiovascular diseases. Focusing on two common diseases in the cardiovascular system,

atherosclerosis and diabetic cardiomyopathy, this dissertation can be divided into two parts. Part 1 is to investigate the alterations of autophagy activity in regulating microtubule stability and VSMCs migration, which facilitates early lesion development in atherosclerosis (107). Part 2 is to investigate the role of mitophagy in diabetic cardiomyopathy and find the potential therapeutic strategy.

Autophagy is an intracellular quality control pathway in which long-lived proteins and organelles are delivered to lysosomes for degradation and recycling. Although autophagy has been considered a non-specific degradation process, increasing evidence demonstrates that autophagy is also critical for the degradation of specific cargoes such as organelles and proteins (108). Tubulin acetylation was first described 20 years ago, but little is known about the enzymes that catalyze this reaction. The role of tubulin acetylation on microtubule stability and VSMCs migration are still poorly understood. Using *in vitro* cell culture system, autophagy-defective *atg5*$^{-/-}$ and *atg7*$^{-/-}$ MEFs and hASMCs, we systemically investigated how autophagy regulates the enzyme that catalyzes tubulin acetylation, how tubulin acetylation affects microtubule stability, and how microtubule stability influences VSMCs migration.

Diabetes mellitus is a devastating disease, affecting 30.3 million (9.4%) people in the United States. Type 2 diabetes is the most common form of diabetes, affecting 90% to 95% of total patients (109). The prevalence of diabetic cardiomyopathy is increasing in parallel with the increase in diabetes mellitus (110,111). Despite its high prevalence, a specific strategy to prevent or treat diabetic cardiomyopathy has not been established. BET family protein BRD4 can facilitate transcriptional activation or suppression of genes by associating with acetylated chromatin. In 2010, two different groups firstly discovered JQ1 and I-BET, the BET bromodomain inhibitors (112,113). Since then, the BET inhibitors have been reported to exert

anti-cancer, immunosuppressive, and anti-hypertensive effects (114). However, the effects of BET inhibitors on diabetic cardiomyopathy remains unknown. We generated diabetic cardiomyopathy mouse model by feeding two-month-old *C57BL/6J* mice with normal diet (ND) or high-fat diet (HFD) for six months. Using comprehensive approaches, including primary cell culture, pharmacological intervention mouse model, and gene knockout mouse model, this work aims to provide insight into the expansion of therapeutic usage of BET inhibitors in cardiovascular system and delineate the underlying molecular mechanisms.

In summary, using a wide selection of biological and biochemical techniques including western blotting, confocal imaging, real-time PCR, ChIP-qPCR, plasmids/siRNA transfection, flow cytometry etc., this dissertation is designed to investigate the role of autophagy and mitophagy in the cardiovascular system. The accomplishment of this work will provide valuable references to design strategies to treat cardiovascular diseases, especially atherosclerosis and diabetic cardiomyopathy.

1.4 References

1. Mizushima N. Autophagy: process and function. Genes Dev **2007**;21(22):2861-73 doi 10.1101/gad.1599207.
2. Zachari M, Ganley IG. The mammalian ULK1 complex and autophagy initiation. Essays Biochem **2017**;61(6):585-96 doi 10.1042/EBC20170021.
3. Hosokawa N, Sasaki T, Iemura S, Natsume T, Hara T, Mizushima N. Atg101, a novel mammalian autophagy protein interacting with Atg13. Autophagy **2009**;5(7):973-9 doi 10.4161/auto.5.7.9296.
4. Ganley IG, Lam du H, Wang J, Ding X, Chen S, Jiang X. ULK1.ATG13.FIP200 complex mediates mTOR signaling and is essential for autophagy. J Biol Chem **2009**;284(18):12297-305 doi 10.1074/jbc.M900573200.
5. Hosokawa N, Hara T, Kaizuka T, Kishi C, Takamura A, Miura Y*, et al.* Nutrient-dependent mTORC1 association with the ULK1-Atg13-FIP200 complex required for autophagy. Mol Biol Cell **2009**;20(7):1981-91 doi 10.1091/mbc.E08-12-1248.
6. Jung CH, Jun CB, Ro SH, Kim YM, Otto NM, Cao J*, et al.* ULK-Atg13-FIP200 complexes mediate mTOR signaling to the autophagy machinery. Mol Biol Cell **2009**;20(7):1992-2003 doi 10.1091/mbc.E08-12-1249.
7. Xie Z, Klionsky DJ. Autophagosome formation: core machinery and adaptations. Nat Cell Biol **2007**;9(10):1102-9 doi 10.1038/ncb1007-1102.

8. Mizushima N, Yoshimori T, Levine B. Methods in mammalian autophagy research. Cell **2010**;140(3):313-26 doi 10.1016/j.cell.2010.01.028.
9. Denton D, Nicolson S, Kumar S. Cell death by autophagy: facts and apparent artefacts. Cell Death Differ **2012**;19(1):87-95 doi 10.1038/cdd.2011.146.
10. Iwata J, Ezaki J, Komatsu M, Yokota S, Ueno T, Tanida I*, et al.* Excess peroxisomes are degraded by autophagic machinery in mammals. J Biol Chem **2006**;281(7):4035-41 doi 10.1074/jbc.M512283200.
11. Bernales S, McDonald KL, Walter P. Autophagy counterbalances endoplasmic reticulum expansion during the unfolded protein response. PLoS Biol **2006**;4(12):e423 doi 10.1371/journal.pbio.0040423.
12. Kraft C, Deplazes A, Sohrmann M, Peter M. Mature ribosomes are selectively degraded upon starvation by an autophagy pathway requiring the Ubp3p/Bre5p ubiquitin protease. Nat Cell Biol **2008**;10(5):602-10 doi 10.1038/ncb1723.
13. Sekine S, Youle RJ. PINK1 import regulation; a fine system to convey mitochondrial stress to the cytosol. BMC Biol **2018**;16(1):2 doi 10.1186/s12915-017-0470-7.
14. Riley BE, Lougheed JC, Callaway K, Velasquez M, Brecht E, Nguyen L*, et al.* Structure and function of Parkin E3 ubiquitin ligase reveals aspects of RING and HECT ligases. Nat Commun **2013**;4:1982 doi 10.1038/ncomms2982.
15. Valente EM, Abou-Sleiman PM, Caputo V, Muqit MM, Harvey K, Gispert S*, et al.* Hereditary early-onset Parkinson's disease caused by mutations in PINK1. Science **2004**;304(5674):1158-60 doi 10.1126/science.1096284.
16. Kitada T, Asakawa S, Hattori N, Matsumine H, Yamamura Y, Minoshima S*, et al.* Mutations in the parkin gene cause autosomal recessive juvenile parkinsonism. Nature **1998**;392(6676):605-8 doi 10.1038/33416.
17. Chen Y, Dorn GW, 2nd. PINK1-phosphorylated mitofusin 2 is a Parkin receptor for culling damaged mitochondria. Science **2013**;340(6131):471-5 doi 10.1126/science.1231031.
18. Yun J, Puri R, Yang H, Lizzio MA, Wu C, Sheng ZH*, et al.* MUL1 acts in parallel to the PINK1/parkin pathway in regulating mitofusin and compensates for loss of PINK1/parkin. Elife **2014**;3:e01958 doi 10.7554/eLife.01958.
19. Nagashima S, Tokuyama T, Yonashiro R, Inatome R, Yanagi S. Roles of mitochondrial ubiquitin ligase MITOL/MARCH5 in mitochondrial dynamics and diseases. J Biochem **2014**;155(5):273-9 doi 10.1093/jb/mvu016.
20. Koyano F, Okatsu K, Kosako H, Tamura Y, Go E, Kimura M*, et al.* Ubiquitin is phosphorylated by PINK1 to activate parkin. Nature **2014**;510(7503):162-6 doi 10.1038/nature13392.
21. Geisler S, Holmstrom KM, Skujat D, Fiesel FC, Rothfuss OC, Kahle PJ*, et al.* PINK1/Parkin-mediated mitophagy is dependent on VDAC1 and p62/SQSTM1. Nat Cell Biol **2010**;12(2):119-31 doi 10.1038/ncb2012.
22. Pankiv S, Clausen TH, Lamark T, Brech A, Bruun JA, Outzen H*, et al.* p62/SQSTM1 binds directly to Atg8/LC3 to facilitate degradation of ubiquitinated protein aggregates by autophagy. J Biol Chem **2007**;282(33):24131-45 doi 10.1074/jbc.M702824200.
23. Boyd JM, Malstrom S, Subramanian T, Venkatesh LK, Schaeper U, Elangovan B*, et al.* Adenovirus E1B 19 kDa and Bcl-2 proteins interact with a common set of cellular proteins. Cell **1994**;79(2):341-51 doi 10.1016/0092-8674(94)90202-x.

24. Hanna RA, Quinsay MN, Orogo AM, Giang K, Rikka S, Gustafsson AB. Microtubule-associated protein 1 light chain 3 (LC3) interacts with Bnip3 protein to selectively remove endoplasmic reticulum and mitochondria via autophagy. J Biol Chem **2012**;287(23):19094-104 doi 10.1074/jbc.M111.322933.
25. Schweers RL, Zhang J, Randall MS, Loyd MR, Li W, Dorsey FC*, et al.* NIX is required for programmed mitochondrial clearance during reticulocyte maturation. Proc Natl Acad Sci U S A **2007**;104(49):19500-5 doi 10.1073/pnas.0708818104.
26. Sandoval H, Thiagarajan P, Dasgupta SK, Schumacher A, Prchal JT, Chen M*, et al.* Essential role for Nix in autophagic maturation of erythroid cells. Nature **2008**;454(7201):232-5 doi 10.1038/nature07006.
27. Bellot G, Garcia-Medina R, Gounon P, Chiche J, Roux D, Pouyssegur J*, et al.* Hypoxia-induced autophagy is mediated through hypoxia-inducible factor induction of BNIP3 and BNIP3L via their BH3 domains. Mol Cell Biol **2009**;29(10):2570-81 doi 10.1128/MCB.00166-09.
28. Quinsay MN, Thomas RL, Lee Y, Gustafsson AB. Bnip3-mediated mitochondrial autophagy is independent of the mitochondrial permeability transition pore. Autophagy **2010**;6(7):855-62 doi 10.4161/auto.6.7.13005.
29. Zhang H, Bosch-Marce M, Shimoda LA, Tan YS, Baek JH, Wesley JB*, et al.* Mitochondrial autophagy is an HIF-1-dependent adaptive metabolic response to hypoxia. J Biol Chem **2008**;283(16):10892-903 doi 10.1074/jbc.M800102200.
30. Liu L, Feng D, Chen G, Chen M, Zheng Q, Song P*, et al.* Mitochondrial outer-membrane protein FUNDC1 mediates hypoxia-induced mitophagy in mammalian cells. Nat Cell Biol **2012**;14(2):177-85 doi 10.1038/ncb2422.
31. Wu W, Tian W, Hu Z, Chen G, Huang L, Li W*, et al.* ULK1 translocates to mitochondria and phosphorylates FUNDC1 to regulate mitophagy. EMBO Rep **2014**;15(5):566-75 doi 10.1002/embr.201438501.
32. Murakawa T, Yamaguchi O, Hashimoto A, Hikoso S, Takeda T, Oka T*, et al.* Bcl-2-like protein 13 is a mammalian Atg32 homologue that mediates mitophagy and mitochondrial fragmentation. Nat Commun **2015**;6:7527 doi 10.1038/ncomms8527.
33. Murakawa T, Okamoto K, Omiya S, Taneike M, Yamaguchi O, Otsu K. A Mammalian Mitophagy Receptor, Bcl2-L-13, Recruits the ULK1 Complex to Induce Mitophagy. Cell Rep **2019**;26(2):338-45 e6 doi 10.1016/j.celrep.2018.12.050.
34. Jing K, Lim K. Why is autophagy important in human diseases? Exp Mol Med **2012**;44(2):69-72 doi 10.3858/emm.2012.44.2.028.
35. Mortimore GE, Schworer CM. Induction of autophagy by amino-acid deprivation in perfused rat liver. Nature **1977**;270(5633):174-6 doi 10.1038/270174a0.
36. Schworer CM, Mortimore GE. Glucagon-induced autophagy and proteolysis in rat liver: mediation by selective deprivation of intracellular amino acids. Proc Natl Acad Sci U S A **1979**;76(7):3169-73 doi 10.1073/pnas.76.7.3169.
37. Wullschleger S, Loewith R, Hall MN. TOR signaling in growth and metabolism. Cell **2006**;124(3):471-84 doi 10.1016/j.cell.2006.01.016.
38. Avruch J, Hara K, Lin Y, Liu M, Long X, Ortiz-Vega S*, et al.* Insulin and amino-acid regulation of mTOR signaling and kinase activity through the Rheb GTPase. Oncogene **2006**;25(48):6361-72 doi 10.1038/sj.onc.1209882.
39. Meijer AJ, Codogno P. Autophagy: regulation and role in disease. Crit Rev Clin Lab Sci **2009**;46(4):210-40 doi 10.1080/10408360903044068.

40. Russell RC, Yuan HX, Guan KL. Autophagy regulation by nutrient signaling. Cell Res **2014**;24(1):42-57 doi 10.1038/cr.2013.166.
41. Kim J, Kundu M, Viollet B, Guan KL. AMPK and mTOR regulate autophagy through direct phosphorylation of Ulk1. Nat Cell Biol **2011**;13(2):132-41 doi 10.1038/ncb2152.
42. Budovskaya YV, Stephan JS, Reggiori F, Klionsky DJ, Herman PK. The Ras/cAMP-dependent protein kinase signaling pathway regulates an early step of the autophagy process in Saccharomyces cerevisiae. J Biol Chem **2004**;279(20):20663-71 doi 10.1074/jbc.M400272200.
43. Stephan JS, Yeh YY, Ramachandran V, Deminoff SJ, Herman PK. The Tor and PKA signaling pathways independently target the Atg1/Atg13 protein kinase complex to control autophagy. Proc Natl Acad Sci U S A **2009**;106(40):17049-54 doi 10.1073/pnas.0903316106.
44. Juhasz G, Puskas LG, Komonyi O, Erdi B, Maroy P, Neufeld TP*, et al.* Gene expression profiling identifies FKBP39 as an inhibitor of autophagy in larval Drosophila fat body. Cell Death Differ **2007**;14(6):1181-90 doi 10.1038/sj.cdd.4402123.
45. Mammucari C, Milan G, Romanello V, Masiero E, Rudolf R, Del Piccolo P*, et al.* FoxO3 controls autophagy in skeletal muscle in vivo. Cell Metab **2007**;6(6):458-71 doi 10.1016/j.cmet.2007.11.001.
46. Zhao J, Brault JJ, Schild A, Cao P, Sandri M, Schiaffino S*, et al.* FoxO3 coordinately activates protein degradation by the autophagic/lysosomal and proteasomal pathways in atrophying muscle cells. Cell Metab **2007**;6(6):472-83 doi 10.1016/j.cmet.2007.11.004.
47. Sardiello M, Palmieri M, di Ronza A, Medina DL, Valenza M, Gennarino VA*, et al.* A gene network regulating lysosomal biogenesis and function. Science **2009**;325(5939):473-7 doi 10.1126/science.1174447.
48. Martina JA, Chen Y, Gucek M, Puertollano R. MTORC1 functions as a transcriptional regulator of autophagy by preventing nuclear transport of TFEB. Autophagy **2012**;8(6):903-14 doi 10.4161/auto.19653.
49. Settembre C, Di Malta C, Polito VA, Garcia Arencibia M, Vetrini F, Erdin S*, et al.* TFEB links autophagy to lysosomal biogenesis. Science **2011**;332(6036):1429-33 doi 10.1126/science.1204592.
50. Settembre C, Zoncu R, Medina DL, Vetrini F, Erdin S, Erdin S*, et al.* A lysosome-to-nucleus signalling mechanism senses and regulates the lysosome via mTOR and TFEB. EMBO J **2012**;31(5):1095-108 doi 10.1038/emboj.2012.32.
51. Chauhan S, Goodwin JG, Chauhan S, Manyam G, Wang J, Kamat AM*, et al.* ZKSCAN3 is a master transcriptional repressor of autophagy. Mol Cell **2013**;50(1):16-28 doi 10.1016/j.molcel.2013.01.024.
52. Sakamaki JI, Wilkinson S, Hahn M, Tasdemir N, O'Prey J, Clark W*, et al.* Bromodomain Protein BRD4 Is a Transcriptional Repressor of Autophagy and Lysosomal Function. Mol Cell **2017**;66(4):517-32 e9 doi 10.1016/j.molcel.2017.04.027.
53. Zhang YL, Cao YJ, Zhang X, Liu HH, Tong T, Xiao GD*, et al.* The autophagy-lysosome pathway: a novel mechanism involved in the processing of oxidized LDL in human vascular endothelial cells. Biochem Biophys Res Commun **2010**;394(2):377-82 doi 10.1016/j.bbrc.2010.03.026.
54. Meng N, Wu L, Gao J, Zhao J, Su L, Su H*, et al.* Lipopolysaccharide induces autophagy through BIRC2 in human umbilical vein endothelial cells. J Cell Physiol **2010**;225(1):174-9 doi 10.1002/jcp.22210.

55. Mattart L, Calay D, Simon D, Roebroek L, Caesens-Koenig L, Van Steenbrugge M*, et al.* The peroxynitrite donor 3-morpholinosydnonimine activates Nrf2 and the UPR leading to a cytoprotective response in endothelial cells. Cell Signal **2012**;24(1):199-213 doi 10.1016/j.cellsig.2011.09.002.
56. Chen G, Zhang W, Li YP, Ren JG, Xu N, Liu H*, et al.* Hypoxia-induced autophagy in endothelial cells: a double-edged sword in the progression of infantile haemangioma? Cardiovasc Res **2013**;98(3):437-48 doi 10.1093/cvr/cvt035.
57. Xie Y, You SJ, Zhang YL, Han Q, Cao YJ, Xu XS*, et al.* Protective role of autophagy in AGE-induced early injury of human vascular endothelial cells. Mol Med Rep **2011**;4(3):459-64 doi 10.3892/mmr.2011.460.
58. Bansode RR, Ahmedna M, Svoboda KR, Losso JN. Coupling in vitro and in vivo paradigm reveals a dose dependent inhibition of angiogenesis followed by initiation of autophagy by C6-ceramide. Int J Biol Sci **2011**;7(5):629-44 doi 10.7150/ijbs.7.629.
59. Wu W, Xu H, Wang Z, Mao Y, Yuan L, Luo W*, et al.* PINK1-Parkin-Mediated Mitophagy Protects Mitochondrial Integrity and Prevents Metabolic Stress-Induced Endothelial Injury. PLoS One **2015**;10(7):e0132499 doi 10.1371/journal.pone.0132499.
60. Torisu T, Torisu K, Lee IH, Liu J, Malide D, Combs CA*, et al.* Autophagy regulates endothelial cell processing, maturation and secretion of von Willebrand factor. Nat Med **2013**;19(10):1281-7 doi 10.1038/nm.3288.
61. Fan Y, Lu H, Liang W, Garcia-Barrio MT, Guo Y, Zhang J*, et al.* Endothelial TFEB (Transcription Factor EB) Positively Regulates Postischemic Angiogenesis. Circ Res **2018**;122(7):945-57 doi 10.1161/CIRCRESAHA.118.312672.
62. Sprott D, Poitz DM, Korovina I, Ziogas A, Phieler J, Chatzigeorgiou A*, et al.* Endothelial-Specific Deficiency of ATG5 (Autophagy Protein 5) Attenuates Ischemia-Related Angiogenesis. Arterioscler Thromb Vasc Biol **2019**;39(6):1137-48 doi 10.1161/ATVBAHA.119.309973.
63. Guo F, Li X, Peng J, Tang Y, Yang Q, Liu L*, et al.* Autophagy regulates vascular endothelial cell eNOS and ET-1 expression induced by laminar shear stress in an ex vivo perfused system. Ann Biomed Eng **2014**;42(9):1978-88 doi 10.1007/s10439-014-1033-5.
64. Bharath LP, Cho JM, Park SK, Ruan T, Li Y, Mueller R*, et al.* Endothelial Cell Autophagy Maintains Shear Stress-Induced Nitric Oxide Generation via Glycolysis-Dependent Purinergic Signaling to Endothelial Nitric Oxide Synthase. Arterioscler Thromb Vasc Biol **2017**;37(9):1646-56 doi 10.1161/ATVBAHA.117.309510.
65. Yau JW, Singh KK, Hou Y, Lei X, Ramadan A, Quan A*, et al.* Endothelial-specific deletion of autophagy-related 7 (ATG7) attenuates arterial thrombosis in mice. J Thorac Cardiovasc Surg **2017**;154(3):978-88 e1 doi 10.1016/j.jtcvs.2017.02.058.
66. Xu K, Yang Y, Yan M, Zhan J, Fu X, Zheng X. Autophagy plays a protective role in free cholesterol overload-induced death of smooth muscle cells. J Lipid Res **2010**;51(9):2581-90 doi 10.1194/jlr.M005702.
67. Ding Z, Wang X, Schnackenberg L, Khaidakov M, Liu S, Singla S*, et al.* Regulation of autophagy and apoptosis in response to ox-LDL in vascular smooth muscle cells, and the modulatory effects of the microRNA hsa-let-7 g. Int J Cardiol **2013**;168(2):1378-85 doi 10.1016/j.ijcard.2012.12.045.
68. Swiader A, Nahapetyan H, Faccini J, D'Angelo R, Mucher E, Elbaz M*, et al.* Mitophagy acts as a safeguard mechanism against human vascular smooth muscle cell apoptosis

induced by atherogenic lipids. Oncotarget **2016**;7(20):28821-35 doi 10.18632/oncotarget.8936.
69. Hu P, Lai D, Lu P, Gao J, He H. ERK and Akt signaling pathways are involved in advanced glycation end product-induced autophagy in rat vascular smooth muscle cells. Int J Mol Med **2012**;29(4):613-8 doi 10.3892/ijmm.2012.891.
70. Ibe JC, Zhou Q, Chen T, Tang H, Yuan JX, Raj JU*, et al.* Adenosine monophosphate-activated protein kinase is required for pulmonary artery smooth muscle cell survival and the development of hypoxic pulmonary hypertension. Am J Respir Cell Mol Biol **2013**;49(4):609-18 doi 10.1165/rcmb.2012-0446OC.
71. Deretic V. Autophagy in immunity and cell-autonomous defense against intracellular microbes. Immunol Rev **2011**;240(1):92-104 doi 10.1111/j.1600-065X.2010.00995.x.
72. Grootaert MO, da Costa Martins PA, Bitsch N, Pintelon I, De Meyer GR, Martinet W*, et al.* Defective autophagy in vascular smooth muscle cells accelerates senescence and promotes neointima formation and atherogenesis. Autophagy **2015**;11(11):2014-32 doi 10.1080/15548627.2015.1096485.
73. Liu M, Gomez D. Smooth Muscle Cell Phenotypic Diversity. Arterioscler Thromb Vasc Biol **2019**;39(9):1715-23 doi 10.1161/ATVBAHA.119.312131.
74. Salabei JK, Cummins TD, Singh M, Jones SP, Bhatnagar A, Hill BG. PDGF-mediated autophagy regulates vascular smooth muscle cell phenotype and resistance to oxidative stress. Biochem J **2013**;451(3):375-88 doi 10.1042/BJ20121344.
75. Nakai A, Yamaguchi O, Takeda T, Higuchi Y, Hikoso S, Taniike M*, et al.* The role of autophagy in cardiomyocytes in the basal state and in response to hemodynamic stress. Nat Med **2007**;13(5):619-24 doi 10.1038/nm1574.
76. Billia F, Hauck L, Konecny F, Rao V, Shen J, Mak TW. PTEN-inducible kinase 1 (PINK1)/Park6 is indispensable for normal heart function. Proc Natl Acad Sci U S A **2011**;108(23):9572-7 doi 10.1073/pnas.1106291108.
77. Kubli DA, Zhang X, Lee Y, Hanna RA, Quinsay MN, Nguyen CK*, et al.* Parkin protein deficiency exacerbates cardiac injury and reduces survival following myocardial infarction. J Biol Chem **2013**;288(2):915-26 doi 10.1074/jbc.M112.411363.
78. Matsui Y, Takagi H, Qu X, Abdellatif M, Sakoda H, Asano T*, et al.* Distinct roles of autophagy in the heart during ischemia and reperfusion: roles of AMP-activated protein kinase and Beclin 1 in mediating autophagy. Circ Res **2007**;100(6):914-22 doi 10.1161/01.RES.0000261924.76669.36.
79. Gurusamy N, Lekli I, Gorbunov NV, Gherghiceanu M, Popescu LM, Das DK. Cardioprotection by adaptation to ischaemia augments autophagy in association with BAG-1 protein. J Cell Mol Med **2009**;13(2):373-87 doi 10.1111/j.1582-4934.2008.00495.x.
80. Kanamori H, Takemura G, Goto K, Maruyama R, Tsujimoto A, Ogino A*, et al.* The role of autophagy emerging in postinfarction cardiac remodelling. Cardiovasc Res **2011**;91(2):330-9 doi 10.1093/cvr/cvr073.
81. Siddall HK, Yellon DM, Ong SB, Mukherjee UA, Burke N, Hall AR*, et al.* Loss of PINK1 increases the heart's vulnerability to ischemia-reperfusion injury. PLoS One **2013**;8(4):e62400 doi 10.1371/journal.pone.0062400.
82. Wang B, Nie J, Wu L, Hu Y, Wen Z, Dong L*, et al.* AMPKalpha2 Protects Against the Development of Heart Failure by Enhancing Mitophagy via PINK1 Phosphorylation. Circ Res **2018**;122(5):712-29 doi 10.1161/CIRCRESAHA.117.312317.

83. Dorn GW, 2nd. Mitochondrial pruning by Nix and BNip3: an essential function for cardiac-expressed death factors. J Cardiovasc Transl Res **2010**;3(4):374-83 doi 10.1007/s12265-010-9174-x.
84. Zhang W, Siraj S, Zhang R, Chen Q. Mitophagy receptor FUNDC1 regulates mitochondrial homeostasis and protects the heart from I/R injury. Autophagy **2017**;13(6):1080-1 doi 10.1080/15548627.2017.1300224.
85. Wu S, Lu Q, Wang Q, Ding Y, Ma Z, Mao X*, et al.* Binding of FUN14 Domain Containing 1 With Inositol 1,4,5-Trisphosphate Receptor in Mitochondria-Associated Endoplasmic Reticulum Membranes Maintains Mitochondrial Dynamics and Function in Hearts in Vivo. Circulation **2017**;136(23):2248-66 doi 10.1161/CIRCULATIONAHA.117.030235.
86. Lusis AJ. Atherosclerosis. Nature **2000**;407(6801):233-41 doi 10.1038/35025203.
87. Hansson GK. Inflammation, atherosclerosis, and coronary artery disease. N Engl J Med **2005**;352(16):1685-95 doi 10.1056/NEJMra043430.
88. Wang JC, Bennett M. Aging and atherosclerosis: mechanisms, functional consequences, and potential therapeutics for cellular senescence. Circ Res **2012**;111(2):245-59 doi 10.1161/CIRCRESAHA.111.261388.
89. Perrotta I. The use of electron microscopy for the detection of autophagy in human atherosclerosis. Micron **2013**;50:7-13 doi 10.1016/j.micron.2013.03.007.
90. Martinet W, De Meyer GR. Autophagy in atherosclerosis: a cell survival and death phenomenon with therapeutic potential. Circ Res **2009**;104(3):304-17 doi 10.1161/CIRCRESAHA.108.188318.
91. Khera AV, Rader DJ. Future therapeutic directions in reverse cholesterol transport. Curr Atheroscler Rep **2010**;12(1):73-81 doi 10.1007/s11883-009-0080-0.
92. Wang X, Li L, Niu X, Dang X, Li P, Qu L*, et al.* mTOR enhances foam cell formation by suppressing the autophagy pathway. DNA Cell Biol **2014**;33(4):198-204 doi 10.1089/dna.2013.2164.
93. Liao X, Sluimer JC, Wang Y, Subramanian M, Brown K, Pattison JS*, et al.* Macrophage autophagy plays a protective role in advanced atherosclerosis. Cell Metab **2012**;15(4):545-53 doi 10.1016/j.cmet.2012.01.022.
94. Razani B, Feng C, Coleman T, Emanuel R, Wen H, Hwang S*, et al.* Autophagy links inflammasomes to atherosclerotic progression. Cell Metab **2012**;15(4):534-44 doi 10.1016/j.cmet.2012.02.011.
95. Sergin I, Evans TD, Zhang X, Bhattacharya S, Stokes CJ, Song E*, et al.* Exploiting macrophage autophagy-lysosomal biogenesis as a therapy for atherosclerosis. Nat Commun **2017**;8:15750 doi 10.1038/ncomms15750.
96. Westermeier F, Riquelme JA, Pavez M, Garrido V, Diaz A, Verdejo HE*, et al.* New Molecular Insights of Insulin in Diabetic Cardiomyopathy. Front Physiol **2016**;7:125 doi 10.3389/fphys.2016.00125.
97. Dandamudi S, Slusser J, Mahoney DW, Redfield MM, Rodeheffer RJ, Chen HH. The prevalence of diabetic cardiomyopathy: a population-based study in Olmsted County, Minnesota. J Card Fail **2014**;20(5):304-9 doi 10.1016/j.cardfail.2014.02.007.
98. Sack MN. Type 2 diabetes, mitochondrial biology and the heart. J Mol Cell Cardiol **2009**;46(6):842-9 doi 10.1016/j.yjmcc.2009.02.001.

99. Xie Z, Lau K, Eby B, Lozano P, He C, Pennington B*, et al.* Improvement of cardiac functions by chronic metformin treatment is associated with enhanced cardiac autophagy in diabetic OVE26 mice. Diabetes **2011**;60(6):1770-8 doi 10.2337/db10-0351.
100. He C, Zhu H, Li H, Zou MH, Xie Z. Dissociation of Bcl-2-Beclin1 complex by activated AMPK enhances cardiac autophagy and protects against cardiomyocyte apoptosis in diabetes. Diabetes **2013**;62(4):1270-81 doi 10.2337/db12-0533.
101. Xu X, Kobayashi S, Chen K, Timm D, Volden P, Huang Y*, et al.* Diminished autophagy limits cardiac injury in mouse models of type 1 diabetes. J Biol Chem **2013**;288(25):18077-92 doi 10.1074/jbc.M113.474650.
102. Kobayashi S, Xu X, Chen K, Liang Q. Suppression of autophagy is protective in high glucose-induced cardiomyocyte injury. Autophagy **2012**;8(4):577-92 doi 10.4161/auto.18980.
103. Mellor KM, Bell JR, Young MJ, Ritchie RH, Delbridge LM. Myocardial autophagy activation and suppressed survival signaling is associated with insulin resistance in fructose-fed mice. J Mol Cell Cardiol **2011**;50(6):1035-43 doi 10.1016/j.yjmcc.2011.03.002.
104. Munasinghe PE, Riu F, Dixit P, Edamatsu M, Saxena P, Hamer NS*, et al.* Type-2 diabetes increases autophagy in the human heart through promotion of Beclin-1 mediated pathway. Int J Cardiol **2016**;202:13-20 doi 10.1016/j.ijcard.2015.08.111.
105. Sciarretta S, Zhai P, Shao D, Maejima Y, Robbins J, Volpe M*, et al.* Rheb is a critical regulator of autophagy during myocardial ischemia: pathophysiological implications in obesity and metabolic syndrome. Circulation **2012**;125(9):1134-46 doi 10.1161/CIRCULATIONAHA.111.078212.
106. Xu X, Hua Y, Nair S, Zhang Y, Ren J. Akt2 knockout preserves cardiac function in high-fat diet-induced obesity by rescuing cardiac autophagosome maturation. J Mol Cell Biol **2013**;5(1):61-3 doi 10.1093/jmcb/mjs055.
107. Johnson JL. Emerging regulators of vascular smooth muscle cell function in the development and progression of atherosclerosis. Cardiovasc Res **2014**;103(4):452-60 doi 10.1093/cvr/cvu171.
108. Johansen T, Lamark T. Selective autophagy mediated by autophagic adapter proteins. Autophagy **2011**;7(3):279-96 doi 10.4161/auto.7.3.14487.
109. Yamamoto S, Kuramoto K, Wang N, Situ X, Priyadarshini M, Zhang W*, et al.* Autophagy Differentially Regulates Insulin Production and Insulin Sensitivity. Cell Rep **2018**;23(11):3286-99 doi 10.1016/j.celrep.2018.05.032.
110. Wild S, Roglic G, Green A, Sicree R, King H. Global prevalence of diabetes: estimates for the year 2000 and projections for 2030. Diabetes Care **2004**;27(5):1047-53 doi 10.2337/diacare.27.5.1047.
111. Matheus AS, Tannus LR, Cobas RA, Palma CC, Negrato CA, Gomes MB. Impact of diabetes on cardiovascular disease: an update. Int J Hypertens **2013**;2013:653789 doi 10.1155/2013/653789.
112. Filippakopoulos P, Qi J, Picaud S, Shen Y, Smith WB, Fedorov O*, et al.* Selective inhibition of BET bromodomains. Nature **2010**;468(7327):1067-73 doi 10.1038/nature09504.
113. Nicodeme E, Jeffrey KL, Schaefer U, Beinke S, Dewell S, Chung CW*, et al.* Suppression of inflammation by a synthetic histone mimic. Nature **2010**;468(7327):1119-23 doi 10.1038/nature09589.

114. Shi J, Vakoc CR. The mechanisms behind the therapeutic activity of BET bromodomain inhibition. Mol Cell **2014**;54(5):728-36 doi 10.1016/j.molcel.2014.05.016.

1.5 Tables and Figures

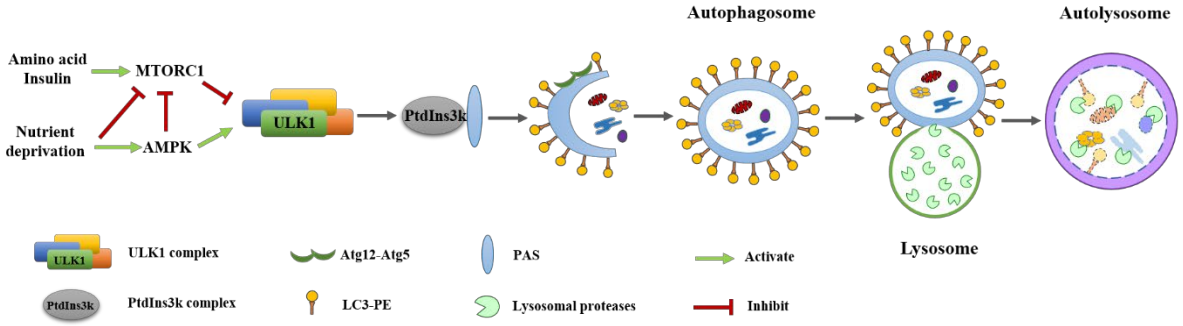

Figure 1.1 Schematic model of autophagy

Autophagy induction is controlled by the ULK1 complex, which consists of ULK1, Atg13, FIP200 and Atg101. Nutrient deprivation generally activates AMPK pathway, which activates ULK1 complex. Excess amino acid and insulin/insulin-like growth factors generally activates MTORC1, which inhibits ULK1 complex. The activated ULK1 complex can regulate class III PtdIns3K complex at PAS, which is responsible for the nucleation of the phagophore membrane. Then Atg12–Atg5 and LC3–PE conjugates are recruited to the phagophore to facilitate the phagophore membrane expansion. Once the autophagosome forms, most of the Atg proteins are dissociated from the surface of autophagosome, allowing fusion of autophagosome and lysosome and cargo degradation by lysosomal proteases.

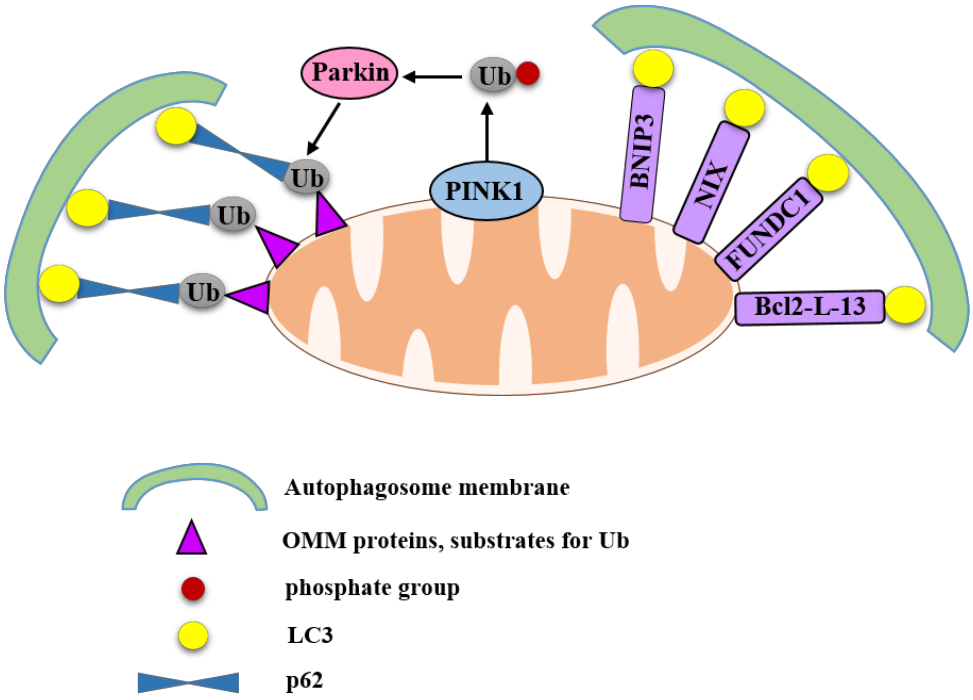

Figure 1.2 Schematic model of mitophagy.

Mitochondrial dysfunction causes PINK1 accumulation on the surface of the mitochondria, where it phosphorylates ubiquitin (Ub) and recruits Parkin from cytosol to mitochondria. Parkin further ubiquitinates some outer mitochondria membrane (OMM) proteins. The adaptor protein p62 binds ubiquitin and autophagosomal LC3 to anchor mitochondria to the autophagosome. OMM proteins such as BNIP3, BNIP3L/NIX, FUNDC1, and Bcl2-L-13 bind to LC3 on autophagosome membrane independent of ubiquitin and adaptor protein p62.

2 Autophagic degradation of KAT2A/GCN5 promotes directional migration of vascular smooth muscle cells by reducing TUBA/α-tubulin acetylation

Changhan Ouyang*, Jing Mu*, Quilun Lu, Jian Li, Huaiping Zhu, Qilong Wang, Ming-Hui Zou#, and Zhonglin Xie#

Center of Molecular and Translational Medicine, Georgia State University, Atlanta, Georgia, 30303

#Address correspondence to:

Zhonglin Xie, MD PhD, Phone: 404-413-6639, Fax: 404-413-3580, E-mail: zxie@gsu.edu

or

Ming-Hui Zou, MD PhD, Phone: 404-413-6637, Fax: 404-413-3580, E-mail: mzou@gsu.edu

*These authors contributed equally to this work.

Ouyang C, Mu J, *et al*. Autophagy. 2020 Oct; 16(10):1753-1770.

2.1 Abstract

Macroautophagy/autophagy, a fundamental process for degradation of macromolecules and organelles, occurs constitutively at a basal level and is upregulated in response to stress. Whether autophagy regulates protein acetylation and microtubule stability in vascular smooth muscle cells (VSMCs) migration, however, remains unknown. Here, we demonstrate that the histone acetyltransferase KAT2A/GCN5 (lysine acetyltransferase 2) binds directly to the autophagosome protein MAP1LC3/LC3 (microtubule associated protein 1 light chain 3) via a conserved LC3-interacting region (LIR) domain. This interaction is required for KAT2A sequestration in autophagosomes and degradation by lysosomal acid hydrolases. Suppression of autophagy results in KAT2A accumulation. KAT2A functions as an acetyltransferase to increase TUBA/α-tubulin acetylation, promote microtubule polymerization and stability, ultimately inhibiting directional cell migration. Our findings indicate that deacetylation of TUBA and perturbation of microtubule stability via selective autophagic degradation of KAT2A are essential for autophagy-promoting VSMC migration.

2.2 Introduction

Cell migration is a central process in the development and maintenance of multicellular organisms. In an adult organism, cell migration is involved in tissue renewal, immune response, and wound repair, and aberrant cell migration is found in various pathologies, including vascular disease, chronic inflammatory diseases, and tumor metastasis. In the vasculature, migration of vascular smooth muscle cells (VSMCs) from the media to intima occurs during the development of intimal hyperplasia and atherosclerosis (1,2). Microtubules are essential components of the cytoskeleton and play a major role in cell migration (3). These polarized polymers are composed of α- and β-Tubulin. Microtubules alternate between phases of growth and shrinkage in a manner

described as dynamic instability (4). Maintaining the balance between dynamically unstable and stable microtubules is required for cell migration. Microtubule stability is regulated by various microtubule-associated proteins and posttranslational modifications, including acetylation, polyglutamylation, and detyrosination. These modifications appear to fine-tune the properties of tubulin and microtubules to facilitate their diverse functions. Acetylation of microtubules in mammalian cells is positively regulated by a variety of acetyltransferases, including, but not limited to, ATAT1 (alpha tubulin acetyltransferase 1) and the elongator protein complex (5,6). To date, the histone deacetylase (HDAC) family member HDAC6 (histone deacetylase 6) and SIRT2 (sirtuin 2) are the only TUBA deacetylases to be described (7,8); however, the enzymes that are responsible for regulating tubulin acetylation and deacetylation in VSMCs remain unknown. Although acetylation of TUBA is always associated with stable microtubules, the precise role of TUBA acetylation in the regulation of microtubule dynamics and cell migration in VSMCs has not been resolved.

Autophagy is a catabolic process that plays a pivotal role in metabolism, cell death, and differentiation (9,10). During autophagy, cytoplasmic components, including long-lived proteins and organelles, are engulfed by a double-membrane structure and targeted for destruction in lysosomes (11). Autophagy initiation requires the activation of ULK1 (unc-51 like autophagy activating kinase 1) and the class III phosphatidylinositol 3-kinase (PtdIns3K)-BECN1 (beclin 1) complex. Once activated, the ULK1 complex drives initiation of autophagosome formation. Elongation and maturation of autophagosomes are regulated by two well-conserved conjugation systems, the conjugation of ATG12 to ATG5 with the help of ATG7 and ATG10 and the conjugation of phosphatidylethanolamine (PE) to MAP1LC3/LC3/Atg8 (microtubule-associated protein 1 light chain 3) by the sequential action of ATG4, ATG7, and ATG3 (12). The

autophagosome then fuses with the lysosome forming autolysosomes within which the cargos are degraded by lysosomal acid hydrolases (11).

Recently, specific autophagic degradation of polyubiquitinated protein aggregates was described, and this substrate-specific autophagy also regulates the turnover of small molecules and entire organelles within cells (13). Many studies have shown that autophagy can be regulated by protein acetylation (14), but whether autophagy can regulate protein acetylation remains unknown. Alterations in autophagy activity have been reported in numerous vascular diseases including pulmonary hypertension (15), vascular aging (16), atherosclerosis (17), and restenosis (18). However, further investigation is required to delineate the mechanism by which autophagy regulates microtubule stability and cell migration and determine the roles of autophagy in vascular diseases. In this study, we demonstrate that activation of autophagy selectively degrades KAT2A, a histone acetyltransferase that acetylates TUBA in VSMCs, leading to microtubule instability and promotion of VSMC migration.

2.3 Materials and methods

2.3.1 Reagents

Antibodies and reagents are from the following companies: ATG5 (Cell Signaling Technology, 8540), ATG7 (Cell Signaling Technology, 8588), SQSTM1/p62 (abcam, 56416), BECN1 (Cell Signaling Technology, 3738), TUBA/α-Tubulin (Cell Signaling Technology, 3873), MAP1LC3A/B (Cell Signaling Technology, 4108), ULK1 (Cell Signaling Technology, 8054), KAT2A/GCN5 (abcam, 137515), acetylated-lysine (Cell Signaling Technology, 9441), MYC-tag (Cell Signaling Technology, 2276), HDAC6 (Cell Signaling Technology, 7612), SIRT1 (Cell Signaling Technology, 9475), mouse secondary antibody (Cell Signaling Technology, 7076), rabbit secondary antibody (Cell Signaling Technology, 7074), ACTB/β-actin

(Santa Cruz Biotechnology, 47778), EP300 (Santa Cruz Biotechnology, 48343), GAPDH (Santa Cruz Biotechnology, 32233), Flag (Sigma-Aldrich, 7425), GFP (Sigma-Aldrich, 1544), goat anti-mouse IgG conjugated to Alexa Fluor 594 red (ThermoFisher Scientific, 11032), goat anti-rabbit IgG conjugated to Alexa Fluor 555 red (ThermoFisher Scientific, 21434), anti-TUBA (Acetyl K40) antibody [6-11B-1] (abcam, 24610). EnVision® + Dual Link System-HRP (DAB+) (Dako Cytomation, 3468). The recombinant KAT2A/GCN5-catalytic domain (362-837) protein (Active Motif, 31204). Purified porcine brain tubulin protein (>99% pure) (Cytoskeleton Inc., T240). Recombinant human GST-LC3 protein and GST protein (Enzo Life Sciences, BML-UW1195-0500). *KAT2A*/*GCN5* siRNA (Santa Cruz Biotechnology, 37946), *ULK1* siRNA (Santa Cruz Biotechnology, 44849), *ATG7* siRNA (Cell Signaling Technology, 6604), *ATG5* siRNA (Cell Signaling Technology, 6345), *SQSTM1* siRNA (Cell Signaling Technology, 6399). The siRNA delivery reagent Lipofectamine RNAiMAX (Life Technologies, 13778150), Lipofectamine® 2000 (Life Technologies, 11668019). Nocodazole (Sigma-Aldrich, 31430), chloroquine (Sigma-Aldrich, 6628), lactacystin (Sigma-Aldrich, 6785).

2.3.2 Plasmids and construction

Plasmids were obtained from Addgene (Cambridge, MA): EGFP-TUBA WT (30487, Tso-Pang Yao's lab), EGFP-TUBA^{K40R} (64059, Weiping Han's lab), Myc-LC3 (24919, Toren Finkel's lab), EGFP-LC3 (11546, Karla Kirkegaard's lab). Flag-KAT2A plasmid was a gift from Dr. Ezra Burstein (Internal Medicine, UT Southwestern Medical Center). To identify the interaction between LC3 and KAT2A, a series of *KAT2A* deletion was constructed by site-directed mutagenesis using a QuikChange II Kit (Stratagene, La Jolla, CA) according to the manufacturer's protocol. The primers used for the deletions were as follows: KAT2AΔ1 (deletion of 661 bp - 664 bp) forward 5'- gcatcccctcccacatcatca -3', reverse 5'- gcatcccctcccacatcatca -3';

KAT2AΔ2 (deletion of 716 bp - 719 bp) forward 5'- agagacaggcgggaaggagaagggga -3', reverse 5'- tcccgcctgtctctcgaatgccag -3'; KAT2AΔ3 (deletion of 734 bp - 737 bp) forward 5'- cgaccagctcaaaaacctgctg -3', reverse 5'- gtttttgagctggtcggggtccttcagc -3'; KAT2AΔ4 (deletion of 826 bp - 829 bp) forward 5'- agttcttcaaggagggaggcctcat -3', reverse 5'- ccctccttgaagaacttctccagggcgctg -3'. In addition, a double-site-mutant (Y734A, L737A) was constructed by multiple site-directed mutagenesis using QuikChange Multi Site-Directed Mutagenesis Kit (#200514. Agilent Technologies) according to the manufacturer's protocol with the following primers: 5'- cagctcgccacaaccgccaaaaacctg-3' and 5'- gtttttggcggttgtggcgagctggtcg-3'. All plasmids were confirmed by sequencing.

2.3.3 Cell culture and transfection

The *atg5*$^{-/-}$ and *atg7*$^{-/-}$ mouse embryonic fibroblasts (MEFs) were a kind gift from Dr. Masaaki Komatsu (The Tokyo Metropolitan Institute Medical Science, Tokyo, Japan). MEFs, HEK293 (ATCC, CRL-1573), and HeLa (ATCC, CCL-2) cells were maintained in Dulbecco's Modified Eagle's Media (DMEM) (Corning, 10-017-CV), supplemented with 10% fetal bovine serum (FBS) (Sigma, F0926). Human aortic smooth muscle cells (HASMCs) was purchased from Invitrogen (Life Technologies, C-007-5C)) and maintained in Medium 231 (ThermoFisher Scientific, M231500) supplemented with 5% smooth muscle cell growth supplements (Sciencell, 1152). During the migration experiment, HASMCs were cultured in complete DMEM medium. All culture media were supplemented with penicillin (100 U/ml) and streptomycin (100 μg/ml) (ThermoFisher Scientific, 15140163). Cultured cells were incubated in a humidified atmosphere of 5% CO_2 and 95% ambient air at 37°C.

ATG5, *ATG7*, and *BECN1* siRNA were obtained from Cell Signaling. For siRNA depletion, HASMCs or MEFs were plated in 6-well plates. After reaching 70% confluence, the

cells were treated with the indicated siRNA at a final concentration of 50 nM using Lipofectamine RNAiMAX reagent (Life Technologies, 13778150) in serum-free medium. After 6 h, the medium was removed and replaced with fresh medium containing 10% FBS. The cells were incubated in the fresh medium for 48 h. HeLa and HEK 293 cells were transfected with 2.5 μg plasmids using Lipofectamine 2000 (Life Technologies, 11668019). HASMCs and MEFs were electroporated with 2.5 μg plasmids using the 4D-Nucleofector™ System (Lonza, Frazer, PA, USA) according to the manufacturer's instructions. *ATG5* adenovirus was purchased from SignaGen Laboratories (Rockville, MD, USA). *ATG7* adenovirus was a gift from Dr. Jeffrey Robbins (Department of Pediatrics, The Cincinnati Children's Hospital Medical Center, Cincinnati, OH, USA). The adenoviruses encoding short hairpin *KAT2A* RNA (sh-*KAT2A*) or *KAT2A* were a gift from Dr. Pere Puigserver (Department of Cell Biology, Harvard Medical School, Boston, MA, USA). The adenoviruses were amplified in HEK293 cells and purified by $CsCl_2$ density gradient ultracentrifugation. Cells were infected with adenovirus at a multiplicity of infection of 100 for 2 h, and then medium was replaced with fresh normal medium. Protein expression was detected 48 h after transfection via immunoblotting analysis with specific antibodies.

2.3.4 Autophagy analysis

Autophagy activity was assessed by measuring GFP-LC3 puncta formation, LC3 cleavage, and SQSTM1 degradation. To determine autophagosome formation, cells were cultured on glass coverslips and allowed to adhere overnight. The cells were transfected with GFP-LC3 adenovirus for 24 h and then incubated with 5 μM chloroquine diphosphate (CQ) for another 24 h. After treatment, cells were fixed, and fluorescence images were obtained using a

fluorescent microscope. Autophagy was measured by enumerating the average number of autophagosomes per cell for each sample. At least 100 cells per sample were counted.

2.3.5 Real-time PCR analysis

Total RNA was extracted from cultured cells using RNeasy Mini Kit (Qiagen, Valencia, CA). For reverse transcription, 1 μg of the total mRNA was converted to first-strand complementary DNA in 20 μL reactions using the iScript cDNA synthesis kit (Bio-Rad Laboratories, Hercules, CA). The primers used for amplification of genes were as follows: KAT2A (mouse) 5'- CGAGTTGTGCCGTAGCTGTGA-3' (forward) and 5'-ACCATTCCCAAGAGCCGGTTA -3' (reverse) and GAPDH (mouse) 5'-CCACTCCTCCACCTTTGAC-3' (forward) and 5'-ACCCTGTTGCTGTAGCCA-3' (reverse). Quantitative RT-PCR reactions were performed using aiQ™ SYBRGreen SupermixKit and a CFX96 real-time PCR detection system (Applied Biosystems, Foster City, CA) as described previously (19). Calculations were performed using the comparative method (2-ΔΔCt) with GAPDH as an internal control (20).

2.3.6 Immunoprecipitation and immunoblotting

Immunoprecipitation (IP) was performed as described previously (21,22). Briefly, cells were collected and lysed in RIPA buffer (10 mM Tris-HCl, pH 8.0, 1 mM EDTA, 140 mM NaCl, 0.1% SDS, 0.1% sodium deoxycholate, 1% Triton X-100; Sigma, R0278) containing a protease inhibitor cocktail (PI; Roche). Protein concentrations were measured with Pierce™ BCA Protein Assay Kit (ThermoFisher Scientific, 23225). After preclearing with protein A agarose beads (GE Healthcare, 17-0780-01) for 30 min at 4°C, whole-cell lysates were subjected to IP with the specific antibodies. Generally, 1 μg of antibody was added to 500 μg of cell lysate and incubated overnight at 4°C. After incubation with protein A agarose beads for 6 h,

immunoprecipitates were eluted with SDS loading buffer by boiling for 10 min. The immunoprecipitated proteins were subjected to immunoblotting analysis.

For immunoblotting, cells were lysed in RIPA buffer containing a protease inhibitor cocktail as described previously (23,24). Protein concentrations were measured with Pierce™ BCA Protein Assay Kit and lysates containing equal amounts of proteins were separated by SDS-PAGE and then transferred to nitrocellulose membranes. The membranes were blocked with 5% non-fat dry milk (LabScientific, M0841) and incubated with specific primary antibodies overnight at 4°C followed by secondary antibodies. All antibodies were used at the manufacturers' recommended dilutions. Immunoreactive bands were visualized by Super Signal™ West Pico PLUS chemiluminescent substrate (ThermoFisher, 34580) using an Odyssey scanner (LI-COR Biosciences, Bad Homburg, Germany) and Photoshop software. For quantification, the protein band intensities of the western blotting images were quantified with Alpha view software (ProteinSimple, San Jose, CA). Data are represented as mean intensity of bands from at least three independent experiments. The membranes were then stripped and probed for total protein and/or ACTB/β-actin to verify equal loading (23,24).

2.3.7 In vitro affinity-isolation assay

Glutathione S-transferase (GST) fusion proteins were immobilized on glutathione Sepharose 4 Fast Flow beads (GE Healthcare, 1707560) for 30 min at 4°C. For GST affinity isolation with purified His-tagged KAT2A protein, 4 μg of GST-LC3 protein was incubated with 1 μg of KAT2A protein in 500 μl of binding buffer (50 mM Tris-HCl, pH 8.0; 250 mM NaCl) for 120 min at 4°C and then washed 5 times with 1 ml of binding buffer. For GST affinity isolation in HeLa cell lysates, 4 μg of GST fusion proteins were incubated with 1,000 μg of HeLa cell lysate for 2 h at 4°C and then washed 5 times with 1 ml of lysis buffer. The precipitate

complex was boiled with 2x Laemmli Sample Buffer (Bio-Rad) containing 1% SDS for 5 min at 95°C (25) and subjected to SDS-PAGE. After transfer to nitrocellulose membranes (Bio-Rad, 1620112), proteins were stained with Ponceau S (Sigma, P3504), followed by immunoblotting with the indicated antibodies.

2.3.8 In vitro tubulin acetylation assay

Purified porcine brain tubulin protein (>99% pure) was incubated with recombinant KAT2A-catalytic domain protein (362-837) protein in acetylation buffer (50 mM Tris, pH 8.0; 50 mM EDTA (Sigma, ED4SS); 10% glycerol; 20 μM acetyl CoA; 10 mM sodium butyrate (Sigma, B5887); 10 mM TSA (SELLECKCHEM, S1045); 1 mM GTP) at 37°C for 1 h. The acetylation of TUBA was assessed by western blotting.

2.3.9 Immunofluorescence

Cells were grown on glass coverslips, fixed with 4% paraformaldehyde for 15 min, and permeabilized with 0.2% Triton X-100 (Sigma, T8787) for 15 min. After blocking with goat serum, the cells were incubated with TUBA antibody (1:2000 dilution) and acetyl-TUBA antibody (1:300 dilution), followed by incubation with fluorescein conjugated secondary antibodies. Slides were mounted with Prolong Gold containing DAPI (Invitrogen) and analyzed with an Olympus microscope or LSM 510 Zeiss confocal microscope.

2.3.10 Microtubule depolymerization

The microtubule depolymerization experiments were performed as described previously (26). Briefly, cells were incubated at 0°C for 5, 10, 15 or 30 min. The morphology of microtubules was then examined by immunostaining of TUBA and confocal microscope.

2.3.11 Nocodazole washout assay

To analyze nocodazole-induced microtubule depolymerization, cells were treated with 10 μM nocodazole for 30 min, and then the cells were washed with pre-warmed PBS (Sigma, D5652) and pre-warmed media and incubated in pre-warmed media without nocodazole for the indicated times. Cell lysates were analyzed by western blot using the indicated antibodies. In addition, cells grown on glass coverslips were incubated in growth media with 10 μM nocodazole for 30 min, and then the drug was washed out to allow the microtubules to repolymerize for the indicated times. The cells were fixed by immersion in ice-cold methanol and processed for immunofluorescence analysis.

2.3.12 Scratch wound healing assay

Monolayer smooth muscle cell migration was performed as described previously (27). Briefly, HASMCs were plated on glass coverslips in 6-well plates at a concentration of 2.5 x 10^5 cells/well and transfected with either siRNA or adenovirus. Forty-eight hours later, a linear wound was gently made in the center of the confluent cell monolayer with a 200-μl pipette tip. The cells were then washed with fresh medium to remove the cellular debris. Repeated observations of the edge of the same scratched lesion were performed. After 10 h, images were captured using a microscope (IX71, Olympus) equipped with a digital camera. The distance of the gap closure was calculated as the total distance of the gap closed over the migration time. For analysis of cell polarity, the cells were fixed and immunostained with a TUBG/γ-tubulin antibody. The angles (θ) of each cell to the scratched line were measured as described by Nakano (25). Briefly, line A was drawn from the point stained with a TUBG antibody to the center of the nucleus, line B was drawn from the center of the nucleus to the scratched line, and the angles (θ) between lines A and B were measured.

2.3.13 Transwell migration assay

Cell migration was examined using a transwell fitted with polycarbonate membrane (8-μm pore size, Corning Inc., Corning, NY). Briefly, growth-arrested HASMCs were trypsinized and resuspended at a concentration of $1x10^6$ cells/ml in DMEM supplemented with 0.5% FBS. HASMC suspension (100 μl) was placed in the upper chamber, and 500 μl of DMEM containing 10% FBS was placed in the lower chamber. Cells were allowed to migrate through the pores of the membrane for 6 h at 37°C in the presence of 5% CO_2. The filter was then removed and fixed in 4% paraformaldehyde. The cells on the upper side of the filter were scraped off with a cotton swab, and the cells that migrated to the lower surface of the filter were stained with 0.2% Crystal violet (ThermoFisher Scientific, C581-100) in 10% methanol for 30 min. The chambers were washed thoroughly with water, and the cells on the lower surface of filters were counted using a light microscope. The experiments were performed at least three times in each group, and cell motility is presented as the number of migrated cells/field.

2.3.14 Statistical analysis

Data are presented as mean ± SEM. The differences between two groups were analyzed using the Student's *t*-test. Comparisons between multiple groups were performed using one-way analysis of variance (ANOVA) followed by Bonferroni post-hoc analysis. A value of $P<0.05$ was considered statistically significant.

2.4 Results

2.4.1 Suppression of autophagy increases TUBA acetylation

Starvation-induced autophagy in mouse embryonic fibroblasts (MEFs) is coupled to reduction of histone H4 lysine 16 acetylation (H4K26ac) (28), prompting us to investigate whether autophagy regulates protein acetylation. We first analyzed the protein acetylation profile

in wild-type (WT) MEFs as well as in MEFs deficient for key autophagy genes (*atg5*$^{-/-}$ and *atg7*$^{-/-}$ MEFs) (29,30). Defective autophagy was verified in *atg5*$^{-/-}$ and *atg7*$^{-/-}$ MEFs, as evidenced by both reduced conversion of LC3-I to LC3-II (a phosphatidylethanolamine derivative of LC3-I) and increased SQSTM1/p62 (sequestosome 1) (a receptor for cargo destined to be degraded by autophagy) levels (**Fig. 2.1A**). The suppression of autophagy was associated with higher levels of acetylated proteins (**Fig. 2.2A**).

We further determined whether activation of autophagy reduces protein acetylation by starvation of MEFs with Hank's buffered salt solution (HBSS) (**Fig. 2.1B)**, which is typically used as a trigger of autophagy (31). Starvation significantly increased the conversion of LC3-I to LC3-II and reduced SQSTM1 levels (**Fig. 2.1B**), indicating activation of autophagy. This increase in autophagy was accompanied by significant reduction in acetylated protein levels (**Fig. 2.2B**).

To determine whether autophagy regulates protein acetylation in non-MEF cells such as VSMCs, we examined protein acetylation in human aortic smooth muscle cells (HASMCs). In line with our findings in MEFs, gene silencing of either *ATG5* or *ATG7* suppressed autophagy by reducing LC3-II levels and increasing SQSTM1 levels (**Fig. 2.1C**), while concomitantly elevating levels of acetylated proteins (**Fig. 2.2C**). Conversely, activation of autophagy by starvation (HBSS treatment) increased conversion of LC3-I to LC3-II and reduced SQSTM1 levels (**Fig. 2.1D**), in concurrence with significant reduction in acetylated protein levels (**Fig. 2.2D**).

We noted a band with a molecular weight of ~50 KD that was significantly increased in autophagy-deficient cells (**Fig. 2.2A and C**). In contrast, this protein was reduced in MEFs and HASMCs upon activation of autophagy (**Fig. 2.2B and D**). Given that a 51-KD TUBA species

has been reported to be acetylated and associated with microtubule stability and cell motility (8), we examined whether inhibition of autophagy promotes the acetylation of TUBA. Using an antibody against acetylated-TUBA (anti-TUBA [acetyl K40] antibody [6-11B-1]), we observed that acetylation of TUBA significantly increased in autophagy-deficient *atg5*$^{-/-}$ and *atg7*$^{-/-}$ MEFs (**Fig. 2.2E**). Similarly, suppression of autophagy in HASMCs by gene silencing of either *ATG5* or *ATG7* also enhanced the levels of acetylated TUBA (**Fig. 2.2G**). On the contrary, activation of autophagy by starvation reduced acetylated TUBA levels in both MEFs and HASMCs (**Fig. 2.2F and H**).

Since autophagy can occur through either the ATG5/ATG7-dependent conventional pathway or the ATG5/ATG7-independent alternative pathway (32), we further explored our hypothesis that autophagy regulates acetylation following inhibition of autophagy using siRNA against *BECN1* and *ULK1*, two proteins that are required for the activation of autophagy through either ATG5/ATG7-dependent or ATG5/ATG7-independent pathway (32). Suppression of autophagy by silencing either *BECN1* or *ULK1* (**Fig. 2.1E and F**) also increased acetylated TUBA levels (**Fig. 2.2I and J**). Collectively, these data indicate that autophagy negatively regulates TUBA acetylation.

2.4.2 Inhibition of autophagy increases KAT2A protein expression

To gain insight into the mechanisms by which autophagy regulates TUBA acetylation, we examined whether autophagy regulates the expression of acetyltransferases, KAT2A, KAT8/hMOF (lysine acetyltransferase 8), EP300, ATAT1, and deacetylases (HDAC6, SIRT1, and SIRT2) in HASMCs. Transfection of HAMSCs with *ATG5*, *ATG7*, *BECN1*, or *ULK1* siRNA resulted in lower levels of ATG5, ATG7, BECN1, or ULK1 respectively, inhibited the conversion of LC3-I to LC3-II, and increased SQSTM1 protein level (**Fig. 2.1C-F, Fig. 2.3A**).

Suppression of autophagy was associated with an increase in KAT2A protein levels (**Fig. 2.4A-C, Fig. 2.3A and B**), but the suppression of autophagy by *ULK1* siRNA did not affect the expression of ATAT1, KAT8, EP300, HDAC6, SIRT1 or SIRT2 (**Fig. 2.3B**).

Next, we determined if autophagy activation by HBSS treatment leads to changed expression of any HDACs including ATAT1, KAT8, EP300, SIRT1 or SIRT2. Activation of autophagy reduced KAT2A protein level but has no effects on the expression of ATAT1, KAT8, EP300, SIRT1, and SIRT2 (**Fig. 2.3C**). We also examined the expression of other HDACs, including HDAC4, HDAC5, HDAC6, HDAC7, and HDAC9, in the autophagy activation (HBSS treatment) condition. The activation of autophagy did not alter the expression of these HDACs either (**Fig. 2.3D**).

We further validated the effect of autophagy on KAT2A expression in WT, *atg5*$^{-/-}$, and *atg7*$^{-/-}$ MEFs and found that deletion of either *Atg5* or *Atg7* significantly increased KAT2A protein expression (**Fig. 2.4E-G**). Notably, defective autophagy had no effect on *KAT2A* mRNA expression (**Fig. 2.4D and H**), suggesting that autophagy regulates KAT2A at the posttranslational level. Conversely, adenovirus overexpression of either ATG5 or ATG7 increased conversion of LC3-I to LC3-II (**Fig. 2.4I and K**) and reduced SQSTM1 levels (**Fig. 2.3E and H**), in concurrence with significant reduction in KAT2A protein levels (**Fig. 2.4I and J**).

We further examined whether activation of autophagy by starvation increases KAT2A degradation in WT and *atg5*$^{-/-}$ MEFs. As expected, starvation (HBSS treatment) activated autophagy as evidenced by increased LC3-II to LC3-I ratios in WT MEFs (**Fig. 2.4L and M**), and HBSS treatments failed to activate autophagy in *atg5*$^{-/-}$ MEFs (**Fig. 2.4L and M**). As autophagy was activated in WT MEFs, KAT2A protein levels declined gradually (**Fig. 2.4I and**

N). More specifically, KAT2A was reduced by 50% in these cells after 24 h HBSS treatment (**Fig. 2.4I and N**). In contrast, in autophagy-defective *atg5*$^{-/-}$ MEFs, HBSS treatment did not alter KAT2A levels compared to levels in the vehicle-treated cells (**Fig. 2.4I and N)**, indicating KAT2A protein degradation by autophagy was inhibited in a*tg5*$^{-/-}$ MEFs. Similarly, starvation also promoted the degradation of exogenous KAT2A in HeLa cells, because following transfection of HeLa cells with *GFP* or *Flag-KAT2A* plasmid and subsequent starvation by incubation of the cells in HBSS, KAT2A levels were decreased in a time-dependent manner (**Fig. 2.4O).** Taken together, autophagy activation promotes KAT2A protein degradation.

To investigate whether the proteasome is involved in this KAT2A degradation, we treated HASMCs with the lysosome inhibitor chloroquine (CQ) (21) or the proteasome inhibitor lactacystin (Lacta) (33). CQ treatment resulted in increased levels of LC3-II and SQSTM1 proteins (inhibition of autophagic flux) in association with an increase in the KAT2A protein level (**Fig. 2.4P**), indicating that defective autophagy reduces KAT2A protein degradation. Conversely, proteasome inhibition with Lacta, which exerts no effect on autophagy activity, increased protein level of RUNX2 (runt related transcription factor 2), a well-known protein degraded by proteasomal pathway (34), but failed to alter KAT2A protein levels (**Fig. 2.4P**). Taken together, these data suggest that KAT2A is degraded through the autophagy-lysosomal pathway.

2.4.3 KAT2A binds to LC3 and co-localizes with autophagosomes

To confirm our results that suggest autophagic degradation of KAT2A, we examined the localization of KAT2A in autophagosomes using immunostaining of KAT2A in HASMCs transfected with *GFP-LC3* adenovirus as a probe for detection of autophagosome formation. Fluorescence microscopy analysis revealed that KAT2A (red) was not only localized in the

nucleus but was also distributed in the cytoplasm. Interestingly, some of the KAT2A protein in the cytoplasm co-localized with GFP-LC3 puncta (**Fig. 2.5A**). The co-localization of KAT2A and LC3 suggests that these two proteins may interact physiologically with each other.

To test this possibility, we first examined the interaction between KAT2A and LC3 in HeLa cells transfected with *EGFP* or *EGFP–LC3* plasmid. Twenty-four h after transfection, cells were collected for immunoprecipitation (IP) with anti-KAT2A antibody and immunoblotting with GFP antibody. A band representing GFP-LC3 was detected in the cells transfected with *EGFP-LC3* and immunoprecipitated with anti-KAT2A but not in the cells transfected with *GFP* (**Fig. 2.5B**). In addition, glutathione S-transferase (GST)-LC3 beads pulled down recombinant full-length KAT2A in binding buffer (**Fig. 2.5C**), indicating that KAT2A physically associates with LC3 in cells.

We next determined whether SQSTM1 mediates the interaction between KAT2A and LC3. In HeLa cells, ectopically overexpressed Myc-LC3 associated with endogenous KAT2A (**Fig. 2.5D)**; however, overexpressed Flag-KAT2A did not associate with SQSTM1 (**Fig. 2.5E**). Importantly, gene silencing of *SQSTM1* did not disrupt the association between KAT2A and LC3 in HeLa cells, (**Fig. 2.6**), suggesting that KAT2A physically interacts with LC3, and SQSTM1 is not involved in the interaction between KAT2A and LC3.

2.4.4 The LC3 interaction region (LIR) domain of KAT2A mediates the association of KAT2A with LC3 and is essential for KAT2A degradation

Next, we investigated whether the LIR domain of KAT2A is required for KAT2A degradation. Autophagy receptor proteins, such as NBR1 (NBR1 autophagy cargo receptor), SQSTM1, Atg32p, and FUNDC1 (FUN14 domain containing 1), bind to LC3 and LC3 homologues through an LIR domain that is typified by the core consensus sequence

W/F/YxxL/I/V (**Fig. 2.7A**) (35,36). To determine whether KAT2A is an autophagy substrate, we analyzed KAT2A protein sequence for predicted LIR domains and found four candidate LIR domains in KAT2A at amino acids 661-664, 716-719, 734-737, and 826-829 (**Fig. 2.7B**). To investigate whether one of these LIR domains mediates the interaction between KAT2A and LC3 and to identify which one, we generated a series of LIR domain deletion mutants (**Fig. 2.7C**). These mutants were overexpressed in HEK293 cells, and the interaction between KAT2A and endogenous LC3 was determined by immunoprecipitation and western blotting. As depicted in **Figure 2.5F**, the mutant with deletion of amino acids 734-737, but not mutants with deletion of the other candidate domains at amino acids 661-664, 716-719, and 826-829, completely disrupted the interaction between KAT2A and LC3. To further demonstrate that KAT2A interacts with LC3 through the LIR (734-737), we mutated Y734 and L737 to alanine and overexpressed this mutant in HeLa cells. Immunoprecipitation and western blotting showed that altering the sequence at the LIR also completely prevented the interactions between KAT2A and LC3 (**Fig. 2.5G**), indicating that amino acids 734-737 comprise the LIR domain that mediates the interaction between KAT2A and LC3.

To determine whether this KAT2A LIR domain is required for KAT2A degradation by autophagy, we expressed WT KAT2A or mutant KAT2A (734-737 deletion) in HEK293 cells. After transfection, the cells were subjected to starvation with HBSS. As depicted in **Figure 2.5H and I**, activation of autophagy reduced WT KAT2A protein levels. Deletion of the LIR domain of KAT2A amino acids 734-737 abrogated this KAT2A reduction induced by autophagy activation (**Fig. 2.5H and I**). Thus, the LIR domain at amino acids 734-737 of KAT2A is required for KAT2A autophagic degradation.

2.4.5 KAT2A induces TUBA acetylation

To investigate whether KAT2A acetylates TUBA, we first examined whether KAT2A interacts with TUBA in WT and *atg5*$^{-/-}$ MEFs. Immunoprecipitation and western blot analysis demonstrated that KAT2A associated with TUBA in WT MEFs, and this association was enhanced in autophagy-deficient *atg5*$^{-/-}$ MEFs, due to the accumulation of KAT2A in the cells (**Fig. 2.8A**), indicating that KAT2A specifically interacts with TUBA. Next, we examined whether KAT2A directly acetylates TUBA in a cell free system by incubating purified porcine brain tubulin protein (>99% pure) with recombinant KAT2A-catalytic domain protein in acetylation buffer, we found that the KAT2A-catalytic domain alone was sufficient to induce TUBA acetylation, as evidenced by increased acetylated TUBA in the purified porcine brain tubulin protein in a dose-dependent manner (**Fig. 2.8B**).

We further examined whether KAT2A induces TUBA acetylation in HASMCs using gain-of- and loss-of-function approaches. As depicted in **Fig. 2.8C-E**, the transfection of *KAT2A* siRNA dramatically reduced KAT2A protein levels as well as levels of TUBA acetylation (**Fig. 2.8C-E**). Immunofluorescence analysis confirmed that *KAT2A* gene silencing reduced the levels of acetylated TUBA (**Fig. 2.8F-H**). In contrast, ectopic expression of KAT2A in HEK 293 cells resulted in increased levels of acetylated TUBA (**Fig. 2.8I and J**).

To date, the most-studied modification of tubulin is acetylation of Lys40 (K40) of TUBA (37). Therefore, we examined whether KAT2A induces acetylation of TUBA specifically at Lys40. We co-transfected HEK293 cells with *KAT2A* adenovirus and WT EGFP-TUBA plasmid, and acetylation-defective TUBA plasmid (EGFP TUBA^{K40R}) (38). Overexpression of KAT2A increased the acetylation of TUBA in the cells transfected with EGFP-WT-TUBA but not in the

cells transfected with mutant EGFP-TUBA^{K40R} (**Fig. 2.8K**), supporting the notion that KAT2A acetylates Lys40 of TUBA.

2.4.6 Autophagy deficiency increases microtubule stability

Acetylation of TUBA is a well-established marker of more stable microtubules in cells (39). We observed that autophagy regulated acetylated TUBA levels (**Fig. 2.2)** and that suppression of autophagy by genetic deletion *(atg5*$^{-/-}$ and *atg7*$^{-/-}$ MEFs) or gene silencing (*ATG5*-, *ATG7*-, *BECN1*-, and *ULK1*-transfected HASMCs) increased the amount of acetylated TUBA (**Fig. 2.2E, G, I, and J**). On the contrary, activation of autophagy by starvation with HBSS decreased TUBA acetylation (**Fig. 2.2F and H)**. We verified the effect of autophagy on acetylation of TUBA using immunofluorescence staining of acetylated TUBA in HASMCs transfected with *ATG7* siRNA (**Fig. 2.9A and B**), compared with control siRNA treatment, *ATG7* siRNA transfection significantly increased the abundance of acetylation of TUBA (**Fig. 2.9A and B**) but had no effect on the abundance of total TUBA. These effects on TUBA acetylation, therefore, suggest that autophagy negatively regulates microtubule stability.

We further determined the effect of autophagy on microtubule stability by examining the morphology of microtubules using immunofluorescence microscopy. HAMSCs were transfected with control or *ATG7* siRNA and then incubated the cells at 0°C for 5, 10, 15 or 30 min. As shown in **Figure 2.9C and D**, cold treatment resulted in the depolymerization of microtubules in a time-dependent manner and microtubules were completely depolymerized after 30 min of cold treatment. In contrast, microtubules were still present in cells transfected with *ATG7* siRNA (**Fig. 2.9C and D**). These data suggest that inhibition of autophagy increased microtubule stability.

To investigate whether autophagy deficiency affects microtubule assembly, we treated both WT and *atg5*$^{-/-}$ MEFs with nocodazole (0.5 μM) for 30 min to depolymerize microtubules,

the drug was then washed out to allow re-polymerization of microtubules. Western blot analysis revealed that K40-acetylated TUBA was barely detectable in WT and *atg5*$^{-/-}$ MEFs following nocodazole treatment compared to levels in untreated MEFs; however, the acetylated TUBA levels recovered more quickly in *atg5*$^{-/-}$ MEFs than in WT cells (**Fig. 2.9E and F**), suggesting that autophagy deficiency promotes microtubule reassembly after nocodazole washout.

2.4.7 KAT2A-mediated acetylation of TUBA increases microtubule reassembly

Since defective autophagy resulted in KAT2A accumulation and KAT2A induced TUBA acetylation, a marker of microtubule stabilization, we assessed whether KAT2A regulates microtubule reassembly. To this end, we transfected HASMCs with adenovirus *encoding Flag-KAT2A* or *GFP* for 48 h and then treated the cells with nocodazole for 30 min to depolymerize microtubules. Tubulin acetylation was assessed by western blot and immunofluorescence microscopy after removal of nocodazole. The results showed that autophagy deficiency results in KAT2A accumulation (**Fig. 2.10A and B**), overexpression of KAT2A in HASMCs promoted the recovery of acetylated TUBA protein levels following nocodazole washout (**Fig. 2.10A and B**). Consistently, immunofluorescence analysis indicated a substantial amount of acetylated TUBA in HASMCs overexpressed KAT2A (**Fig. 2.10C and D**). On the contrary, KAT2A silencing reduced acetylated TUBA protein levels under basal conditions and delayed the recovery of acetylated TUBA protein levels after nocodazole washout **(Fig. 2.10E and F**). Collectively, KAT2A-induced TUBA acetylation increases microtubule reassembly under autophagy-deficient conditions.

2.4.8 Autophagy controls the directional migration of VSMCs

As autophagy dynamically modulates microtubule stability, which is an essential requirement for directional cell migration (40), we examined the role of the autophagy-KAT2A-

TUBA acetylation axis in cell polarization and subsequent cell migration. We first examined the effect of autophagy inhibition on cell polarity using the scratch wound healing assay. We found that inhibition of autophagy by *ATG7* siRNA interfered with microtubule-organizing center (MTOC) reorientation in the leading cells (**Fig. 2.11A and B**), as evidenced by larger angles (θ) in *ATG7* siRNA-treated cells relative to those of control siRNA-treated cells. In addition, in control siRNA-treated HASMCs, the first two layers of leading cells were clearly polarized toward the leading edge, as shown via staining of the stabilized microtubules with acetylated-TUBA antibody. Inhibition of autophagy by *ATG7* silencing, however, dramatically increased the level of stable microtubules in the first two layers of leading cells and resulted in a loss of orientation toward the leading edge in these cells (**Fig. 2.11C**).

Finally, we tested the effect of autophagy on HASMC migration. In the scratch wound healing assay, control siRNA-treated cells migrated into the wound area and organized a dense cellular network, resulting in nearly complete wound recovery after 48 h, while siRNA silencing of either *ATG7* or *BECN1* significantly inhibited cell migration into the wound area (**Fig. 2.11D and E**). The transwell assay also showed that transfection of HASMCs with *ATG7* or *BECN1* siRNA drastically reduced cell migration through the filter membrane (**Fig. 2.11F and G**). Conversely, adenoviral overexpression of ATG5 or ATG7 significantly promoted cell migration into the wound areas (**Fig. 2.11H and I**) and significantly increased the numbers of HASMCs that migrated through the filter membrane (**Fig. 2.11J and K)**. These data suggest that autophagy is required to establish front-rear polarity and proper cell migration, presumably through the regulation of microtubule acetylation and stabilization.

2.4.9 KAT2A is required for autophagy regulation of VSMC migration

To determine whether KAT2A-acetylated TUBA mediated autophagy-regulated cell migration, we first examined whether KAT2A regulates cell migration. We transfected HASMCs with control or *KAT2A* siRNA and found that *KAT2A* silencing (**Fig. 2.12A**) promoted cell migration into the wound areas in the scratch wound healing assay (**Fig. 2.12B, C**). Conversely, adenoviral overexpression of KAT2A inhibited cell migration through the membrane in the transwell assay (**Fig. 2.12D-F**). We then co-transfected HASMCs with *ATG7* and *KAT2A* siRNA and examined cell migration. Transfection of *ATG7* siRNA reduced ATG7 protein expression and concomitantly increased protein levels of KAT2A and acetylated TUBA. Administration of *KAT2A* siRNA prevented *ATG7* siRNA-enhanced acetylation of TUBA (**Fig. 2.12G**). Notably, *ATG7* silencing inhibited VSMCs migration into the wound area, while *KAT2A* silencing promoted this VSMC migration. The observed inhibition of VSMCs migration attained by *ATG7* silencing was attenuated by silencing of *KAT2A* (**Fig. 2.12H and I**).

To establish links between KAT2A, TUBA acetylation, and VSMCs migration, we co-transfected HASMCs with *KAT2A* adenovirus and WT TUBA plasmid or with *KAT2A* adenovirus and a dominant negative Lys40 acetylation-defective TUBA plasmid ($TUBA^{K40R}$) (38). In the cells transfected with WT TUBA, overexpression of KAT2A reduced the numbers of cells that migrated through the membrane compared with overexpression of GFP. Transfection of cells with the $TUBA^{K40R}$ mutant, however, significantly prevented KAT2A-induced reduction in VSMCs migration (**Fig. 2.12J, K**). Together, these findings indicate that KAT2A-mediated acetylation of TUBA is required for defective autophagy inhibition of VSMC migration.

2.5 Discussion

In this study, we showed that selective autophagic degradation of histone acetyltransferase KAT2A controls cell migration by regulating microtubule stability. KAT2A binds directly to the autophagic effector protein LC3 via an LIR motif, which mediates autophagic degradation of KAT2A. Suppression of autophagy resulted in KAT2A accumulation, and KAT2A-induced TUBA acetylation increased microtubule stability, leading to an inhibition of cell migration. Together, our results demonstrate that autophagy controls microtubule stability by regulating KAT2A protein expression.

Although autophagy has been considered a non-specific degradation process, recent studies demonstrated that autophagy is also critical for the degradation of specific cargo, such as organelles and proteins (13,41,42). In agreement with these findings, we observed that inhibition of autophagy led to an increase in KAT2A protein levels but had no effect on *KAT2A* mRNA expression, whereas activation of autophagy reduced KAT2A protein expression and administration of a proteasome inhibitor had no effect on KAT2A protein expression. In addition, KAT2A contains an LIR motif, which mediates the association between KAT2A and LC3, recruiting KAT2A to autophagosomes. Deletion of the LIR motif prevented the degradation of KAT2A by starvation-induced autophagy. These data indicate that KAT2A is selectively degraded through the autophagy-lysosomal pathway and that the interaction between KAT2A and LC3 via the LIR motif is required for degradation of KAT2A by autophagy.

SQSTM1 has been proposed to contribute to selective autophagy of protein aggregates and depolarized mitochondria (43). Thus, we investigated whether SQSTM1 is required for KAT2A degradation by autophagy. Although LC3 bound to SQSTM1 and KAT2A separately, KAT2A was not associated with SQSTM1. Importantly, gene silencing of *SQSTM1* did not

disrupt the association between KAT2A and LC3, indicating that SQSTM1 is not involved in the interaction between KAT2A and LC3 and that direct binding between KAT2A and LC3 mediates autophagic degradation of KAT2A.

Tubulin acetylation was first described 20 years ago, but little is known about the enzymes that catalyze this reaction. Recent evidence suggests that *Atat1*/*atat-2* may function as the major TUBA acetyltransferase in C. elegans (44) and mice (45). In C. elegans, loss of *atat-2* leads to disruption of microtubule structural integrity and axonal morphologic defects in touch receptor neurons (46). In mice, ATAT1 is highly expressed in testis, kidney, and brain (45), the loss of ATAT1 results in brain abnormalities (45) and abnormal sperm morphology and motility (47). Because neither activation nor suppression of autophagy alters ATAT1 expression, it is unlikely that autophagy via ATAT1 regulates TUBA acetylation in our system.

In the current study, we demonstrated that KAT2A is the enzyme that mediates acetylation of TUBA in VSMCs, The following lines of evidence support this conclusion: co-immunoprecipitation indicated that KAT2A physically associates with TUBA, immunofluorescence analysis revealed that endogenous KAT2A colocalized with acetylated TUBA, and an *in vitro* tubulin acetylation assay showed that full-length recombinant KAT2A induces acetylation of TUBA. Furthermore, KAT2A silencing decreased TUBA acetylation, while overexpression of KAT2A increased TUBA acetylation. Importantly, overexpression of KAT2A increased acetylation of WT-TUBA but failed to induce acetylation of $TUBA^{K40R}$ mutant, in which Lys40 was substituted with arginine (38). Thus, KAT2A represents a newly described acetyltransferase that targets TUBA. KAT2A, which is first identified as a global coactivator, and transcription-related histone acetyl transferase (48), has been reported to be involved in a broad range of cellular processes including gene transcription, differentiation, DNA

repair, nucleosome assembly, and cell cycle regulation (49). Although our results strongly indicate suggests that KAT2A directly acetylates TUBA, we cannot exclude that it can indirectly regulates TUBA acetylation via other molecules. Deacetylation of TUBA is mediated by both HDAC6 and SIRT2 (7,8); however, the increased acetylation of TUBA in autophagy-deficient conditions may not be mediated by either of these deacetylases because neither activation nor suppression of autophagy alters the expression of HDAC6 or SIRT2.

The extent and duration of autophagy are crucial for cell heath, and acute and chronic manipulations of autophagy have led to, in several instances, controversial conclusion. Our results are consistent with the findings that induction of autophagy is coupled to reduction of H4K16ac (28), and α-lipoic acid inhibits cellular autophagic flux and promotes the rapid hyperacetylation of TUBA (50). However, other groups also showed that nutritional stress triggers hyperacetylation of tubulin in HeLa cells by an unidentified mechanism (51), and voluntary exercise increases acetylated tubulin levels, associated with activation of autophagy in mutated $CRYAB^{R120G}$ (CryABR120G) transgenic mouse hearts (52).

Accumulating evidence suggests that microtubules regulate autophagosome formation and transportation in axon (53,54). Whether autophagy in turn modulates microtubule stability in VSMCs is not known. In the present study we found that suppression of autophagy resulted in KAT2A accumulation, and KAT2A-induced TUBA acetylation increased microtubule stability, leading to an inhibition of cell migration. This finding is consistent with the report that inhibition of the HDAC6 by siRNA or tributyrin increased tubulin acetylation and inhibited endothelial cell migration (55). However the role of autophagy on microtubule stability seems to be different in different cell types, because a recent study showed that activation of autophagy increases microtubule stability through the degradation of STMN2 (stathmin 2), a microtubule

destabilization protein, and promotes axon regeneration after spinal cord injury (56). STMN2 is a neuron-specific, membrane-associated protein that is highly concentrated in growth cones of developing neurons. Thus, further investigations are warranted to determine the role of autophagy on microtubule stability in different cell types.

Microtubule stability plays important roles in autophagy. Treatment of cells with nocodazole leads to complete depolymerization of both labile and stable microtubules and fully inhibits autophagic flux. Autophagosome formation is also inhibited by treatment with taxol, a drug that stabilizes microtubules and interferes with the dynamic turnover of the microtubule network (57). It is now clear that microtubules are involved in autophagosome formation (58). First, microtubules interact with ATG proteins, including LC3, ULK1, BECN1, ATG5, and ATG12, supporting the assembly of pre-autophagosomal structure (59). Second, microtubules regulate two major complexes (MTORC1 and PtdIns3K complex) (59) involved in the initiation of autophagy. In VSMCs, activation of autophagy results in destabilization of microtubules, which may inhibit the interaction between microtubules and ATG proteins and prevent the formation of initiation complexes, MTORC1 and PtdIns3K complex, therefore tuning down autophagy.

The role of TUBA acetylation on microtubule stability has been controversial. Early studies indicated that TUBA acetylation had no effect on microtubule polymerization (60); however, more recent studies reported that increased acetylation of TUBA by HDAC6 inhibition increases microtubule stability and inhibits cell motility (61,62). Since HDAC6 may regulate many other proteins in addition to TUBA, it has been difficult to determine whether these results are direct effects of HDAC6-mediated deacetylation of microtubules or indirect effects via other molecules. In our study, we found that KAT2A induced TUBA acetylation and dose-dependently

increased microtubule polymerization. Overexpression of KAT2A protected microtubules from nocodazole-induced depolymerization, supporting the notion that acetylation of TUBA stabilizes microtubules. We also observed that KAT2A silencing increased cell migration into the wound area in a scratch wound healing assay. Overexpression of KAT2A inhibited cell migration in cells transfected with WT TUBA, but transfection of cells with the $TUBA^{K40R}$ mutant significantly attenuated this KAT2A-induced inhibition of VSMC migration, suggesting that KAT2A-mediated acetylation of TUBA inhibits cell migration. However, the role of stabilized microtubules in migration is greatly understudied. It has been reported that reduced TUBA acetylation impairs migration in neuronal cell lines (5,63), and in breast cancer cells (64). Conflicting reports have suggested that HDAC inhibitors, specifically targeting HDAC6's tubulin deacetylase activity, reduces cancer migration by increasing TUBA acetylation in estrogen receptor-positive breast cancer (65), in addition, enhanced acetylated TUBA decreased cell motility in a human non-small cell lung carcinoma cell line (H1299) and NIH 3T3 fibroblasts (8,66). Moreover, hyperacetylation of tubulin suppressed cell migration in endothelial cells (55). Our results suggest that acetylation of TUBA increases microtubule stability and inhibits cell motility in VSMCs.

Recent studies have clearly demonstrated that autophagy has a greater variety of physiological and pathophysiological roles, including starvation adaptation, intracellular protein and organelle clearance, elimination of microorganisms, and antigen presentation (42,67,68). We further demonstrated that autophagy regulates microtubule dynamics and cell motility through modulating TUBA acetylation. The role of autophagy in regulation of VSMC migration remains a subject of debate in the literature. Consistent with our findings, both PDGF-BB and 1-palmitoyl-2-(5-oxovaleroyl)-sn-glycero-3-phosphocholine (POVPC) induce autophagy and

concomitantly promote the loss of contractile gene expression and increase cell proliferation and migration (69,70). By contrast, administration of the autophagy inducer rapamycin inhibits cell proliferation and prevents restenosis after angioplasty (71,72). These effects of rapamycin are unlikely due to its activation of autophagy (70). Rather, the drugs appear to prevent proliferation and migration by inhibiting RPS6KB1/S6K1 (ribosomal protein S6 kinase, polypeptide 1) (73,74) and regulating the expression of key cell cycle protein CDKN1B/$p27^{Kip1}$ (75). Intriguingly, rapamycin promotes Schwann cell migration via unidentified mechanisms (76). Another study demonstrated that VSMC-specific deletion of *ATG7* accelerates senescence and promotes neointimal formation and atherogenesis (18). One explanation for this discrepancy is that autophagy can also occur in the absence of some key autophagy proteins, such as ATG5 and ATG7, through unconventional biogenesis of canonical autophagosomes (32). In addition, ATG7 has been reported to regulate TRP53/p53-dependent cell cycle and cell death pathways independent of autophagy during metabolic stress (77). Thus, further investigation is necessary to determine the role of autophagy in regulating VSMC migration. A mouse with VSMC-specific deletion of ULK1, a protein essential for regulating both ATG5/ATG7-dependent and ATG5/ATG7-independent autophagy (32), may be useful for these investigations.

In conclusion, KAT2A is the acetyltransferase responsible for acetylation of TUBA and is selectively degraded by the autophagy-lysosomal pathway. Stabilization of microtubules by KAT2A-mediated acetylation of TUBA is an important mechanism by which defective autophagy inhibits VSMC migration. Our findings suggest that autophagy suppression in VSMCs may be an important therapeutic target for atherosclerosis and intimal hyperplasia.

2.6 Acknowledgments

This study was supported by funding from the following agencies: NHLBI (HL079584, HL080499, HL089920, HL110488, HL128014, HL132500, HL137371, and HL142287), NCI (CA213022), NIA (AG047776), and AHA (16GRANT29590003). Dr. Zou is the Eminent Scholar in Molecular and Translational Medicine of the Georgia Research Alliance.

2.7 References

1. Kenagy RD, Fukai N, Min SK, Jalikis F, Kohler TR, Clowes AW. Proliferative capacity of vein graft smooth muscle cells and fibroblasts in vitro correlates with graft stenosis. J Vasc Surg **2009**;49(5):1282-8 doi 10.1016/j.jvs.2008.12.020.
2. Schaper W, Ito WD. Molecular mechanisms of coronary collateral vessel growth. Circ Res **1996**;79(5):911-9 doi 10.1161/01.res.79.5.911.
3. Etienne-Manneville S. Microtubules in cell migration. Annu Rev Cell Dev Biol **2013**;29:471-99 doi 10.1146/annurev-cellbio-101011-155711.
4. Mitchison T, Kirschner M. Dynamic instability of microtubule growth. Nature **1984**;312(5991):237-42 doi 10.1038/312237a0.
5. Creppe C, Malinouskaya L, Volvert ML, Gillard M, Close P, Malaise O*, et al.* Elongator controls the migration and differentiation of cortical neurons through acetylation of alpha-tubulin. Cell **2009**;136(3):551-64 doi 10.1016/j.cell.2008.11.043.
6. Akella JS, Wloga D, Kim J, Starostina NG, Lyons-Abbott S, Morrissette NS*, et al.* MEC-17 is an alpha-tubulin acetyltransferase. Nature **2010**;467(7312):218-22 doi 10.1038/nature09324.
7. North BJ, Marshall BL, Borra MT, Denu JM, Verdin E. The human Sir2 ortholog, SIRT2, is an NAD+-dependent tubulin deacetylase. Mol Cell **2003**;11(2):437-44 doi 10.1016/s1097-2765(03)00038-8.
8. Hubbert C, Guardiola A, Shao R, Kawaguchi Y, Ito A, Nixon A*, et al.* HDAC6 is a microtubule-associated deacetylase. Nature **2002**;417(6887):455-8 doi 10.1038/417455a.
9. Chimal-Monroy J, Abarca-Buis RF, Cuervo R, Diaz-Hernandez M, Bustamante M, Rios-Flores JA*, et al.* Molecular control of cell differentiation and programmed cell death during digit development. IUBMB Life **2011**;63(10):922-9 doi 10.1002/iub.563.
10. Sridhar S, Botbol Y, Macian F, Cuervo AM. Autophagy and disease: always two sides to a problem. J Pathol **2012**;226(2):255-73 doi 10.1002/path.3025.
11. Cuervo AM. Autophagy: in sickness and in health. Trends Cell Biol **2004**;14(2):70-7 doi 10.1016/j.tcb.2003.12.002.
12. Kroemer G, Marino G, Levine B. Autophagy and the integrated stress response. Mol Cell **2010**;40(2):280-93 doi 10.1016/j.molcel.2010.09.023.
13. Kim PK, Hailey DW, Mullen RT, Lippincott-Schwartz J. Ubiquitin signals autophagic degradation of cytosolic proteins and peroxisomes. Proc Natl Acad Sci U S A **2008**;105(52):20567-74 doi 10.1073/pnas.0810611105.

14. Popelka H, Klionsky DJ. Post-translationally-modified structures in the autophagy machinery: an integrative perspective. FEBS J **2015**;282(18):3474-88 doi 10.1111/febs.13356.
15. Long L, Yang X, Southwood M, Lu J, Marciniak SJ, Dunmore BJ*, et al.* Chloroquine prevents progression of experimental pulmonary hypertension via inhibition of autophagy and lysosomal bone morphogenetic protein type II receptor degradation. Circ Res **2013**;112(8):1159-70 doi 10.1161/CIRCRESAHA.111.300483.
16. LaRocca TJ, Gioscia-Ryan RA, Hearon CM, Jr., Seals DR. The autophagy enhancer spermidine reverses arterial aging. Mech Ageing Dev **2013**;134(7-8):314-20 doi 10.1016/j.mad.2013.04.004.
17. Martinet W, De Meyer GR. Autophagy in atherosclerosis: a cell survival and death phenomenon with therapeutic potential. Circ Res **2009**;104(3):304-17 doi 10.1161/CIRCRESAHA.108.188318.
18. Grootaert MO, da Costa Martins PA, Bitsch N, Pintelon I, De Meyer GR, Martinet W*, et al.* Defective autophagy in vascular smooth muscle cells accelerates senescence and promotes neointima formation and atherogenesis. Autophagy **2015**;11(11):2014-32 doi 10.1080/15548627.2015.1096485.
19. Tedesco L, Valerio A, Cervino C, Cardile A, Pagano C, Vettor R*, et al.* Cannabinoid type 1 receptor blockade promotes mitochondrial biogenesis through endothelial nitric oxide synthase expression in white adipocytes. Diabetes **2008**;57(8):2028-36 doi 10.2337/db07-1623.
20. Pfaffl MW. A new mathematical model for relative quantification in real-time RT-PCR. Nucleic Acids Res **2001**;29(9):e45 doi 10.1093/nar/29.9.e45.
21. He C, Zhu H, Li H, Zou MH, Xie Z. Dissociation of Bcl-2-Beclin1 complex by activated AMPK enhances cardiac autophagy and protects against cardiomyocyte apoptosis in diabetes. Diabetes **2013**;62(4):1270-81 doi 10.2337/db12-0533.
22. Xie Z, Dong Y, Zhang J, Scholz R, Neumann D, Zou MH. Identification of the serine 307 of LKB1 as a novel phosphorylation site essential for its nucleocytoplasmic transport and endothelial cell angiogenesis. Mol Cell Biol **2009**;29(13):3582-96 doi 10.1128/MCB.01417-08.
23. Zou MH, Li H, He C, Lin M, Lyons TJ, Xie Z. Tyrosine nitration of prostacyclin synthase is associated with enhanced retinal cell apoptosis in diabetes. Am J Pathol **2011**;179(6):2835-44 doi 10.1016/j.ajpath.2011.08.041.
24. Xie Z, Singh M, Siwik DA, Joyner WL, Singh K. Osteopontin inhibits interleukin-1beta-stimulated increases in matrix metalloproteinase activity in adult rat cardiac fibroblasts: role of protein kinase C-zeta. J Biol Chem **2003**;278(49):48546-52 doi 10.1074/jbc.M302727200.
25. Nakano A, Kato H, Watanabe T, Min KD, Yamazaki S, Asano Y*, et al.* AMPK controls the speed of microtubule polymerization and directional cell migration through CLIP-170 phosphorylation. Nat Cell Biol **2010**;12(6):583-90 doi 10.1038/ncb2060.
26. Sun X, Shi X, Liu M, Li D, Zhang L, Liu X*, et al.* Mdp3 is a novel microtubule-binding protein that regulates microtubule assembly and stability. Cell Cycle **2011**;10(22):3929-37 doi 10.4161/cc.10.22.18106.
27. Liang CC, Park AY, Guan JL. In vitro scratch assay: a convenient and inexpensive method for analysis of cell migration in vitro. Nat Protoc **2007**;2(2):329-33 doi 10.1038/nprot.2007.30.

28. Fullgrabe J, Lynch-Day MA, Heldring N, Li W, Struijk RB, Ma Q*, et al.* The histone H4 lysine 16 acetyltransferase hMOF regulates the outcome of autophagy. Nature **2013**;500(7463):468-71 doi 10.1038/nature12313.
29. Komatsu M, Waguri S, Ueno T, Iwata J, Murata S, Tanida I*, et al.* Impairment of starvation-induced and constitutive autophagy in Atg7-deficient mice. J Cell Biol **2005**;169(3):425-34 doi 10.1083/jcb.200412022.
30. Kuma A, Hatano M, Matsui M, Yamamoto A, Nakaya H, Yoshimori T*, et al.* The role of autophagy during the early neonatal starvation period. Nature **2004**;432(7020):1032-6 doi 10.1038/nature03029.
31. Mizushima N. Autophagy: process and function. Genes Dev **2007**;21(22):2861-73 doi 10.1101/gad.1599207.
32. Nishida Y, Arakawa S, Fujitani K, Yamaguchi H, Mizuta T, Kanaseki T*, et al.* Discovery of Atg5/Atg7-independent alternative macroautophagy. Nature **2009**;461(7264):654-8 doi 10.1038/nature08455.
33. Tomoda H, Omura S. Lactacystin, a proteasome inhibitor: discovery and its application in cell biology. Yakugaku Zasshi **2000**;120(10):935-49 doi 10.1248/yakushi1947.120.10_935.
34. Shen R, Wang X, Drissi H, Liu F, O'Keefe RJ, Chen D. Cyclin D1-cdk4 induce runx2 ubiquitination and degradation. J Biol Chem **2006**;281(24):16347-53 doi 10.1074/jbc.M603439200.
35. Suzuki H, Tabata K, Morita E, Kawasaki M, Kato R, Dobson RC*, et al.* Structural basis of the autophagy-related LC3/Atg13 LIR complex: recognition and interaction mechanism. Structure **2014**;22(1):47-58 doi 10.1016/j.str.2013.09.023.
36. Alemu EA, Lamark T, Torgersen KM, Birgisdottir AB, Larsen KB, Jain A*, et al.* ATG8 family proteins act as scaffolds for assembly of the ULK complex: sequence requirements for LC3-interacting region (LIR) motifs. J Biol Chem **2012**;287(47):39275-90 doi 10.1074/jbc.M112.378109.
37. Magiera MM, Janke C. Post-translational modifications of tubulin. Curr Biol **2014**;24(9):R351-4 doi 10.1016/j.cub.2014.03.032.
38. Dompierre JP, Godin JD, Charrin BC, Cordelieres FP, King SJ, Humbert S*, et al.* Histone deacetylase 6 inhibition compensates for the transport deficit in Huntington's disease by increasing tubulin acetylation. J Neurosci **2007**;27(13):3571-83 doi 10.1523/JNEUROSCI.0037-07.2007.
39. Piperno G, LeDizet M, Chang XJ. Microtubules containing acetylated alpha-tubulin in mammalian cells in culture. J Cell Biol **1987**;104(2):289-302 doi 10.1083/jcb.104.2.289.
40. Kaverina I, Straube A. Regulation of cell migration by dynamic microtubules. Semin Cell Dev Biol **2011**;22(9):968-74 doi 10.1016/j.semcdb.2011.09.017.
41. Lu K, Psakhye I, Jentsch S. A new class of ubiquitin-Atg8 receptors involved in selective autophagy and polyQ protein clearance. Autophagy **2014**;10(12):2381-2 doi 10.4161/15548627.2014.981919.
42. Steele S, Brunton J, Kawula T. The role of autophagy in intracellular pathogen nutrient acquisition. Front Cell Infect Microbiol **2015**;5:51 doi 10.3389/fcimb.2015.00051.
43. Rogov V, Dotsch V, Johansen T, Kirkin V. Interactions between autophagy receptors and ubiquitin-like proteins form the molecular basis for selective autophagy. Mol Cell **2014**;53(2):167-78 doi 10.1016/j.molcel.2013.12.014.

44. Shida T, Cueva JG, Xu Z, Goodman MB, Nachury MV. The major alpha-tubulin K40 acetyltransferase alphaTAT1 promotes rapid ciliogenesis and efficient mechanosensation. Proc Natl Acad Sci U S A **2010**;107(50):21517-22 doi 10.1073/pnas.1013728107.
45. Kim GW, Li L, Ghorbani M, You L, Yang XJ. Mice lacking alpha-tubulin acetyltransferase 1 are viable but display alpha-tubulin acetylation deficiency and dentate gyrus distortion. J Biol Chem **2013**;288(28):20334-50 doi 10.1074/jbc.M113.464792.
46. Topalidou I, Keller C, Kalebic N, Nguyen KC, Somhegyi H, Politi KA*, et al.* Genetically separable functions of the MEC-17 tubulin acetyltransferase affect microtubule organization. Curr Biol **2012**;22(12):1057-65 doi 10.1016/j.cub.2012.03.066.
47. Kalebic N, Sorrentino S, Perlas E, Bolasco G, Martinez C, Heppenstall PA. alphaTAT1 is the major alpha-tubulin acetyltransferase in mice. Nat Commun **2013**;4:1962 doi 10.1038/ncomms2962.
48. Kikuchi H, Barman HK, Nakayama M, Takami Y, Nakayama T. Participation of histones, histone modifying enzymes and histone chaperones in vertebrate cell functions. Subcell Biochem **2006**;40:225-43 doi 10.1007/978-1-4020-4896-8_13.
49. Burgess RJ, Zhou H, Han J, Zhang Z. A role for Gcn5 in replication-coupled nucleosome assembly. Mol Cell **2010**;37(4):469-80 doi 10.1016/j.molcel.2010.01.020.
50. Stoner MW, Thapa D, Zhang M, Gibson GA, Calderon MJ, St Croix CM*, et al.* alpha-Lipoic acid promotes alpha-tubulin hyperacetylation and blocks the turnover of mitochondria through mitophagy. Biochem J **2016**;473(12):1821-30 doi 10.1042/BCJ20160281.
51. Geeraert C, Ratier A, Pfisterer SG, Perdiz D, Cantaloube I, Rouault A*, et al.* Starvation-induced hyperacetylation of tubulin is required for the stimulation of autophagy by nutrient deprivation. J Biol Chem **2010**;285(31):24184-94 doi 10.1074/jbc.M109.091553.
52. McLendon PM, Ferguson BS, Osinska H, Bhuiyan MS, James J, McKinsey TA*, et al.* Tubulin hyperacetylation is adaptive in cardiac proteotoxicity by promoting autophagy. Proc Natl Acad Sci U S A **2014**;111(48):E5178-86 doi 10.1073/pnas.1415589111.
53. Fu MM, Nirschl JJ, Holzbaur ELF. LC3 binding to the scaffolding protein JIP1 regulates processive dynein-driven transport of autophagosomes. Dev Cell **2014**;29(5):577-90 doi 10.1016/j.devcel.2014.04.015.
54. Maday S, Wallace KE, Holzbaur EL. Autophagosomes initiate distally and mature during transport toward the cell soma in primary neurons. J Cell Biol **2012**;196(4):407-17 doi 10.1083/jcb.201106120.
55. Wang YH, Yan ZQ, Qi YX, Cheng BB, Wang XD, Zhao D*, et al.* Normal shear stress and vascular smooth muscle cells modulate migration of endothelial cells through histone deacetylase 6 activation and tubulin acetylation. Ann Biomed Eng **2010**;38(3):729-37 doi 10.1007/s10439-009-9896-6.
56. He M, Ding Y, Chu C, Tang J, Xiao Q, Luo ZG. Autophagy induction stabilizes microtubules and promotes axon regeneration after spinal cord injury. Proc Natl Acad Sci U S A **2016**;113(40):11324-9 doi 10.1073/pnas.1611282113.
57. Kochl R, Hu XW, Chan EY, Tooze SA. Microtubules facilitate autophagosome formation and fusion of autophagosomes with endosomes. Traffic **2006**;7(2):129-45 doi 10.1111/j.1600-0854.2005.00368.x.
58. Fass E, Shvets E, Degani I, Hirschberg K, Elazar Z. Microtubules support production of starvation-induced autophagosomes but not their targeting and fusion with lysosomes. J Biol Chem **2006**;281(47):36303-16 doi 10.1074/jbc.M607031200.

59. Mackeh R, Perdiz D, Lorin S, Codogno P, Pous C. Autophagy and microtubules - new story, old players. J Cell Sci **2013**;126(Pt 5):1071-80 doi 10.1242/jcs.115626.
60. Maruta H, Greer K, Rosenbaum JL. The acetylation of alpha-tubulin and its relationship to the assembly and disassembly of microtubules. J Cell Biol **1986**;103(2):571-9 doi 10.1083/jcb.103.2.571.
61. Matsuyama A, Shimazu T, Sumida Y, Saito A, Yoshimatsu Y, Seigneurin-Berny D*, et al.* In vivo destabilization of dynamic microtubules by HDAC6-mediated deacetylation. EMBO J **2002**;21(24):6820-31 doi 10.1093/emboj/cdf682.
62. Tran AD, Marmo TP, Salam AA, Che S, Finkelstein E, Kabarriti R*, et al.* HDAC6 deacetylation of tubulin modulates dynamics of cellular adhesions. J Cell Sci **2007**;120(Pt 8):1469-79 doi 10.1242/jcs.03431.
63. Li L, Wei D, Wang Q, Pan J, Liu R, Zhang X*, et al.* MEC-17 deficiency leads to reduced alpha-tubulin acetylation and impaired migration of cortical neurons. J Neurosci **2012**;32(37):12673-83 doi 10.1523/JNEUROSCI.0016-12.2012.
64. Boggs AE, Vitolo MI, Whipple RA, Charpentier MS, Goloubeva OG, Ioffe OB*, et al.* alpha-Tubulin acetylation elevated in metastatic and basal-like breast cancer cells promotes microtentacle formation, adhesion, and invasive migration. Cancer Res **2015**;75(1):203-15 doi 10.1158/0008-5472.CAN-13-3563.
65. Saji S, Kawakami M, Hayashi S, Yoshida N, Hirose M, Horiguchi S*, et al.* Significance of HDAC6 regulation via estrogen signaling for cell motility and prognosis in estrogen receptor-positive breast cancer. Oncogene **2005**;24(28):4531-9 doi 10.1038/sj.onc.1208646.
66. Jung HY, Jung JS, Whang YM, Kim YH. RASSF1A Suppresses Cell Migration through Inactivation of HDAC6 and Increase of Acetylated alpha-Tubulin. Cancer Res Treat **2013**;45(2):134-44 doi 10.4143/crt.2013.45.2.134.
67. Mizushima N. The pleiotropic role of autophagy: from protein metabolism to bactericide. Cell Death Differ **2005**;12 Suppl 2:1535-41 doi 10.1038/sj.cdd.4401728.
68. Choi AM, Ryter SW, Levine B. Autophagy in human health and disease. N Engl J Med **2013**;368(7):651-62 doi 10.1056/NEJMra1205406.
69. Salabei JK, Cummins TD, Singh M, Jones SP, Bhatnagar A, Hill BG. PDGF-mediated autophagy regulates vascular smooth muscle cell phenotype and resistance to oxidative stress. Biochem J **2013**;451(3):375-88 doi 10.1042/BJ20121344.
70. Salabei JK, Hill BG. Implications of autophagy for vascular smooth muscle cell function and plasticity. Free Radic Biol Med **2013**;65:693-703 doi 10.1016/j.freeradbiomed.2013.08.003.
71. Kim J, Kundu M, Viollet B, Guan KL. AMPK and mTOR regulate autophagy through direct phosphorylation of Ulk1. Nat Cell Biol **2011**;13(2):132-41 doi 10.1038/ncb2152.
72. Jung CH, Ro SH, Cao J, Otto NM, Kim DH. mTOR regulation of autophagy. FEBS Lett **2010**;584(7):1287-95 doi 10.1016/j.febslet.2010.01.017.
73. Martin KA, Merenick BL, Ding M, Fetalvero KM, Rzucidlo EM, Kozul CD*, et al.* Rapamycin promotes vascular smooth muscle cell differentiation through insulin receptor substrate-1/phosphatidylinositol 3-kinase/Akt2 feedback signaling. J Biol Chem **2007**;282(49):36112-20 doi 10.1074/jbc.M703914200.
74. Gallo R, Padurean A, Jayaraman T, Marx S, Roque M, Adelman S*, et al.* Inhibition of intimal thickening after balloon angioplasty in porcine coronary arteries by targeting

regulators of the cell cycle. Circulation **1999**;99(16):2164-70 doi 10.1161/01.cir.99.16.2164.
75. Sun J, Marx SO, Chen HJ, Poon M, Marks AR, Rabbani LE. Role for p27(Kip1) in Vascular Smooth Muscle Cell Migration. Circulation **2001**;103(24):2967-72 doi 10.1161/01.cir.103.24.2967.
76. Liu F, Zhang H, Zhang K, Wang X, Li S, Yin Y. Rapamycin promotes Schwann cell migration and nerve growth factor secretion. Neural Regen Res **2014**;9(6):602-9 doi 10.4103/1673-5374.130101.
77. Lee IH, Kawai Y, Fergusson MM, Rovira, II, Bishop AJ, Motoyama N*, et al.* Atg7 modulates p53 activity to regulate cell cycle and survival during metabolic stress. Science **2012**;336(6078):225-8 doi 10.1126/science.1218395.

2.8 Tables and Figures

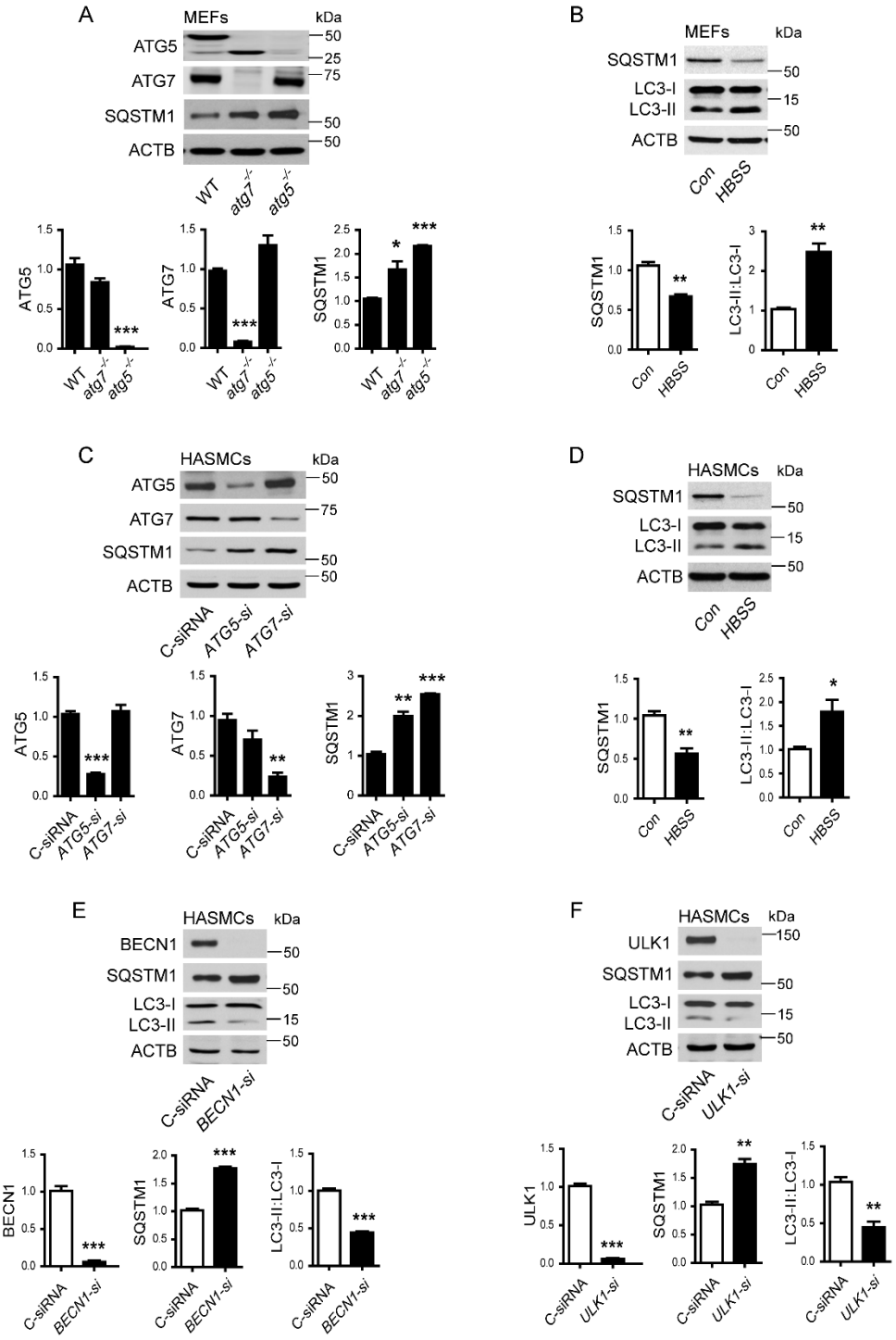
A
MEFs
kDa
ATG5
ATG7
SQSTM1
ACTB
50
25
75
50
50
WT
atg7-/-
atg5-/-
ATG5
ATG7
SQSTM1
B
MEFs
kDa
SQSTM1
LC3-I
LC3-II
ACTB
50
15
50
Con
HBSS
SQSTM1
LC3-II:LC3-I
C
HASMCs
kDa
ATG5
ATG7
SQSTM1
ACTB
50
75
50
50
C-siRNA
ATG5-si
ATG7-si
ATG5
ATG7
SQSTM1
D
HASMCs
kDa
SQSTM1
LC3-I
LC3-II
ACTB
50
15
50
Con
HBSS
SQSTM1
LC3-II:LC3-I
E
HASMCs
kDa
BECN1
SQSTM1
LC3-I
LC3-II
ACTB
50
50
15
50
C-siRNA
BECN1-si
BECN1
SQSTM1
LC3-II:LC3-I
F
HASMCs
kDa
ULK1
SQSTM1
LC3-I
LC3-II
ACTB
150
50
15
50
C-siRNA
ULK1-si
ULK1
SQSTM1
LC3-II:LC3-I

Figure 2.1 Manipulation of autophagy in mouse embryonic fibroblasts (MEFs) and human aortic smooth muscle cells (HASMCs).

(A) Protein levels of ATG5, ATG7, SQSTM1, LC3, and ACTB/β-actin in wild-type (WT), *atg5*$^{-/-}$, and *atg7*$^{-/-}$ MEFs were analyzed by western blot. n=3, **P<0.05*, ****P<0.001* vs. WT. (B) WT MEFs were starved with Hanks balanced salt solution (HBSS) for 3 h, and protein levels of SQSTM1, LC3, and ACTB/β-actin were analyzed by western blot. n=3, ***P<0.01* vs. Con. (C) HASMCs were transfected with control siRNA (C-siRNA), *ATG5* siRNA, or *ATG7* siRNA for 48 h. Protein levels of ATG5, ATG7, SQSTM1, LC3, and ACTB/β-actin were measured by western blot. n=3, ***P<0.01*, ****P<0.001* vs. C-siRNA. (D) HASMCs were starved with HBSS for 3 h, and protein levels of SQSTM1, LC3, and ACTB/β-actin were analyzed by western blotting. n=3, **P<0.05*, ***P<0.01* vs. Con. (E) HASMCs were transfected with control siRNA (C-siRNA) or *BECN1* siRNA, and protein levels of SQSTM1, LC3, and ACTB/β-actin were detected by western blotting. n=3, ****P<0.001* vs. C-siRNA. (F) Western blot analysis of ULK1, SQSTM1, LC3, and ACTB/β-actin in HASMCs transfected with control siRNA (C-siRNA) or *ULK1* siRNA (*ULK1-si*). n=3, ***P<0.01*, ****P<0.001* vs. C-siRNA.

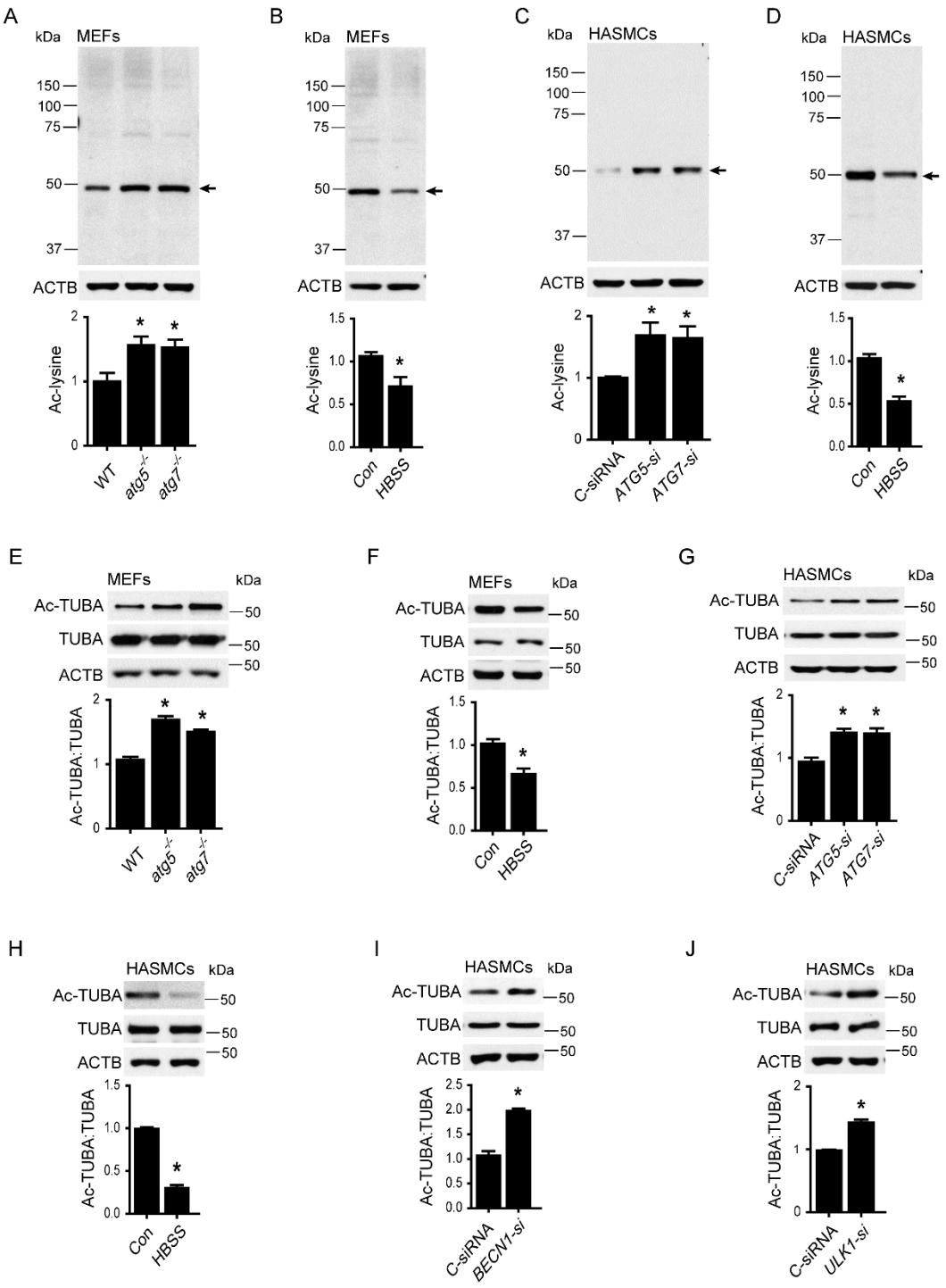

Figure 2.2 Autophagy regulates TUBA acetylation.

(A) Western blot analysis of protein acetylation in wild-type (WT), *atg5*$^{-/-}$, and *atg7*$^{-/-}$ mouse embryonic fibroblasts (MEFs). n=5, **P<0.05 vs.* WT. (B) WT MEFs were starved with Hank's balanced salt solution

(HBSS) for 3 h, and acetylated proteins were analyzed by western blotting. n=5, **P*<0.05 vs. control (con). (C) Human aortic smooth muscle cells (HASMCs) were transfected with control siRNA (C-siRNA) or siRNA targeting *ATG5* (*ATG5*-si) or *ATG7* (*ATG7*-si) for 48 h. Protein acetylation was measured by western blotting. n=5, **P*<0.05 vs. C-siRNA. (D) HASMCs were starved with HBSS for 3 h. Protein acetylation was analyzed by western blot. n=5, **P*<0.05 vs. Con (E) Western blot analysis of acetylation of TUBA (Ac-TUBA) in WT, *atg5*$^{-/-}$*, and atg7*$^{-/-}$ MEFs. n=5, **P*<0.05 vs. WT. (F) Western blot analysis of Ac-TUBA in MEFs subjected to starvation. n=5, **P*<0.05 *vs.* Con. (G) Levels of Ac-TUBA were determined by western blot in HASMCs transfected with C-siRNA, *ATG5* siRNA, or *ATG7* siRNA. n=5, **P*<0.05 vs. C-siRNA. (H) Western blot analysis of Ac-TUBA in HASMCs subjected to starvation. n=5, **P*<0.05 vs. Con. (I) Western blots detected the indicated proteins in HASMCs transfected with C-siRNA or *BECN1* siRNA (*BECN1*-si). n=5, **P*<0.05 vs. C-siRNA. (J) Western blot analysis of Ac-TUBA in HASMCs transfected with C-siRNA or *ULK1* siRNA (*ULK1*-si). n=5, **P*<0.05 vs. C-siRNA.

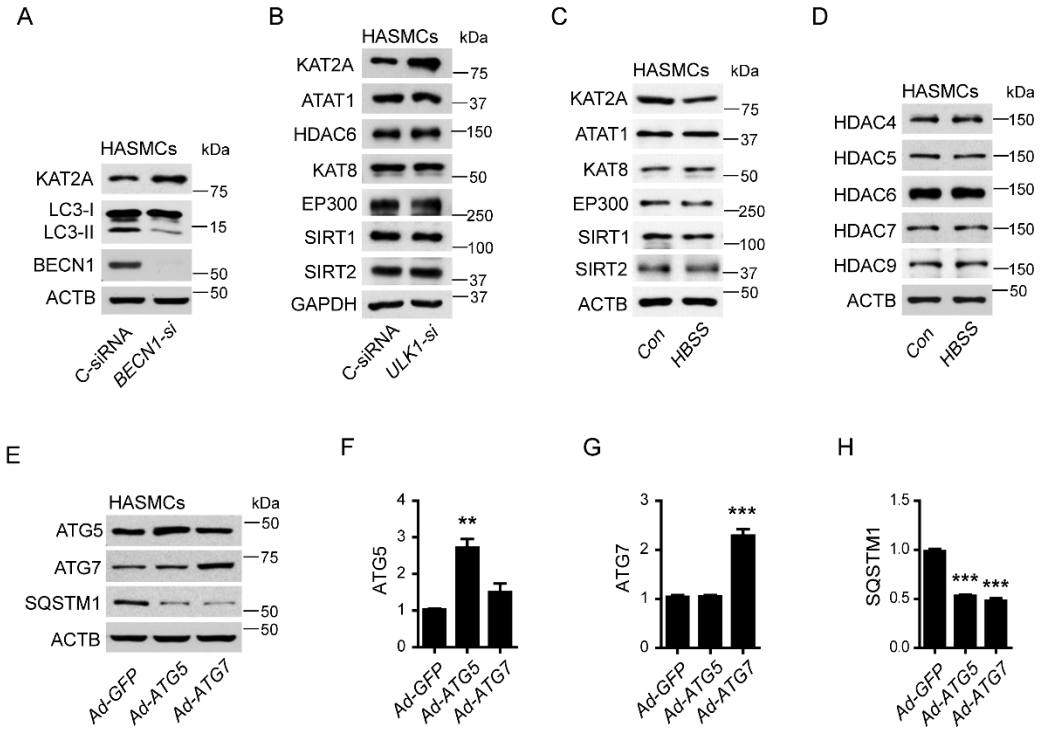

Figure 2.3 Autophagy inhibition increases KAT2A protein levels.

(A) HASMCs were transfected with control siRNA (C-siRNA) or *BECN1* siRNA for 48 h. Protein levels of KAT2A/GCN5, LC3, and BECN1 were determined by western blotting. (B) Levels of KAT2A, ATAT1, HDAC6, KAT8/hMOF, EP300, SIRT1, and SIRT2 in HASMC lysates transfected with control siRNA (C-siRNA) or *ULK1* siRNA were detected by western blotting. (C and D) HASMCs were starved with HBSS for 3 h. (C) Protein levels of KAT2A, ATAT1, KAT8, EP300, SIRT1, and SIRT2 were analyzed by western blot. (D) Protein levels of HDAC4, HDAC5, HDAC6, HDAC7, and HDAC9 were analyzed by western blot. (E-H) HASMCs were transfected with adenovirus encoding *GFP* (*Ad-GFP*), *ATG5* (*Ad-ATG5*), or *ATG7* (*Ad-ATG7*) for 48 h. Protein levels of ATG5, ATG7, SQSTM1, and ACTB/β-actin were analyzed by western blot and densitometry. n=3, ***P<0.01*, ****P<0.001* vs. Ad-GFP.

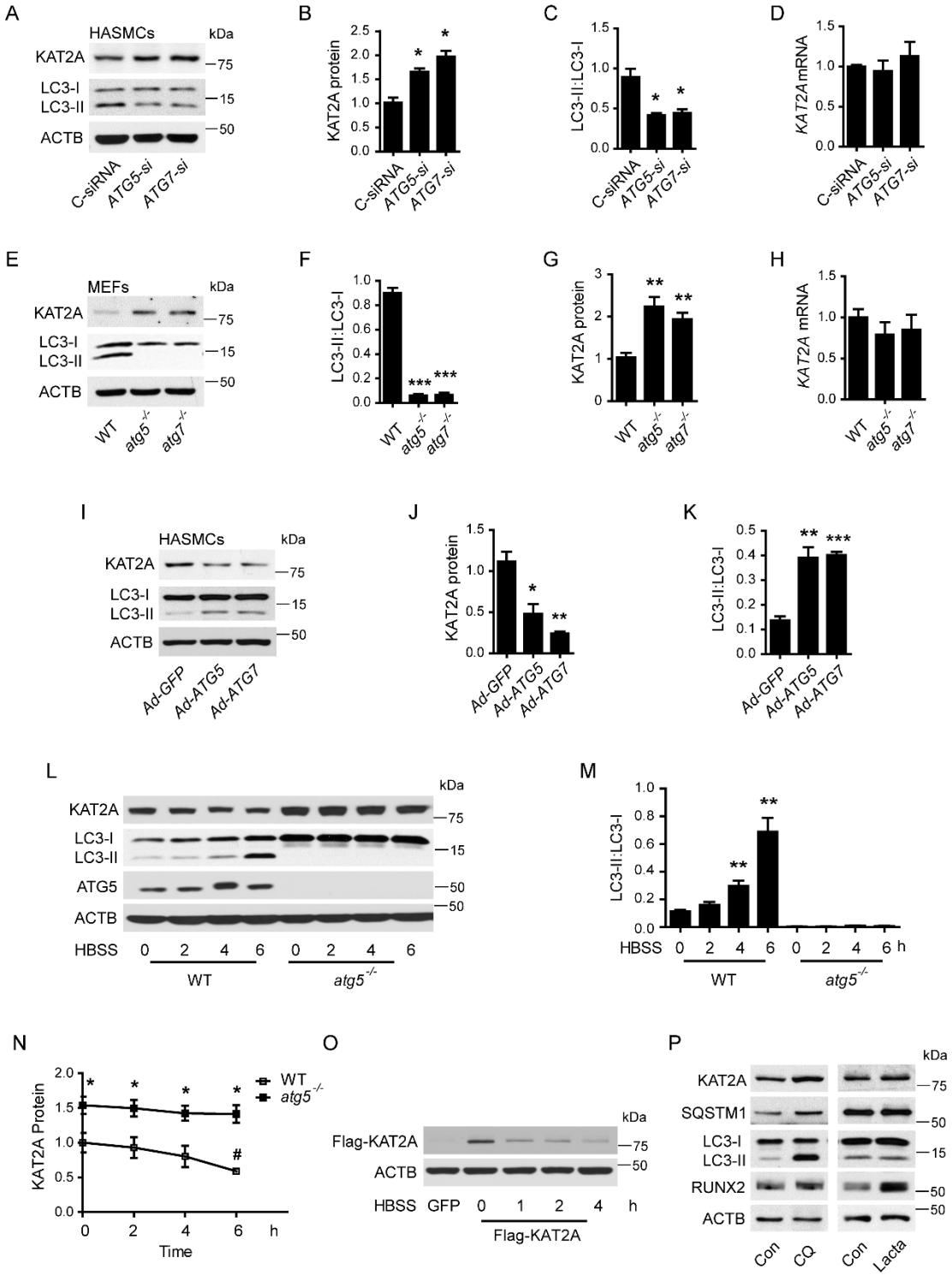
A
HASMCs
kDa
KAT2A
LC3-I
LC3-II
ACTB
75
15
50
C-siRNA
ATG5-si
ATG7-si
B
KAT2A protein
C
LC3-II:LC3-I
D
KAT2A mRNA
E
MEFs
WT
atg5-/-
atg7-/-
F
G
H
I
Ad-GFP
Ad-ATG5
Ad-ATG7
J
K
L
ATG5
HBSS
0 2 4 6 0 2 4 6
M
N
KAT2A Protein
Time
h
WT
atg5-/-
O
Flag-KAT2A
HBSS GFP 0 1 2 4 h
P
SQSTM1
RUNX2
Con
CQ
Lacta

Figure 2.4 Autophagy inhibition increases KAT2A protein levels.

(A-C) HASMCs were transfected with control siRNA (C-siRNA), *ATG5* siRNA (*ATG5*-si), or *ATG7* siRNA (*ATG7*-si) for 48 h. Protein levels of KAT2A and LC3-I or LC3-II were analyzed by western blotting and densitometry. n=3, **P*<0.05 vs. C-siRNA. (D) *KAT2A* mRNA was measured by quantitative real-time PCR. (E-G) Western blot and densitometry analysis of KAT2A and LC3-I or LC3-II protein levels in WT, *atg5*$^{-/-}$, and *atg7*$^{-/-}$ MEFs. n=3, ***P*<0.01 vs. WT, ****P*<0.001 vs. WT. (H) Expression of *KAT2A* mRNA in WT, *atg5*$^{-/-}$, and *atg7*$^{-/-}$ MEFs. (I-K) HASMCs were transfected with Ad-*GFP*, Ad-*ATG5*, or Ad-*ATG7* for 48 h. Protein levels of KAT2A and LC3-I or LC3-II were evaluated by western blotting and densitometry. n=3, **P*<0.05, ***P*<0.01, ****P*<0.001 vs. ad-GFP. (L) WT and *atg5*$^{-/-}$ MEFs were starved with HBSS for the indicated time points. Protein levels of KAT2A, LC3-I or LC3-II, and ATG5 were analyzed by western blotting. (M) The LC3-II to LC3-I ratio was analyzed by densitometry. n=3, ***P*<0.01 vs. control. (N) KAT2A degradation was analyzed by densitometry. n=3, **P*<0.05 vs. *atg5*$^{-/-}$ MEFs; $^{\#}$*P*<0.05 vs. *atg5*$^{-/-}$ 0 h. (O) HeLa cells were transfected with plasmid encoding GFP or Flag-KAT2A for 48 h and then starved with HBSS for the indicated time points. Expression of Flag-KAT2A was determined by western blotting. (P) HASMCs were treated with chloroquine (CQ, 10 μM) or lactacystin (Lacta, 5 μM) for 24 h. Levels of KAT2A, SQSTM1, LC3-I or LC3-II and RUNX2 were analyzed by western blotting.

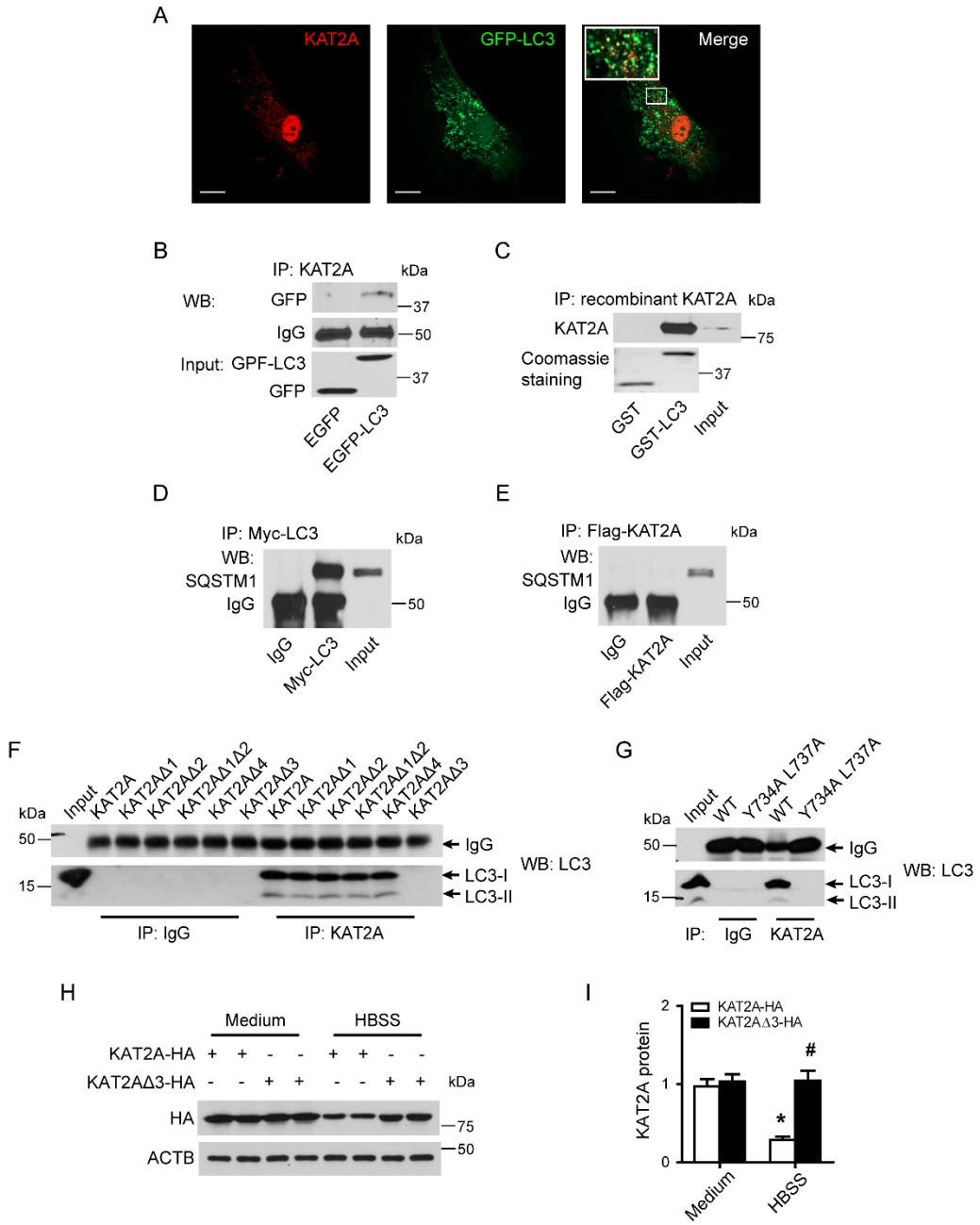

Figure 2.5 KAT2A is degraded through the autophagic-lysosomal pathway.

(A) HASMCs were transfected with an adenovirus encoding GFP-LC3 for 24 h and then treated with chloroquine for 16 h. KAT2A was stained by immunocytochemistry, and the co-localization (yellow) of KAT2A (red) and GFP-LC3 puncta was evaluated by immunofluorescence microscopy. Scale bar, 20 μm.

(B) HeLa cells were transfected with EGFP or EGFP-LC3 plasmid for 24 h. The interaction between

KAT2A and LC3B was determined by immunoprecipitation (IP) of KAT2A and subsequent western blotting (WB) with GFP. (C) Recombinant full-length KAT2A was incubated with GST- or GST-LC3-immobilized beads and then subjected to SDS-PAGE. KAT2A was detected with KAT2A antibody. Coomassie staining was used to visualize GST and GST-LC3 proteins. (D) HeLa cells were transfected with plasmid encoding Myc-LC3 for 48 h, and the interaction between LC3 and SQSTM1 was determined by IP and WB as indicated. (E) HeLa cells were transfected with plasmid encoding Flag-KAT2A for 48 h, and the interaction between KAT2A and SQSTM1 was determined by IP and WB as indicated. (F) HeLa cells were transfected with the indicated KAT2A constructs for 24 h. Cell lysates were immunoprecipitated using IgG or KAT2A antibody, and LC3B antibody was used for WB. (G) HeLa cells were transfected with plasmids encoding WT and KAT2A$^{Y734A,\ L737A}$ mutant for 24 h. Cells were lysed and immunoprecipitated using IgG or KAT2A antibody. The immunoprecipitated proteins were detected by western blotting with LC3B antibody. (H and I) HeLa cells were transfected with WT or KAT2A$^{Y734A,\ L737A}$ mutant for 48 h and then starved with incubation in HBSS for 3 h to activate autophagy. KAT2A protein levels were analyzed by WB and densitometry. n=3, ***$P<0.001$ *vs.* KAT2A-HA/Medium; ###$P<0.001$ *vs.* KAT2A-HA/HBSS.

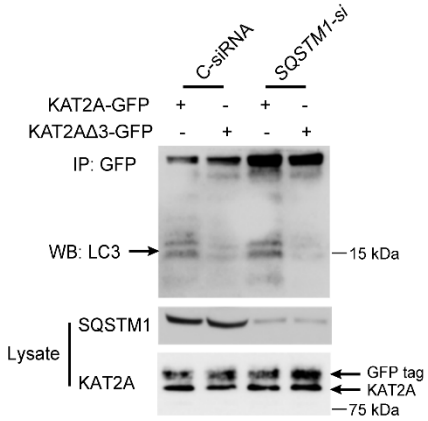

Figure 2.6 SQSTM1 is not involved in the interaction between KAT2A and LC3.

HEK293 cells were transfected with KAT2A-GFP or KAT2AΔ3-GFP plasmid for 48 h, and the interaction between KAT2A and LC3 was analyzed by immunoprecipitation (IP) and western blot (WB).

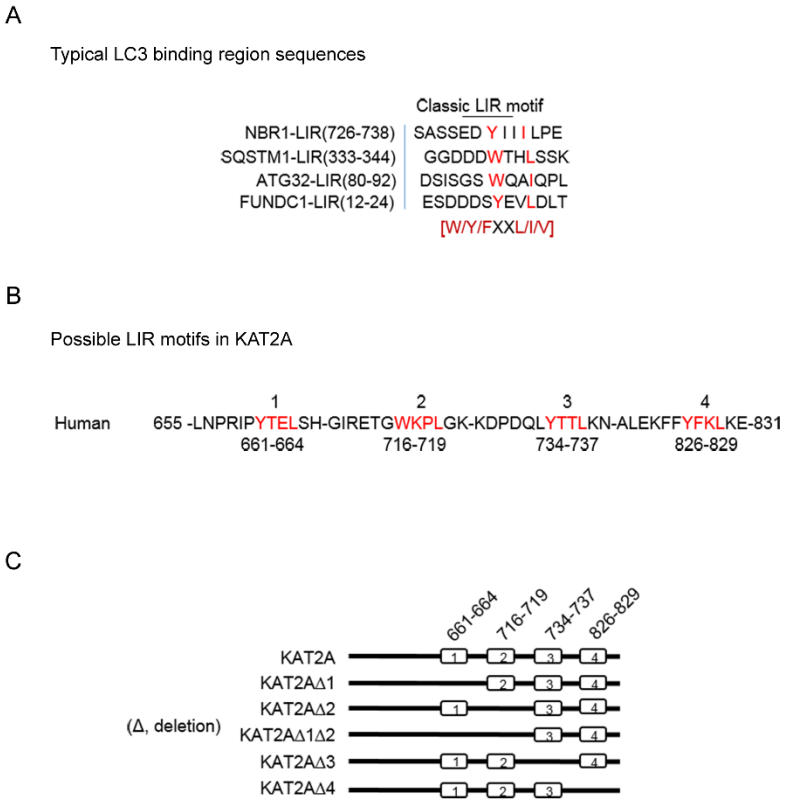

Figure 2.7 Analysis of LC3 binding region (LIR) in KAT2A and KAT2A truncation variants.

(A) Typical LC3 binding region sequences (W/F/YxxL/I/V) in known autophagy substrates are shown. (B) Sequence alignment of KAT2A with candidate LIR domains depicted in red. (C) Illustration of the different KAT2A truncation variants.

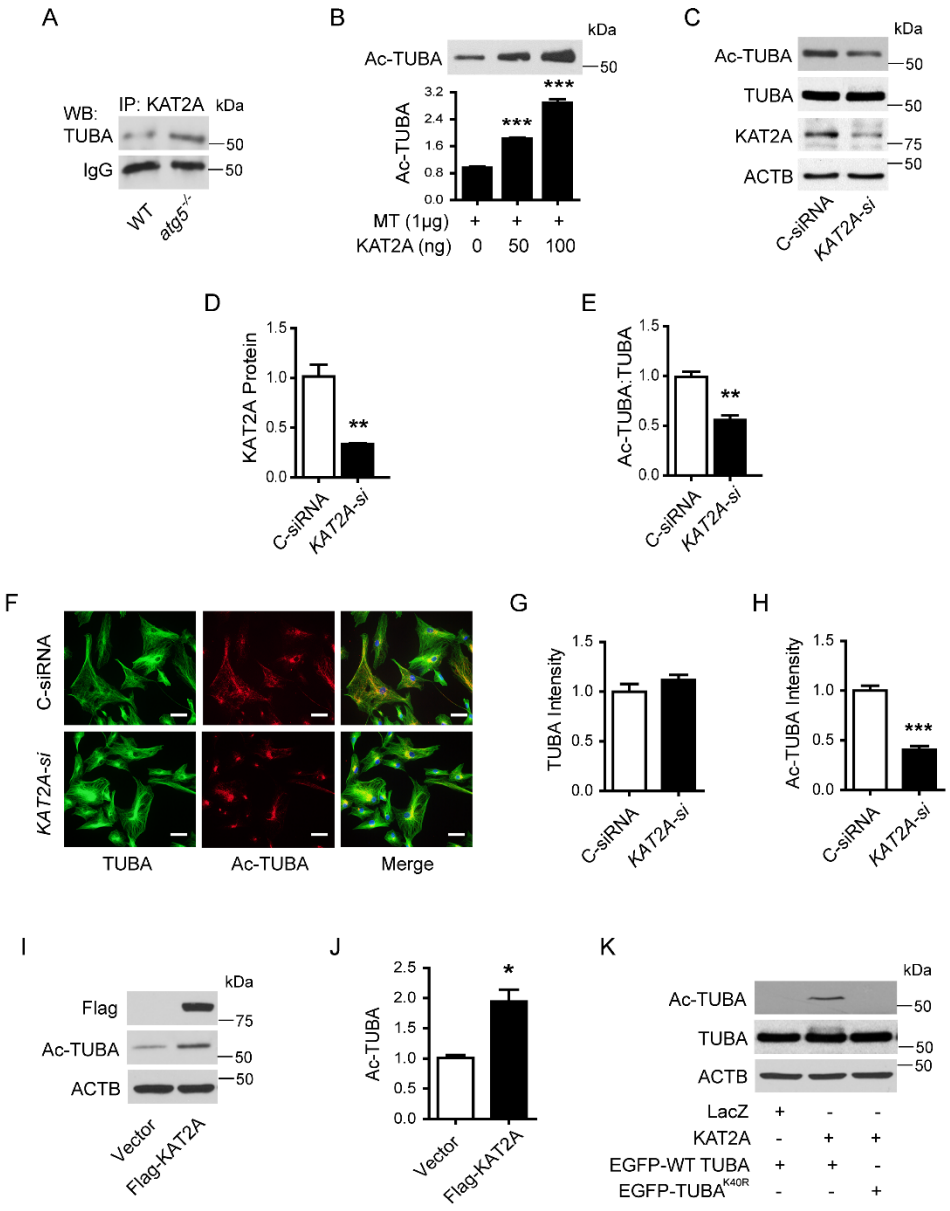

Figure 2.8 KAT2A acetylates TUBA.

(A) The interaction of KAT2A and TUBA in *atg5*$^{-/-}$ MEFs was determined by immunoprecipitation and western blotting. (B) Purified porcine brain tubulin protein was incubated with recombinant KAT2A-catalytic domain protein in acetylation buffer at 37°C for 1 h. The acetylation of TUBA (Ac-tubulin) was assessed by western blotting. n=3, ***P<0.001. (C-E) HASMCs were transfected with control siRNA (C-siRNA) or *KAT2A* siRNA (*KAT2A*-si). Expression of KAT2A and acetylation of TUBA were examined

by western blot and densitometry. n=3, $^{**}P<0.01$. (F-H) HASMCs were transfected with control siRNA (C-siRNA) or *KAT2A* siRNA (*KAT2A*-si). Acetylation of TUBA was analyzed by immunofluorescence. Scale bar, 50 μm. n= 3, $^{***}P<0.001$. (I and J) HEK 293 cells were transfected with a plasmid encoding Flag-KAT2A for 48 h. Acetylation of TUBA was assayed by western blotting and densitometry. n=3, $^{*}P<0.01$. (K) HEK293 cells were co-transfected with plasmid encoding LacZ, KAT2A, EGFP-WT-TUBA, or EGFP-TUBA^{K40R} for 48 h. Acetylation of TUBA was examined by western blotting.

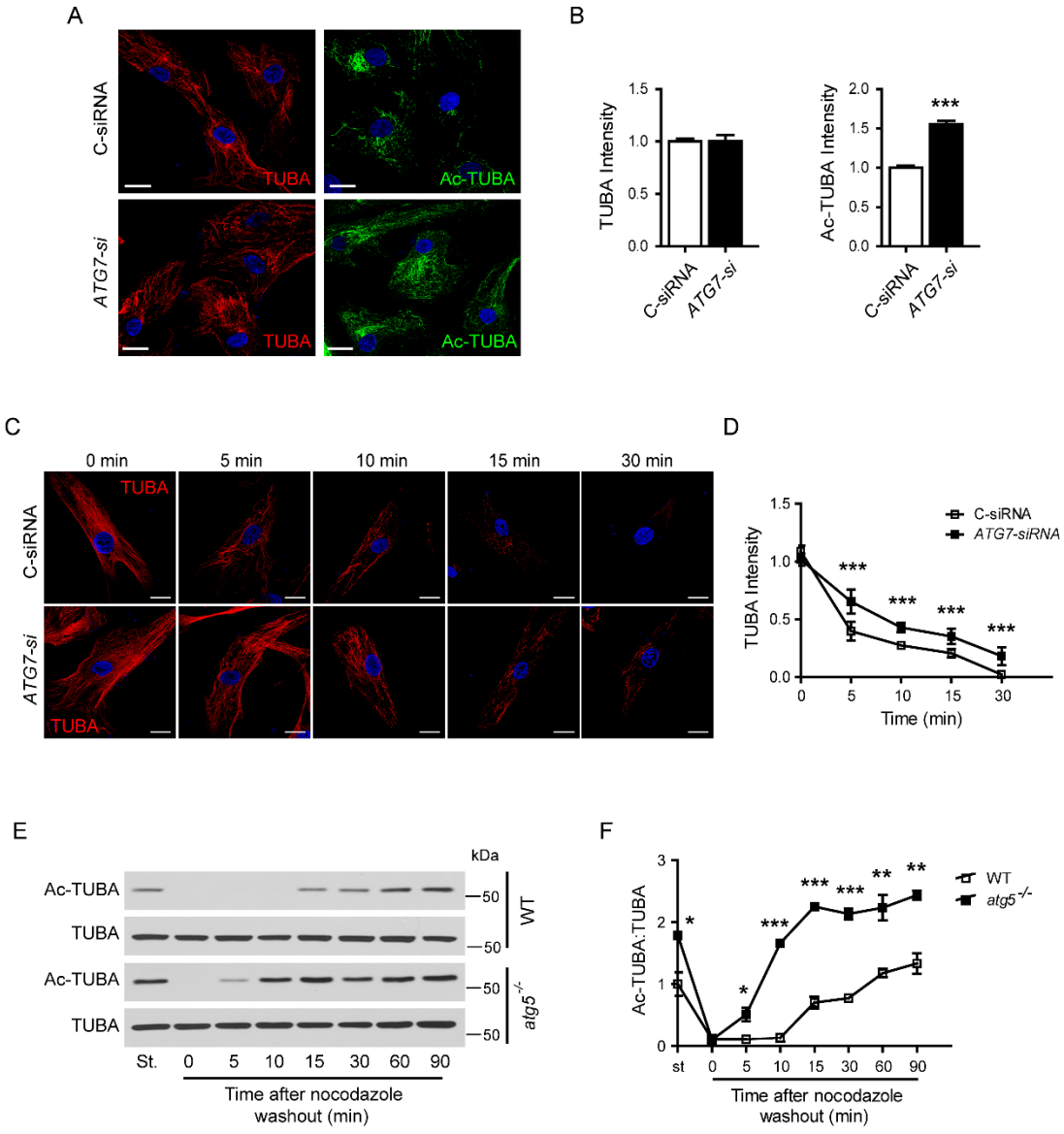

Figure 2.9 Autophagy deficiency increases microtubule stability.

(A) HASMCs were transfected with control siRNA (C-siRNA) or *ATG7* siRNA (*ATG7*-si) for 48 h. TUBA and Ac-TUBA was stained by immunocytochemistry. Scale bar, 20 μm. (B) Quantitative analysis of TUBA and Ac-TUBA intensity. n=3, ***P<0.001. (C) HASMCs transfected with C-siRNA or *ATG7*-si were incubated at 0ºC for 0, 5, 10, 15, or 30 min. The morphology of microtubules was examined using immunostaining of TUBA and confocal microscope. Scale bar, 20 μm. (D) Quantitative analysis of microtubule intensity. n=25/group, ***P<0.001. (E) WT and *atg5*$^{-/-}$ MEFs were treated with nocodazole

for 30 min, and then the drug was washed out to allow the microtubules to repolymerize for the indicated times. Acetylation of TUBA (Ac-TUBA) in cell lysates were analyzed by western blot. St, steady-state situation without nocodazole treatment. (F) Densitometry analysis of acetylation of TUBA levels. n=3, **P*<0.05, ***P*<0.01, ****P*<0.001.

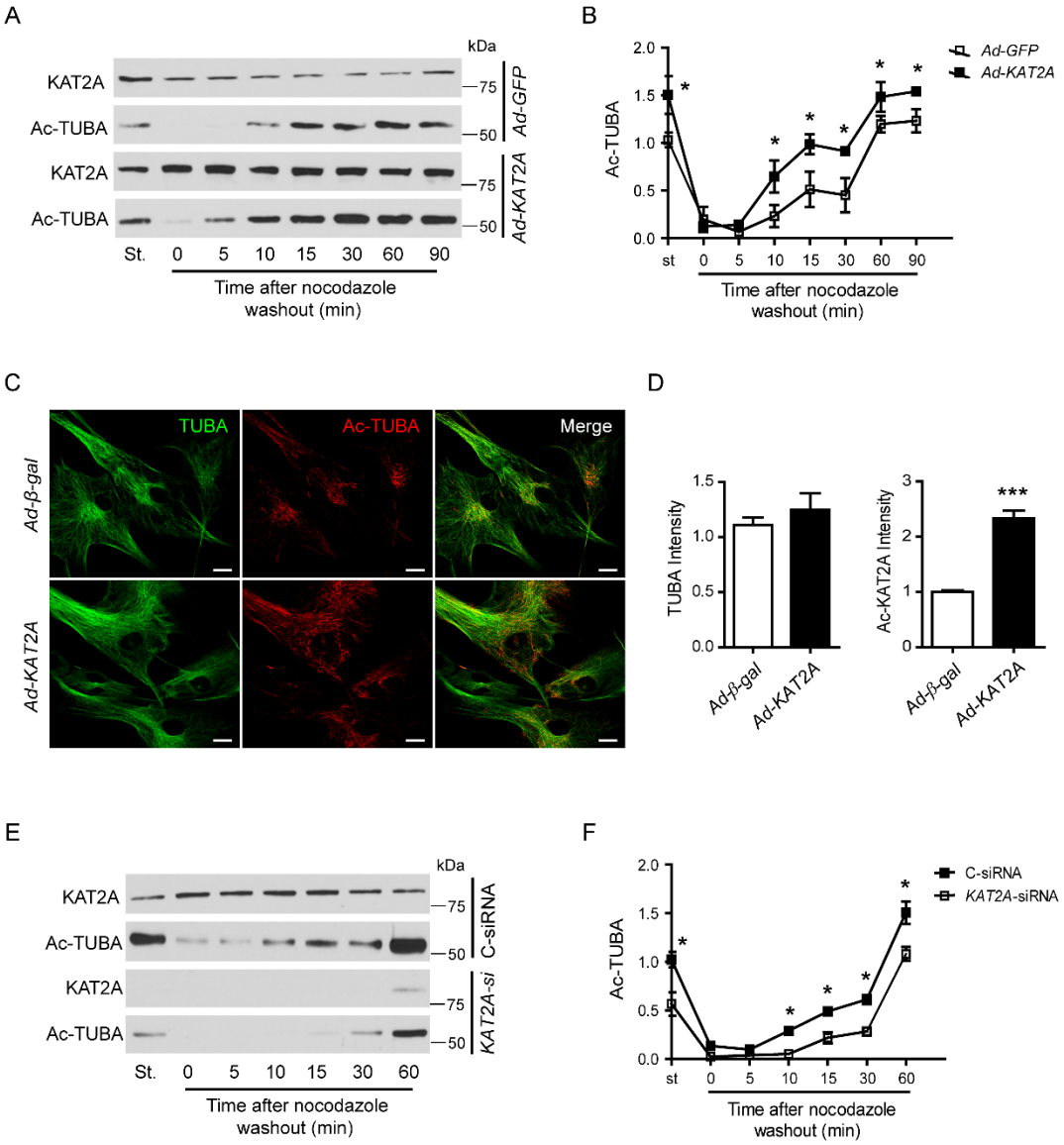

Figure 2.10 KAT2A-mediated acetylation of TUBA increases microtubule reassembly.

(A) HASMCs were transfected with adenovirus encoding GFP and KAT2A. Cells were treated with nocodazole for 30 min, and then the drug was washed out to allow the microtubules to repolymerize for the indicated times. Cell lysates were analyzed by western blot. St, steady-state situation without nocodazole treatment. (B) Densitometry analysis of acetylated TUBA level. n=3, **P*<0.05. (C) HASMCs were transfected with adenovirus encoding β-gal or KAT2A for 48 h, and acetylation of TUBA was measured using immunofluorescence. Scale bar, 20 μm. (D) Quantitative analysis of TUBA and Ac-

TUBA intensity. n=3, ***P<0.001. (E) HASMCs were transfected with control siRNA (C-siRNA) or *KAT2A*-siRNA (*KAT2A*-si), and cells were subjected to the nocodazole-washout assay as described. (F) Densitometry analysis of acetylated TUBA levels. n=3, *P<0.05.

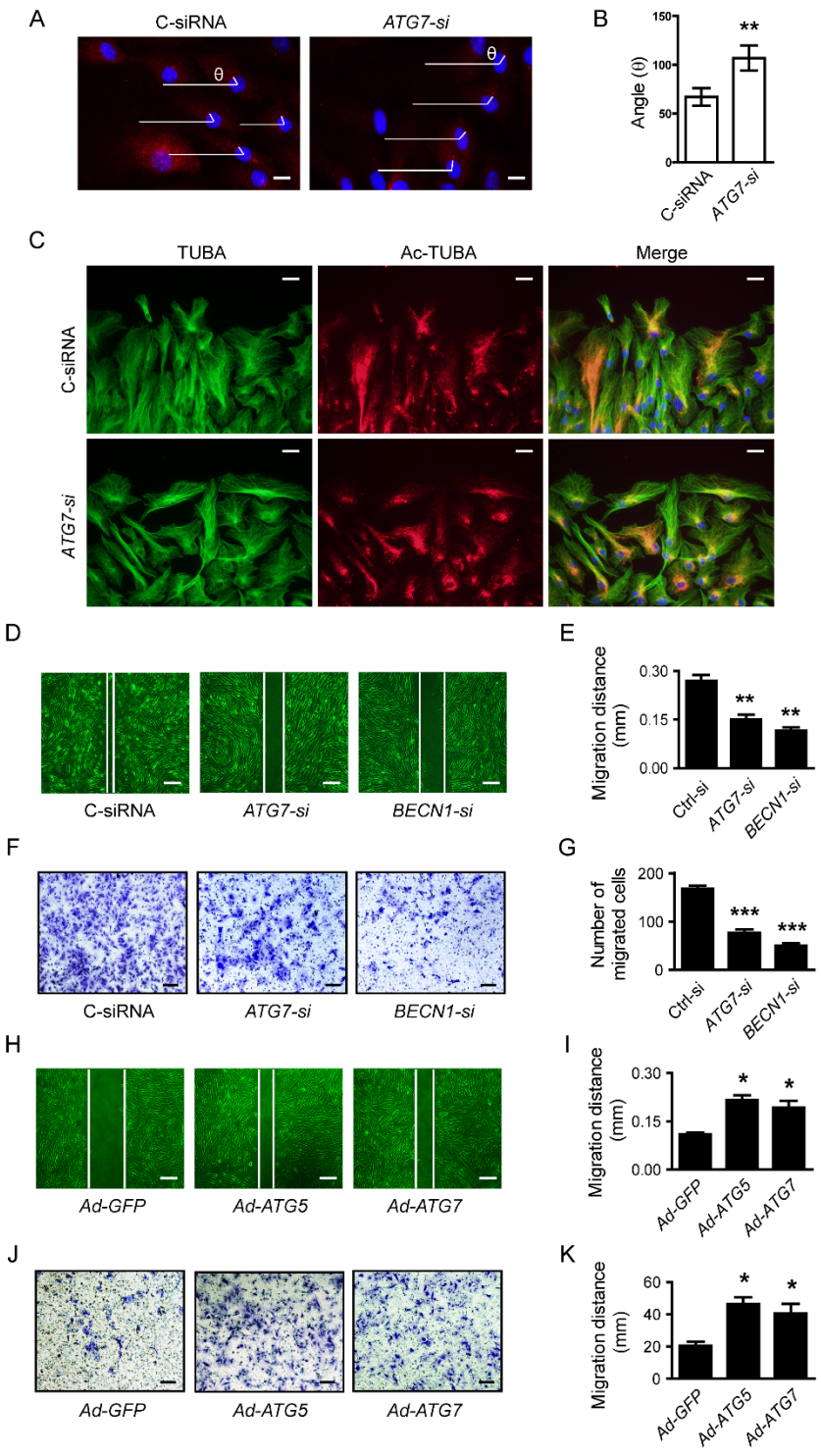

Figure 2.11 Autophagy is required for polarization and directional migration of VSMCs in vitro.

(A) Representative images of HASMCs stained with TUBG antibody in cells subjected to a scratch wound assay. The cells were treated with control siRNA or *ATG7* siRNA for 48 h, and the images were

captured 6 h after the scratch. Scale bar, 20 μm. The cell polarization was assessed by the angles (θ) between the lines of TUBG and the scratched line at the center of each nucleus as a marker for microtubule-organizing center (MTOC) reorientation. (B) Quantitation of the angles (θ). n=100, **P*<0.01 vs. C-siRNA. (C) Images of HASMC stained with TUBA (green) and Ac-TUBA (red) antibodies in cells subjected to the scratch wound assay. Nuclei were stained with DAPI (blue). The cells were transfected with control siRNA or *ATG7* siRNA. Scale bar, 50 μm. (D-G) HASMCs were transfected with control siRNA (C-siRNA), *ATG7* siRNA (*ATG7*-si), or *BECN1* siRNA (*BECN1*-si) for 48 h. (D) Representative images of HASMC migration in the scratch wound assay. Scale bar, 1 mm. (E) Migration distances of HASMCs. n=4, ***P*<0.01 vs. C-siRNA. (F) Cell migration was determined by transwell migration assays. Scale bar, 1 mm. (G) Migrated cells were quantified. n=5, ****P*<0.001 vs. C-siRNA. (H-K) HASMCs were transfected with adenovirus encoding GFP, ATG5, or ATG7 for 48 h. (H) Representative images of HASMC migration in the scratch wound assay. Scale bar, 1 mm. (I) Migration distances of HASMCs. n=4, **P*<0.05 vs. C-siRNA. (J) Cell migration was determined by transwell migration assays. Scale bar, 1 mm. (K) Migrated cells were quantified. n=4, **P*<0.05 vs. C-siRNA.

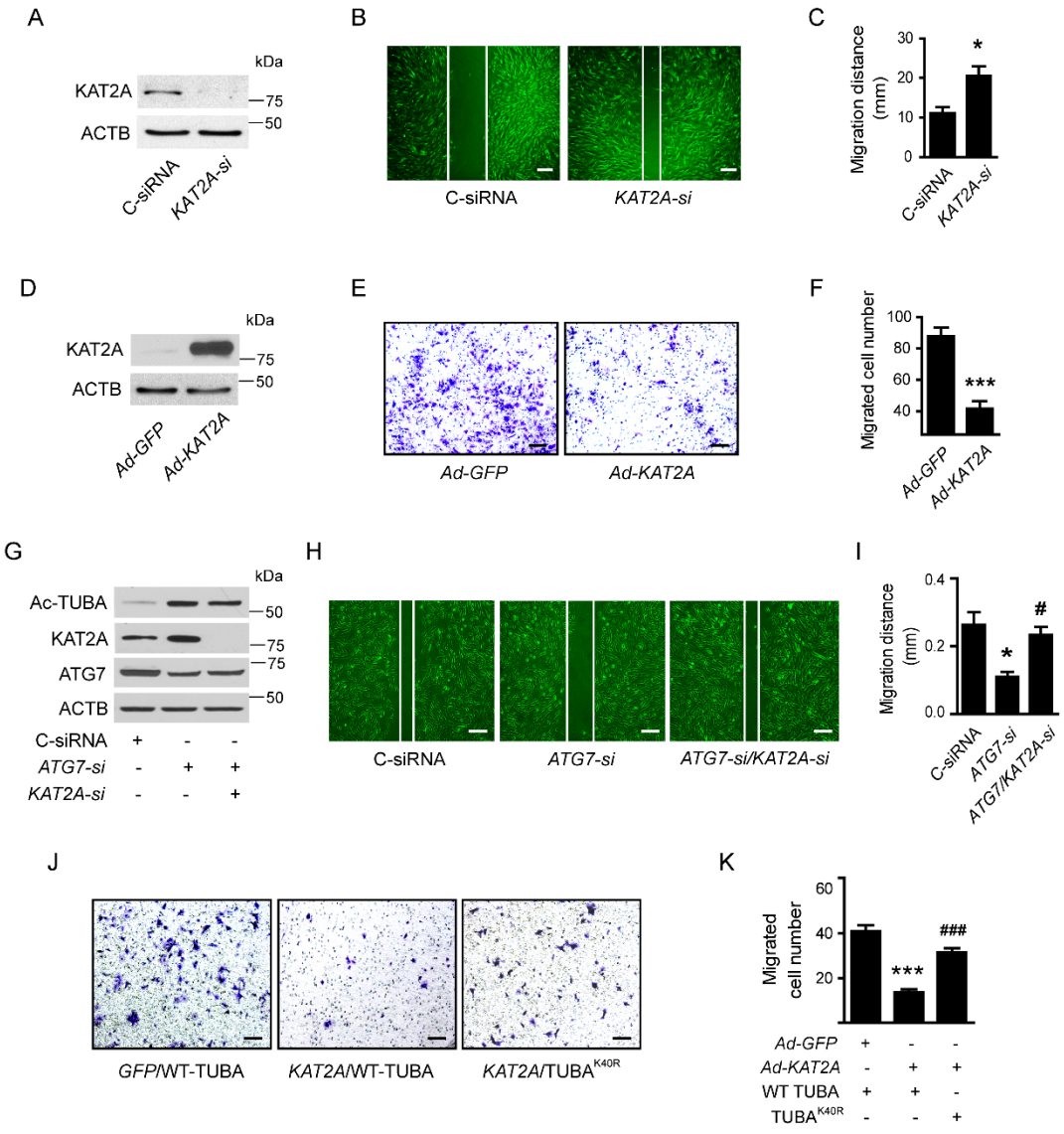

Figure 2.12 KAT2A inhibits VSMC migration by acetylating TUBA.

(A-C) HASMCs were transfected with control siRNA (C-siRNA) or *KAT2A*-siRNA (*KAT2A*-si) for 48 h. (A) KAT2A levels were analyzed by western blot. (B) Representative images of HASMC migration in the scratch wound assay. Scale bar, 1 mm. (C) Migration distances of HASMCs. n=4, * P<0.05 vs. C-siRNA. (D-F) HASMCs were transfected with *Ad-GFP* or *Ad-KAT2A* for 48 h. (D) Levels of KAT2A were analyzed by western blotting. (E) Cell migration was determined by transwell migration assays. Scale bar, 1 mm. (F) Migrated cells were quantified. n=5, *P<0.05 vs. C-siRNA. (G-I) HASMCs were transfected

with control siRNA (C-siRNA), *ATG7* siRNA, or *ATG7* and *KAT2A* siRNA for 48 h. (G) Levels of acetylated TUBA (Ac-TUBA), KAT2A, and ATG7 in cell lysates were measured by western blotting. (H) Representative images of HASMC migration in the scratch wound assay. Scale bar, 1 mm. (I) Migration distances of HASMCs. n=3, **P*<0.05 vs. C-siRNA. $^{\#}$*P*<0.05 vs. *ATG7*-siRNA. (J) HASMCs were co-transfected with *Ad-GFP*/WT TUBA, *Ad-KAT2A*/WT TUBA, or *Ad-KAT2A*/TUBA^{K40R} mutant for 48 h. Cell migration was determined by transwell migration assays. Scale bar, 1 mm. (K) Migrated cells were quantified. n=5, ****P*<0.001 vs. *Ad-GFP*/WT TUBA; $^{\#\#\#}$*P*<0.001 vs. *Ad-KAT2A*/WT TUBA.

3 BRD4 inhibition by JQ1 prevents high-fat diet-induced diabetic cardiomyopathy by activating PINK1/Parkin-mediated mitophagy *in vivo*

Jing Mu[1,2], Donghong Zhang[2], Yunli Tian[2], Zhonglin Xie[2]*, Ming-hui Zou[1,2]*

[1]Department of Chemistry, [2]Center for Molecular and Translational Medicine,

Georgia State University, Atlanta, GA, 30303

*Address correspondence to:

Ming-Hui Zou, MD PhD, Phone: 404-413-6637, Fax: 404-413-3580, E-mail: mzou@gsu.edu

or

Zhonglin Xie, MD PhD, Phone: 404-413-6639, Fax: 404-413-3580, E-mail: zxie@gsu.edu

Mu J, *et al.* J Mol Cell Cardiol. 2020 Sep 15; 149:1-14.

3.1 Abstract

BRD4 is a member of the BET family of epigenetic regulators. Inhibition of BRD4 by the selective bromodomain inhibitor JQ1, alleviates thoracic aortic constriction-induced cardiac hypertrophy and heart failure. However, whether BRD4 inhibition by JQ1 has therapeutic effect on diabetic cardiomyopathy, a major cause of heart failure in patients with Type 2 diabetes, remains unknown. Here, we discover a novel link between BRD4 and PINK1/Parkin-mediated mitophagy during diabetic cardiomyopathy. Upregulation of BRD4 in diabetic mouse hearts inhibits PINK1/Parkin-mediated mitophagy, resulting in accumulation of damaged mitochondria and subsequent impairment of cardiac structure and function. BRD4 inhibition by JQ1 improves mitochondrial function, and repairs the cardiac structure and function of the diabetic heart. These effects depended on rewiring of the BRD4-driven transcription and repression of PINK1. Deletion of *Pink1* suppresses mitophagy, exacerbates cardiomyopathy, and abrogates the therapeutic effect of JQ1 on diabetic cardiomyopathy. Our results illustrate a valid therapeutic strategy for treating diabetic cardiomyopathy by inhibition of BRD4.

3.2 Introduction

Diabetes affects 30.3 million people in the United States (9.4% of the population) and more than 347 million people worldwide. Type 2 diabetes is the most common form of diabetes, affecting 90% to 95% of all patients with diabetes. Diabetic cardiomyopathy is a major cause of heart failure in patients with Type 2 diabetes (1). Although multiple factors may collectively contribute to the development of diabetic cardiomyopathy, the exact mechanisms underlying this pathological process are poorly understood.

Autophagy is an intracellular catabolic pathway by which long-lived proteins and organelles are delivered to lysosomes for degradation. Autophagy is controlled by autophagy-

related genes (Atgs) and is critical for cardiac homeostasis (2). Increasing evidence demonstrates that autophagy is inhibited in the cardiac tissue of Type 1 (3,4) and Type 2 (5-8) diabetic mouse models and contributes to the development of diabetic cardiomyopathy. Mitophagy is a specific type of autophagy that specifically degrades impaired mitochondria (9). In addition to core autophagic machinery components, mitophagy exploits a variety of molecules to identify and eliminate damaged or superfluous mitochondria (10). PTEN-induced putative kinase protein 1 (PINK1) and the Parkin pathway, which activates mitophagy in an ubiquitination-dependent manner, is the most well studied mitophagy pathway (11). Bromodomain-containing protein 4 (BRD4) belongs to bromodomain and extra-terminal domain (BET) family of proteins. It binds to acetylated histones and transcription factors through its bromodomains and recruits transcriptional regulators (12). JQ1, one of the BET bromodomain inhibitors, has therapeutic effect on different diseases (13-15). In the cardiovascular system, administration of JQ1 attenuates pulmonary arterial hypertension (16), angiotensin II-induced hypertension (17), abdominal aortic aneurysm (18), transverse aortic constriction-induced cardiac hypertrophy, and heart failure (19,20) in animal models. Furthermore, a recent study showed that administration of JQ1 prevents high glucose-induced hypertrophy and fibrosis-associated gene expression in H9c2 cardiomyoblast cells (21). Collectively, these data suggest the involvement of BET family proteins in cardiovascular diseases. However, the role of BRD4 in the development of cardiomyopathy in Type 2 diabetes remains unknown.

Here we report that cardiac BRD4 is upregulated in high-fat diet (HFD)-induced diabetic cardiomyopathy and inhibits PINK1/Parkin-mediated mitophagy, which impairs mitochondria and cardiac structure and function. BRD4 inhibition with JQ1 restores PINK1/Parkin-mediated mitophagy and prevents HFD-induced diabetic cardiomyopathy.

3.3 Materials and methods

3.3.1 Mouse models and JQ1 treatment

Wild-type (WT, *C57BL/6J*, stock number 000664) and *Pink1-/-* mice (B6.129S4 *Pink1*^{tm1Shn}/J, stock number 017946) were purchased from Jackson Laboratories. 2-month-old male mice were subjected to ND (normal diet) or HFD (Research Diets D12492) consumption for 6 months. To determine if PINK1 mediates the therapeutic effect of JQ1, we divided male WT and *Pink1-/-* mice into four groups: ND + DMSO, ND + JQ1, HFD + DMSO, and HFD + JQ1. JQ1 (MedChem Express) and vehicle preparation were described previously (19). In the last month of ND or HFD treatment, WT and *Pink1-/-* mice were treated intraperitoneally with DMSO or JQ1 (10 mg/kg/day). Body weights were recorded daily. All animal protocols were approved by the Institutional Animal Care and Use Committee of Georgia State University.

3.3.2 Comprehensive metabolic monitoring

Mice were analyzed for whole energy expenditure, oxygen consumption, carbon dioxide production, and respiratory exchange ratio (vCO2/vO2) using calorimetric systems (PhenoMaster, TSE Systems, Bad Homburg, Germany). Mice were individually housed and acclimated to chambers for 3 days before experimental measurements and allowed free access to food and water.

3.3.3 Echocardiography

Echocardiography was performed using a Vevo 3100 High-Resolution Micro-Ultrasound System (FUJIFILM Visual Sonics Inc., Toronto, Canada) as previously described (22). M-mode tracings were used to measure LV wall thickness, LV end-systolic diameter, and LV end-diastolic diameter. FS and EF were calculated from LV dimensions in the 2D short-axis view. Diastolic function was measured using tissue Doppler imaging and color Doppler imaging.

Tissue Doppler was used to measure the peak myocardial relaxation velocity at the mitral valve annulus during early diastole and early filling deceleration time. Color Doppler was used to obtain a sharper signal from the early ventricular filling peak velocity (E wave) and late filling velocity (A wave). All examinations were analyzed using Vevo Lab 2.1.0 software.

3.3.4 Cell culture and treatment

Mouse neonatal cardiomyocytes were isolated from *C57BL/6J* mice using an adapted protocol from the Pierce Primary Cardiomyocyte Isolation Kit (#88281, Thermo Fisher Scientific). Briefly, neonatal mouse hearts were freshly dissected and incubated with Cardiomyocyte Isolation Enzyme 1 and Enzyme 2 at 37°C for 30-35 minutes. Then, the tissue was disrupted in complete DMEM with cardiomyocyte growth supplement. Total cell yield was determined using a TC20™ Automated Cell Counter (Bio-Rad Laboratories) and cell viability was determined using a trypan blue exclusion assay. Isolated neonatal cardiomyocytes were then plated on dishes and incubated at 37°C in 5% CO_2 for further experiments.

Palmitate (PA) was prepared as a PA-BSA conjugate. Mouse neonatal cardiomyocytes were treated with 200 μM of PA for 48 hours or 500 nM of JQ1 for 24 hours. Control groups were treated with bovine serum albumin (BSA) or DMSO.

3.3.5 Quantification of lysosomal-mitochondrial interactions

Mouse neonatal cardiomyocytes were treated with JQ1 or DMSO in the present of BSA or PA for 48h, labeled with LysoTracker™ Deep Red (#12492, ThermoFisher Scientific) and MitoTracker® Green FM (#7514, Thermo Fisher Scientific) for 30 min at 37°C, and subjected to confocal microscopy (LSM800, Carl Zeiss Microscopy). Manders' Correlation Coefficient was calculated using Image J software (National Institute of Health).

3.3.6 Immunofluorescence

Mid-ventricles were fixed in phosphate buffered saline (PBS)/4% paraformaldehyde and embedded in paraffin. 4 μm-thick sections were subjected to xylene and alcohol for dehydration. Then, the slides were subjected to antigen retrieval using citrate buffer, permeabilized with 0.2% Triton X-100 and blocked with 5% normal goat serum (BioGenex, Fremont, CA). Or OCT embedded mid-ventricles were sliced to 6 μm-thick sections. The slides were rinsed with ddH_2O and fixed in ice-cold acetone for 10 minutes. Then, the slides were permeabilized with 0.2% Triton X-100 and blocked with 5% normal goat serum. For primary antibodies, slides were incubated with rabbit anti-BRD4 (Abcam, 1:100 dilution) and mouse anti-cardiac troponin T (ThermoFisher Scientific, 1:1000 dilution) at 4°C overnight. Or slides were incubated with rabbit anti-LC3A/B (CST, 1:100 dilution) and mouse anti-ATP5A1 (proteintech, 1:200 dilution) at 4°C overnight. Alexa Fluor 555 goat anti-rabbit and 488 goat anti-mouse IgG (Invitrogen, 1:200 dilution) were used as secondary antibodies, incubated at RT for 1 hour. Cell nuclei were stained with 4′, 6-diamidino-2-phenylindole (DAPI, Sigma). Samples were mounted with VectaMount™ AQ (#5501, Vector Laboratories) for fluorescence microscopy.

3.3.7 Histological analysis

Heart sections from the mid-ventricle were fixed in paraformaldehyde and embedded in paraffin; morphology was determined by H&E staining. Cardiomyocyte cross-sectional area was determined by staining with rhodamine-conjugated wheat germ agglutinin (Vector Laboratories RL-1022). Oil red O staining was performed to determined lipid accumulation. Fibrosis was visualized using a Picro-Sirius Red Stain Kit (#ab150681, Abcam). Terminal deoxynucleotidyl transferase dUTP nick-end label (TUNEL) staining was performed in wax sections of the left ventricle using TUNEL Enzyme and TUNEL Label Mix (Roche, 11767305001; 11767291910).

Cardiomyocyte cross-sectional area, lipid area, and fibrosis area were calculated using Image J software (National Institute of Health).

3.3.8 Mouse heart mitochondrial isolation

Adult mouse cardiac mitochondria was isolated using Mitochondrial Isolation Kits (#ab110168, abcam). All procedures followed manufacturer instructions. Briefly, freshly isolated left ventricle heart tissue was washed with pre-chilled washing buffer, and minced in pre-chilled isolation buffer. After spinning down at 1,000g, supernatant was transferred to a new tube. After a second spinning down at 12,000g, supernatant containing cytosol protein was collected. Then the pellet containing mitochondria was washed in isolation buffer supplemented with protease inhibitor cocktail (#7012, CST), and was collected for further use after spinning down at 12,000g.

3.3.9 Measurement of mitochondrial OCR

Mitochondrial OCR was determined using an XFᵉ96 extracellular flux analyzer (Seahorse Biosciences) following the manufacturer's instructions. All analyses were reported using the XF Cell Mito Stress Test Report Generator. Coupling Assay and Electron Transport Assay were performed in isolated mitochondria from adult mouse hearts according to the published protocol (23).

3.3.10 Flow cytometry

Mitochondrial ROS level was determined using MitoSOX™ Red (5 μM, M36008, ThermoFisher Scientific) as previously described (24). Briefly, mouse neonatal cardiomyocytes were incubated with the probe in analysis buffer (HBSS containing calcium and Magnesium), and cells were washed, trypsinized, and collected. Isolated mitochondria from adult mouse hearts were incubated with the probe and washed with analysis buffer as previously described (24).

Then, levels of mitochondrial ROS was measured using a Fortessa Flow Cytometer (BD Bioscience). A minimum of 10,000 events was collected for each sample. Quantitative analysis of the data was determined using *FlowJo* (v10) software.

3.3.11 Transmission electron microscopy (TEM)

Mouse heart samples were removed and fixed with 2.5% glutaraldehyde in 0.1 M cacodylate buffer (pH 7.4). Heart samples were then rinsed with 0.1 M cacodylate buffer (pH 7.4) twice before post-fixation in 1% osmium tetroxide for 1 hour. After additional buffer rinses, heart samples were dehydrated through an ethanol series to 100% ethanol, infiltrated with a mixture of 100% propylene oxide and Eponate 12 resin (Ted Pella Inc., Redding, CA), followed by pure Eponate 12 resin overnight. Heart samples were embedded in beem capsules and placed in a 60°C oven for polymerization. Ultrathin sections were cut on a Leica UltraCut microtome at 70-80 nm and placed on 200 mesh copper grids. Sections were then stained with 5% uranyl acetate for 15 minutes followed by 2% lead citrate for 15 minutes. Samples were imaged with a JEOL JEM-1400 transmission electron microscope (Tokyo, Japan) equipped with a Gatan US1000 CCD camera (Pleasanton, CA). Mitochondrial mass and lipid content were measured using Image J software (National Institute of Health).

3.3.12 Western blotting

Mouse tissues and cultured cardiomyocytes were homogenized using ice cold RIPA lysis buffer (#sc-24948, Santa Cruz Biotechnology). Protein contents were measured using the Bradford assay (#23225, Pierce Biotechnology). Detailed steps for western blotting were described previously (25). Primary antibodies information was shown in Table 3.1.

3.3.13 Quantitative real-time PCR

Total RNA was extracted from cultured cardiomyocytes or mouse hearts using the RNeasy Mini Kit (#74106, QIAGEN) or TRIzol according to the manufacturer's instructions. cDNA was synthesized using the iScript™ cDNA Synthesis Kit (#170-8891, Bio-Rad Laboratories). All samples were run in triplicate and underwent initial denaturation at 95°C for 5 min, followed by 40 rounds of amplification (95°C for 30 s, 60°C for 30 s) using iQ™ SYBR® Green Supermix (#720001059, Bio-Rad Laboratories) and the CFX96™ Real-Time System (Bio-Rad Laboratories). All data were analyzed using the $2^{-\Delta\Delta CT}$ method as previously described (26). Primers information was shown in Table 3.2.

3.3.14 ChIP-qPCR

ChIP-qPCR was performed with the SimpleChIP® Enzymatic Chromatin IP Kit (# 9003, CST) following the manufacturer's instructions. As previously described (27,28), mouse whole heart tissues from indicated treatment groups were homogenized and crosslinked with 1% formaldehyde and quenched with glycine. Then, nucleus samples were isolated and sonicated into 100-500 bp DNA fragments. Lysates in each chromatin solution then underwent immunoprecipitation with 5 μg of antibody, including anti-Brd4 (A301-985A100, BETHYL Laboratories, Inc.), anti-H3K27ac (8173S, CST), or anti-IgG (171870, Abcam) overnight at 4°C. The immunoprecipitated DNA samples were reversed crosslinked, purified, and amplified by quantitative PCR with specific primers designed to amplify the *Pink1* promoter region (forward: 5'-GGACCGCTACCGCTTCTTC-3'; reverse: 5'- CTTCCGCCTGCTTCTCCTC-3'). The enrichment of *Pink1* gene DNA fragments was normalized against total genomic DNA input.

3.3.15 Statistical analysis

All values are presented as mean ± SEM. Differences between experimental groups were determined by one-way or two-way ANOVA, followed by the Tukey post hoc test, as appropriate. Student *t*-tests were performed for single comparisons between groups. $P < 0.05$ was considered statistically significant.

3.4 Results

3.4.1 Increased BRD4 protein in HFD-induced Type 2 diabetic cardiomyopathy

We fed 2-month-old WT mice a ND or a HFD for 6 months to build Type 2 diabetic cardiomyopathy mouse model. To address the relationship between BET family proteins and diabetic cardiomyopathy, we first examined mRNA levels of *Brd2*, *Brd3*, and *Brd4* in adult mouse hearts and mouse neonatal cardiomyocytes (**Fig. 3.1A and B**), and found that *Brd4* expression was most abundant in cardiomyocytes. Then we examined BRD2, BRD3, and BRD4 protein expression in HFD-induced Type 2 diabetic mouse hearts. Compared with ND-fed mice, HFD-fed mice exhibited a significantly higher BRD4 level and normal BRD2 and BRD3 protein levels (**Fig. 3.2A and B**). However, HFD feeding did not increase *Brd4* mRNA expression (**Fig. 3.1C**). Finally, co-staining of BRD4 and the cardiomyocyte marker cardiac troponin T indicated that the increase in BRD4 expression mainly occurred in cardiomyocytes (**Fig. 3.2C and D**). Collectively, these results suggest a potential role for BRD4 in the development of diabetic cardiomyopathy.

3.4.2 Suppression of PINK1/Parkin-mediated mitophagy in diabetic cardiomyopathy

Next, we investigated the effects of HFD-feeding on the process of autophagy/mitophagy. We found that HFD feeding reduced PINK1 protein levels but had no effect on Parkin protein expression (**Fig. 3.2E-G**). Since cells possess several mitophagy

mechanisms, we further examined expression of mitophagy receptors and other proteins regulating mitophagy and found that HFD exposure did not alter expression of these proteins (**Fig. 3.3A and B**). Moreover, mitochondria can also be cleared through general autophagy pathway. Therefore, we investigated the effects of HFD-feeding on this process (**Fig. 3.3C-F**). We found the inhibition of autophagic flux in HFD-fed mice was likely due to blockage of lysosomal degradation of cargos, but not to autophagy initiation. Taken together, we reasoned that an accumulation of dysfunctional mitochondria may occurred in HFD-fed mouse heart.

As shown in **Figure 3.2H to J**, protein levels of translocase of the inner membrane 23 (TIM23) and voltage-dependent anion channel 1 (VDAC1) were markedly increased in the hearts of mice fed a HFD. Despite the increase in mitochondrial content, peroxisome proliferator-activated receptor γ coactivator-1α (PGC-1α) and mitochondrial transcription factor A (Tfam), two important molecules regulating mitochondrial biogenesis were decreased in hearts from mice fed a HFD (**Fig. 3.3G and H).** Since mitochondrial content homeostasis is dependent on the generation of new and the removal of damaged or unwanted mitochondria, our results suggested the increase in mitochondrial proteins in HFD-fed hearts is due to impairment of the ability of cardiomyocytes to remove damaged mitochondria. Then, we characterized mitochondrial function using Seahorse XF96 metabolic flux analyzer by directly isolating mitochondria from hearts of mice fed a ND or HFD. A significant reduction in State 3 and State 3_u oxygen consumption rate (OCR) were observed between HFD-fed and ND-fed mice (**Fig. 3.2K and L**). OCR decreased dramatically in State 3_u, but not State 4_0, suggesting a decreased mitochondrial respiratory control ratio (RCR) (State 3_u/State 4_0) in HFD-fed mice hearts (**Fig. 3.2M**). These data suggest that HFD feeding inhibits PINK1/Parkin-dependent mitophagy, leading to the accumulation of dysfunctional mitochondria in the hearts of diabetic mice.

3.4.3 Knockout of Pink1 worsens HFD-induced diabetic cardiomyopathy in mice

Given that a HFD induces diabetic cardiomyopathy and concurrently suppresses PINK1/Parkin-mediated mitophagy, we examined the effect of *Pink1* deficiency on the development of diabetic cardiomyopathy *in vivo*. After 4 months of HFD feeding, *Pink1-/-* mice developed diastolic dysfunction, indicated by reduced E/A-wave ratio (E-wave and A-wave represent LV early filling and filling from atrial contraction, respectively) (**Fig. 3.4A and B**), increased LV isovolumic relaxation time (IVRT) (**Fig. 3.4C**) and the ratio between early mitral inflow velocity wave (E) and mitral annular early diastolic velocity (E′) (E/E′) (**Fig. 3.5A and B)**. *Pink1-/-* mice also developed profound systolic dysfunction, indicated by reduced ejection fraction (EF) and fractional shortening (FS) (**Fig. 3.4D-F**). However, WT mice exhibited no significant cardiac dysfunction between ND and HFD groups. After 6 months, WT mice developed profound diabetic cardiomyopathy. Deletion of *Pink1* worsened diastolic and systolic dysfunction in both ND and HFD groups relative to those after 4-month HFD feeding (**Fig. 3.4A-F**). In addition, interstitial fibrosis, lipid accumulation, and cell apoptosis were more apparent in *Pink1-/-* mice after 6-month HFD feeding **(Fig. 3.4G-L)**. These data suggest the lack of *Pink1* accelerates and exacerbates HFD-induced cardiomyopathy.

3.4.4 Deletion of Pink1 aggravates the accumulation of dysfunctional mitochondria in the hearts of diabetic mice

We next investigated the influence of *Pink1* loss on mitophagy. We found that mitochondrial makers TIM23 and VDAC1 were markedly increased in HFD-fed WT mice; these increases were significantly aggravated in *Pink1-/-* mice (**Fig. 3.6A-C**). Transmission electron microscope (TEM) revealed that mitochondrial area and lipid droplet area were markedly increased in the hearts of HFD-fed WT mice and were further augmented in *Pink1-/-* mice (**Fig.**

3.6D-F). In addition, mitochondria isolated from the hearts of HFD-fed WT and ND-fed *Pink1-/-* mice exhibited reduced OCR in state 3 and state 3_u, while HFD-fed *Pink1-/-* mice showed a dramatic OCR decrease in all states of respiration (**Fig. 3.6G and H**). Furthermore, HFD-fed WT mice exhibited a reduction in mitochondrial RCR, and this reduction was further decreased in *Pink1-/-* mice (**Fig. 3.6I**). Both HFD consumption and *Pink1* deletion increased mitochondrial ROS production, and HFD-induced ROS overproduction was exacerbated by *Pink1* deletion (**Fig. 3.6J and K**). These data suggest that lack of *Pink1* exacerbates HFD-impaired mitophagy.

3.4.5 Inhibition of BRD4 attenuates HFD-induced cardiomyopathy

Since upregulation of BRD4 is associated with development of diabetic cardiomyopathy, we investigated if BRD4 inhibition prevents diabetic cardiomyopathy. We exposed 2-month-old WT mice to a ND or HFD for 7 months. During the last month, we randomized mice to receive JQ1 (10 mg/kg daily via intraperitoneal injection) or vehicle (DMSO). We found although administration of JQ1 resulted in minor reductions in EF, FS, and E/A ratio in ND-treated mice, JQ1 treatment completely prevented cardiac abnormalities in HFD-fed mice, restoring normal EF, FS, E/A ratio, IVRT, and E/E′ ratio (**Fig. 3.7A-D, Fig. 3.8A-C**). Concurrently, JQ1 treatment ameliorated HFD-induced cardiac hypertrophy (**Fig. 3.7E**), cardiomyocyte cross sectional area (**Fig. 3.7F and G**), interstitial fibrosis (**Fig. 3.7I and J**), lipid accumulation (**Fig. 3.7K and L**), and cardiomyocyte apoptosis (**Fig. 3.7M and N**). We further examined if JQ1 ameliorated cardiomyopathy in Type 2 diabetes by preventing metabolic abnormalities. We found that JQ1 treatment prevented HFD-induced body weight increases, but did not affect mouse body weight in the ND group (**Fig. 3.9A and B**). Moreover, JQ1 treatment did not affect fasting blood glucose (**Fig. 3.7H**) or mouse whole-body energetics, as evidenced by a consistent respiratory

exchange ratio (RER) in the DMSO group (**Fig. 3.9C and D**). Together, these data suggest that BRD4 plays an important role in the pathogenesis of HFD-induced cardiomyopathy.

3.4.6 BRD4 inhibition restores mitophagy and improves mitochondrial function in HFD-fed mice

Next, we investigated if BRD4 inhibition could prevent diabetic cardiomyopathy by activating PINK1/Parkin-mediated mitophagy. We found that JQ1 treatment dramatically increased PINK1 expression in hearts from ND mice and attenuated HFD-induced reduction of PINK1 protein expression, but did not affect expression of BRD4 and Parkin. Concomitantly, JQ1 treatment attenuated the accumulation of mitochondria in HFD-fed mice, as evidenced by comparable levels of TIM23 and VDAC1 in JQ1-treated HFD mice and DMSO-treated ND mice (**Fig. 3.10A-E**). In addition, HFD feeding increased mitochondrial area, which was almost completely prevented by JQ1 treatment. JQ1 also significantly mitigated the increases in lipid droplet size and density in hearts from HFD-fed mice (**Fig. 3.10F-H**). To further investigate mitophagy *in vivo*, we co-stained mitochondria marker ATP synthase subunit alpha mitochondria-like protein (ATP5A1) with autophagosome marker LC3, using frozen section of mouse heart samples. We found HFD feeding decreased the colocalization of ATP5A1 and LC3, while JQ1 treatment elevated the colocalization, suggesting that mitophagy was rescued with JQ1 under HFD consumption (**Fig. 3.11A and B**). We next assessed the respiration capacity of adult mouse cardiac mitochondria, and found that JQ1 treatment significantly attenuated OCR reduction in state 3 and state 3_u induced by HFD feeding (**Fig. 3.10I and J**). It also significantly prevented HFD inhibited RCR (**Fig. 3.10K**). Additionally, compared with ND feeding, HFD exposure markedly increased mitochondrial ROS production, and this increase was abolished by JQ1 treatment (**Fig. 3.10L and M**). Since the clearance of dysfunctional mitochondria can

through both mitophagy and general autophagy pathways (9), we also investigated the effect of JQ1 on general autophagy in mouse heart. As shown in **Figure 3.12A to E**, JQ1 administration increased overall autophagic flux under HFD condition, as evidenced by reducing the accumulation of LC3 II and p62 proteins. Moreover, JQ1 treatment significantly increased LAMP1 protein expression under both ND and HFD condition. Taken together, these results suggest that JQ1 treatment mitigates HFD-induced cardiomyopathy by activating PINK1/Parkin-mediated mitophagy and general autophagy pathways.

We further tested if BRD4 inhibition with JQ1 increased mitophagy in mouse neonatal cardiomyocytes. Consistent with our findings *in vivo*, compared with BSA-treated control cardiomyocytes, PA treatment reduced lysosomal-mitochondrial interactions. In contrast, JQ1 treatment significantly increased the colocalization of lysosome and mitochondria in both BSA- and PA-treated cardiomyocytes (**Fig. 3.13A and B**). We then examined the effect of JQ1 on mitochondrial function and found that PA treatment significantly reduced basal and maximal respiration rate compared with BSA-treated controls. JQ1 treatment also significantly attenuated PA-enhanced maximal respiration rate and reduced proton leak, although it inhibited maximal respiration rate in BSA-treated cardiomyocytes (**Fig. 3.13C and D**). Moreover, PA-enhanced mitochondrial ROS production was completely abolished by JQ1 treatment (**Fig. 3.13E and F**). These results support the notion that the BRD4 inhibitor JQ1 prevents mitophagy suppression and improves mitochondrial function in HFD-fed conditions.

3.4.7 Inhibition of BRD4 association with the Pink1 gene promoter activates PINK1/Parkin- mediated mitophagy

BRD4 is a transcriptional regulator that recruits regulatory complexes to acetylated chromatin (29). We therefore examined whether HFD exposure and JQ1 treatment affect histone

acetylation in the heart. We found that HFD feeding increased histone protein acetylation and this increase was mitigated by JQ1 treatment (**Fig. 3.14A and B**). Interestingly, acetylated histone H3 lysine 27 (H3K27ac), a major site of BRD4 occupancy in the mouse heart (19), was increased in HFD-fed mice and this increase was attenuated by administration of JQ1 (**Fig. 3.14C and D**). Thus, we reasoned that JQ1 regulates *Pink1* gene expression by disrupting association of BRD4 with H3K27ac at the *Pink1* promoter. To test this, we performed chromatin immunoprecipitation coupled with real-time PCR (ChIP-qPCR) using hearts from ND- or HFD-fed and DMSO- or JQ1-treated mice. We observed an enrichment of both BRD4 (**Fig. 3.14E and F**) and H3K27ac (**Fig. 3.14G and H**) at the *Pink1* promoter in HFD-fed mouse hearts and this enrichment was abolished by JQ1 administration.

Next, we examined whether enrichment of BRD4 and H3K27ac at the *Pink1* promoter affects *Pink1* gene expression in cardiac tissues. We found that in the hearts of HFD-fed mice, *Pink1* mRNA expression was significantly reduced. Administration of JQ1 restored normal levels of *Pink1* mRNA in the hearts of HFD-fed mice (**Fig. 3.14I**). Since BRD4 knockdown induces the expression of a subset of autophagy and lysosome genes in KP-4 cells (30), we also studied if BET inhibition by JQ1 could regulate the expression of genes related to autophagy/mitophagy in cultured neonatal cardiomyocytes. PA induced significant decreases in *Map1lc3b* and *Pink1* gene expression. JQ1 treatment markedly upregulated gene expressions of Atgs, including *Map1lc3b*, *Sqstm1*, *Ulk1*, *Lamp1*, *Ctss*, and *Pink1* in both BSA- and PA-treated cells (**Fig. 3.14J**). These data suggest that BRD4 suppresses the expression of *Pink1* gene, as well as genes regulating autophagy and lysosomal function.

To further characterize the mechanisms by which JQ1 regulates mitophagy, we isolated mitochondrial fractions from ND- or HFD-fed and DMSO- or JQ1-treated mouse hearts to

analyze mitochondrial-associated Parkin translocation and downstream mitophagy events. Administration of JQ1 increased mitochondrial localization of PINK1, Parkin, and p62 in BSA-treated cells, and it prevented PA-inhibited mitochondrial localization of PINK1, Parkin, and p62 (**Fig. 3.14K-N**). Moreover, JQ1 treatment dramatically increased mitochondrial protein ubiquitination in both ND- and HFD-fed mouse hearts (**Fig. 3.14O and P**). Taken together, these data suggest that JQ1 inhibition stimulates PINK1/Parkin-mediated mitophagy signaling.

3.4.8 Pink1 deletion abrogates JQ1-alleviated diabetic cardiomyopathy induced by HFD feeding

To establish the essential role of PINK1/Parkin-mediated mitophagy in JQ1-alleviated diabetic cardiomyopathy**,** we fed 2-month-old *Pink1-/-* mice a ND or HFD for 7 months and treated mice with JQ1 or vehicle (DMSO) during the last month combined with HFD feeding. In contrast to the complete abrogation of HFD-induced diastolic and systolic dysfunctions under JQ1 treatment in WT mice, JQ1 treatment failed to restore normal cardiac functions in *Pink1-/-* mice, as evidenced by comparable EF, FS, and E/E′ values in JQ1- and DMSO-treated *Pink1-/-* mice fed a HFD (**Fig. 3.15C and D, Fig. 3.16A-C**); however, administration of JQ1 slightly alleviated HFD-reduced E/A ratio and IVRT values (**Fig. 3.15A and B**). Similarly, JQ1 treatment did not prevent HFD-induced cardiac hypertrophy in *Pink1-/-* mice (**Fig. 3.15E-G**). Next, we assessed the effects of JQ1 on cardiac histopathological features. JQ1 administration significantly attenuated HFD-induced interstitial fibrosis (**Fig. 3.15H and I**), but could not alleviate HFD-induced lipid accumulation and cardiomyocyte apoptosis in *Pink1-/-* mice (**Fig. 3.15J-M**). Taken together, these results support the notion that PINK1/Parkin-mediated mitophagy is an essential mediator for JQ1-induced improvement of diabetic cardiomyopathy.

3.5 Discussion

In this study, we show that aberrant expression of BRD4 suppresses PINK1/Parkin-mediated mitophagy, resulting in accumulation of dysfunctional mitochondria and development of diabetic cardiomyopathy. Inhibition of BRD4 using the selective bromodomain inhibitor JQ1 restores PINK1/Parkin-mediated mitophagy, improves mitochondrial function, and consequently prevents impairment of cardiac structure and function in the hearts of diabetic mice. Importantly, *Pink1* deletion suppresses mitophagy, exacerbates cardiomyopathy, and abrogates the therapeutic effect of JQ1 on diabetic cardiomyopathy.

Mitophagy is a cellular process that removes dysfunctional or superfluous mitochondria (31), and shares its core molecular machinery with the autophagy pathway. Since damaged mitochondria lead to over-production of ROS and cell death (32,33), selective removal of dysfunctional mitochondria via mitophagy is an important mechanism of maintaining mitochondrial homeostasis and preserving cell viability. We previously showed that defective autophagy promotes heart failure, concurrent with enhanced protein aggregation and accumulation of damaged mitochondria in Type 1 diabetic mice (4,34). However, the functional role of autophagy/mitophagy in metabolic stress-induced cardiomyopathy remains controversial. Autophagy can either be suppressed (5-8) or activated (35,36) in the metabolically stressed heart. Notably, a recent study reported that 2 months of HFD feeding activated autophagic flux and mitophagy in mice. At the same time, these mice exhibited cardiac hypertrophy, diastolic dysfunction, and lipid accumulation (37).

In the present study, we find that HFD-induced Type 2 diabetic mice exhibit marked increase in LC3-II and p62 protein levels and significant reduction in LAMP1 protein level. Notably, the BET inhibitor JQ1 promotes autophagic flux in HFD-fed mouse hearts and

increases expression of genes related to autophagy and lysosomal function in neonatal cardiomyocytes. However, we cannot determine whether the suppression of autophagy and lysosomal-related genes is also dependent on BRD4 binding to H3K27ac at their promoter regions. Concomitantly, we find that HFD exposure inhibits mitophagy, as indicated by increases in the mitochondrial proteins, TIM23 and VDAC1, with an even decreasing of mitochondrial biogenesis markers. Although the PINK1/Parkin pathway is considered the most important regulatory pathway in controlling mitophagy, the outer mitochondrial membrane proteins BNIP3L/Nix, BCL2-L-13, and FUNDC1 are also involved. In our study, suppression of mitophagy may be a result of PINK1 down-regulation, as HFD feeding only reduced PINK1 protein and mRNA expression, but had no effect on other proteins regulating mitophagy. Furthermore, deletion of *Pink1*, which impairs PINK1/Parkin-mediated mitophagy, worsened HFD-induced diabetic cardiomyopathy. These observations strongly support the notion that suppression of PINK1/Parkin-mediated mitophagy may represent an essential mechanism for the pathogenesis of diabetic cardiomyopathy in Type 2 diabetes. However, multiple factors may collectively contribute to the development of diabetic cardiomyopathy in Type 2 diabetes, such as lipotoxicity, insulin resistance, and Ca^{+} imbalance, and possible molecular mechanisms linked to the development of cardiomyopathy include abnormalities in AMP-activated protein kinase, peroxisome proliferator-activated receptors, O-linked N-acetylglucosamine, protein kinase C, microRNA, and exosome pathways (38). Also, it is important to bear in mind that genetic *Pink1* gene deletion mice exhibit pathological cardiac phenotype at basal conditions due to disrupted mitophagy (39). Thus, HFD feeding worsened cardiomyopathy in *Pink1-/-* mice may be the combined effects of obesity in addition to inhibition of PINK1-mediated mitophagy.

Despite the fact that cardiac complications are a major cause of death in patients with diabetes, therapeutic strategies to effectively prevent or mitigate diabetic heart failure are still unavailable due to an incomplete understanding of the underlying mechanisms. Our work provides direct experimental evidence demonstrating that aberrant expression of cardiac BRD4 is a critical event in the development of diabetic cardiomyopathy, and inhibition of BRD4 with the selective bromodomain inhibitor JQ1 prevents HFD-induced impairment of cardiac structure and function. First, BRD4 is the most abundant BET family protein in cardiomyocytes; HFD-feeding significantly increased BRD4 protein levels, but did not alter those of BRD2 and BRD3. Second, upregulation of BRD4 is associated with the development of diabetic cardiomyopathy. Third, administration of JQ1 completely restored normal cardiac diastolic and systolic function in HFD-fed mice. Finally, JQ1 treatment almost completely prevented HFD-induced cardiac hypertrophy, interstitial fibrosis, lipid accumulation, and cardiomyocyte apoptosis.

BRD4 binds to acetylated histones and transcription factors through bromodomains and recruits transcriptional regulators such as positive transcription elongation factor b and the mediator complex (40). JQ1 is a selective bromodomain inhibitor that binds the bromodomain of BET proteins, resulting in transient displacement of bromodomain-containing proteins from acetylated chromatin (13). In this study, we observed an enrichment of both BRD4 and H3K27ac at the *Pink1* gene promoter in hearts of HFD-fed mice, implying that BRD4 binds to H3K27ac at the *Pink1* gene promoter region. However, enrichment of BRD4 and H3K27ac occupancy at *Pink1* gene promotor was abolished by JQ1 treatment. Importantly, we found that mRNA expression of *Pink1* and *Atgs* were significantly reduced in hearts of HFD-fed mice, in which association of BRD4 and H3K27ac at the *Pink1* gene promoter was increased. JQ1 treatment abolished enrichment of BRD4 and H3K27ac at the *Pink1* gene promoter and restored *Pink1*

mRNA to normal levels in hearts from HFD-fed mice, demonstrating that JQ1 upregulates *Pink1* mRNA expression by dissociating BRD4 from the *Pink1* gene promoter.

It is noteworthy that we used a dose of 10 mg/kg/day for the JQ1 treatment, which is four-times less than that used by other groups (16,17,19). We found that 50 mg/kg/day caused a dramatic body weight loss and HFD-fed mice died within one week (data not shown). The discrepancy may be due to differently aged mice. In our study, we treated mice at 8-9 months of age, while other groups treated mice at 10-12 weeks of age. In addition, diabetes is a metabolic syndrome that induces multi-organ dysfunction, including hepatic and renal dysfunction, which inhibits drug metabolism and excretion. Thus, it is of great importance to determine JQ1 dosage based on age, disease, disease stage, and disease severity.

In summary, the present study establish that the selective bromodomain inhibitor JQ1 prevents HFD-induced diabetic cardiomyopathy and provide mechanistic insights into the role of BRD4 in regulating PINK1/Parkin-mediated mitophagy. This mechanism provides a rationale for the development of BET bromodomain inhibitors as a new therapeutic approach for diabetic cardiomyopathy.

3.6 Acknowledgments

This study was supported by funding from the following agencies: National Heart, Lung, and Blood Institute (HL079584, HL080499, HL089920, HL110488, HL128014, HL132500, HL137371, and HL142287), National Cancer Institute (CA213022), National Institute on Aging (AG047776), and American Heart Association (16GRANT29590003). Dr. Zou is the Eminent Scholar in Molecular and Translational Medicine of the Georgia Research Alliance.

3.7 References

1. Westermeier F, Riquelme JA, Pavez M, Garrido V, Diaz A, Verdejo HE*, et al.* New Molecular Insights of Insulin in Diabetic Cardiomyopathy. Front Physiol **2016**;7:125 doi 10.3389/fphys.2016.00125.
2. Nakai A, Yamaguchi O, Takeda T, Higuchi Y, Hikoso S, Taniike M*, et al.* The role of autophagy in cardiomyocytes in the basal state and in response to hemodynamic stress. Nat Med **2007**;13(5):619-24 doi 10.1038/nm1574.
3. Xu X, Kobayashi S, Chen K, Timm D, Volden P, Huang Y*, et al.* Diminished autophagy limits cardiac injury in mouse models of type 1 diabetes. J Biol Chem **2013**;288(25):18077-92 doi 10.1074/jbc.M113.474650.
4. Xie Z, Lau K, Eby B, Lozano P, He C, Pennington B*, et al.* Improvement of cardiac functions by chronic metformin treatment is associated with enhanced cardiac autophagy in diabetic OVE26 mice. Diabetes **2011**;60(6):1770-8 doi 10.2337/db10-0351.
5. Sciarretta S, Zhai P, Shao D, Maejima Y, Robbins J, Volpe M*, et al.* Rheb is a critical regulator of autophagy during myocardial ischemia: pathophysiological implications in obesity and metabolic syndrome. Circulation **2012**;125(9):1134-46 doi 10.1161/CIRCULATIONAHA.111.078212.
6. Guo R, Zhang Y, Turdi S, Ren J. Adiponectin knockout accentuates high fat diet-induced obesity and cardiac dysfunction: role of autophagy. Biochim Biophys Acta **2013**;1832(8):1136-48 doi 10.1016/j.bbadis.2013.03.013.
7. An M, Ryu DR, Won Park J, Ha Choi J, Park EM, Eun Lee K*, et al.* ULK1 prevents cardiac dysfunction in obesity through autophagy-meditated regulation of lipid metabolism. Cardiovasc Res **2017**;113(10):1137-47 doi 10.1093/cvr/cvx064.
8. Kanamori H, Takemura G, Goto K, Tsujimoto A, Mikami A, Ogino A*, et al.* Autophagic adaptations in diabetic cardiomyopathy differ between type 1 and type 2 diabetes. Autophagy **2015**;11(7):1146-60 doi 10.1080/15548627.2015.1051295.
9. Ashrafi G, Schwarz TL. The pathways of mitophagy for quality control and clearance of mitochondria. Cell Death Differ **2013**;20(1):31-42 doi 10.1038/cdd.2012.81.
10. Vasquez-Trincado C, Garcia-Carvajal I, Pennanen C, Parra V, Hill JA, Rothermel BA*, et al.* Mitochondrial dynamics, mitophagy and cardiovascular disease. J Physiol **2016**;594(3):509-25 doi 10.1113/JP271301.
11. Sekine S, Youle RJ. PINK1 import regulation; a fine system to convey mitochondrial stress to the cytosol. BMC Biol **2018**;16(1):2 doi 10.1186/s12915-017-0470-7.
12. Shi J, Vakoc CR. The mechanisms behind the therapeutic activity of BET bromodomain inhibition. Mol Cell **2014**;54(5):728-36 doi 10.1016/j.molcel.2014.05.016.
13. Filippakopoulos P, Qi J, Picaud S, Shen Y, Smith WB, Fedorov O*, et al.* Selective inhibition of BET bromodomains. Nature **2010**;468(7327):1067-73 doi 10.1038/nature09504.
14. Korb E, Herre M, Zucker-Scharff I, Darnell RB, Allis CD. BET protein Brd4 activates transcription in neurons and BET inhibitor Jq1 blocks memory in mice. Nat Neurosci **2015**;18(10):1464-73 doi 10.1038/nn.4095.
15. Civenni G, Bosotti R, Timpanaro A, Vazquez R, Merulla J, Pandit S*, et al.* Epigenetic Control of Mitochondrial Fission Enables Self-Renewal of Stem-like Tumor Cells in Human Prostate Cancer. Cell Metab **2019**;30(2):303-18 e6 doi 10.1016/j.cmet.2019.05.004.

16. Meloche J, Potus F, Vaillancourt M, Bourgeois A, Johnson I, Deschamps L*, et al.* Bromodomain-Containing Protein 4: The Epigenetic Origin of Pulmonary Arterial Hypertension. Circ Res **2015**;117(6):525-35 doi 10.1161/CIRCRESAHA.115.307004.
17. Das S, Senapati P, Chen Z, Reddy MA, Ganguly R, Lanting L*, et al.* Regulation of angiotensin II actions by enhancers and super-enhancers in vascular smooth muscle cells. Nat Commun **2017**;8(1):1467 doi 10.1038/s41467-017-01629-7.
18. Duan Q, Mao X, Liao C, Zhou H, Sun Z, Deng X*, et al.* Inhibition of BET bromodomain attenuates angiotensin II induced abdominal aortic aneurysm in ApoE(-/-) mice. Int J Cardiol **2016**;223:428-32 doi 10.1016/j.ijcard.2016.08.238.
19. Anand P, Brown JD, Lin CY, Qi J, Zhang R, Artero PC*, et al.* BET bromodomains mediate transcriptional pause release in heart failure. Cell **2013**;154(3):569-82 doi 10.1016/j.cell.2013.07.013.
20. Duan Q, McMahon S, Anand P, Shah H, Thomas S, Salunga HT*, et al.* BET bromodomain inhibition suppresses innate inflammatory and profibrotic transcriptional networks in heart failure. Sci Transl Med **2017**;9(390) doi 10.1126/scitranslmed.aah5084.
21. Guo M, Wang HX, Chen WJ. BET-inhibition by JQ1 alleviates streptozotocin-induced diabetic cardiomyopathy. Toxicol Appl Pharmacol **2018**;352:9-18 doi 10.1016/j.taap.2018.05.018.
22. Wu S, Lu Q, Ding Y, Wu Y, Qiu Y, Wang P*, et al.* Hyperglycemia-Driven Inhibition of AMP-Activated Protein Kinase alpha2 Induces Diabetic Cardiomyopathy by Promoting Mitochondria-Associated Endoplasmic Reticulum Membranes In Vivo. Circulation **2019**;139(16):1913-36 doi 10.1161/CIRCULATIONAHA.118.033552.
23. Rogers GW, Brand MD, Petrosyan S, Ashok D, Elorza AA, Ferrick DA*, et al.* High throughput microplate respiratory measurements using minimal quantities of isolated mitochondria. PLoS One **2011**;6(7):e21746 doi 10.1371/journal.pone.0021746.
24. Mattiasson G. Flow cytometric analysis of isolated liver mitochondria to detect changes relevant to cell death. Cytometry A **2004**;60(2):145-54 doi 10.1002/cyto.a.20024.
25. Zou MH, Li H, He C, Lin M, Lyons TJ, Xie Z. Tyrosine nitration of prostacyclin synthase is associated with enhanced retinal cell apoptosis in diabetes. Am J Pathol **2011**;179(6):2835-44 doi 10.1016/j.ajpath.2011.08.041.
26. Livak KJ, Schmittgen TD. Analysis of relative gene expression data using real-time quantitative PCR and the 2(-Delta Delta C(T)) Method. Methods **2001**;25(4):402-8 doi 10.1006/meth.2001.1262.
27. Zhang D, Wu B, Wang P, Wang Y, Lu P, Nechiporuk T*, et al.* Non-CpG methylation by DNMT3B facilitates REST binding and gene silencing in developing mouse hearts. Nucleic Acids Res **2017**;45(6):3102-15 doi 10.1093/nar/gkw1258.
28. Zhang D, Wang Y, Lu P, Wang P, Yuan X, Yan J*, et al.* REST regulates the cell cycle for cardiac development and regeneration. Nat Commun **2017**;8(1):1979 doi 10.1038/s41467-017-02210-y.
29. Dawson MA, Kouzarides T, Huntly BJ. Targeting epigenetic readers in cancer. N Engl J Med **2012**;367(7):647-57 doi 10.1056/NEJMra1112635.
30. Sakamaki JI, Wilkinson S, Hahn M, Tasdemir N, O'Prey J, Clark W*, et al.* Bromodomain Protein BRD4 Is a Transcriptional Repressor of Autophagy and Lysosomal Function. Mol Cell **2017**;66(4):517-32 e9 doi 10.1016/j.molcel.2017.04.027.

31. Kubli DA, Gustafsson AB. Unbreak my heart: targeting mitochondrial autophagy in diabetic cardiomyopathy. Antioxid Redox Signal **2015**;22(17):1527-44 doi 10.1089/ars.2015.6322.
32. Fleury C, Mignotte B, Vayssiere JL. Mitochondrial reactive oxygen species in cell death signaling. Biochimie **2002**;84(2-3):131-41 doi 10.1016/s0300-9084(02)01369-x.
33. Marchi S, Giorgi C, Suski JM, Agnoletto C, Bononi A, Bonora M*, et al.* Mitochondria-ros crosstalk in the control of cell death and aging. J Signal Transduct **2012**;2012:329635 doi 10.1155/2012/329635.
34. He C, Zhu H, Li H, Zou MH, Xie Z. Dissociation of Bcl-2-Beclin1 complex by activated AMPK enhances cardiac autophagy and protects against cardiomyocyte apoptosis in diabetes. Diabetes **2013**;62(4):1270-81 doi 10.2337/db12-0533.
35. Mellor KM, Bell JR, Young MJ, Ritchie RH, Delbridge LM. Myocardial autophagy activation and suppressed survival signaling is associated with insulin resistance in fructose-fed mice. J Mol Cell Cardiol **2011**;50(6):1035-43 doi 10.1016/j.yjmcc.2011.03.002.
36. Munasinghe PE, Riu F, Dixit P, Edamatsu M, Saxena P, Hamer NS*, et al.* Type-2 diabetes increases autophagy in the human heart through promotion of Beclin-1 mediated pathway. Int J Cardiol **2016**;202:13-20 doi 10.1016/j.ijcard.2015.08.111.
37. Tong M, Saito T, Zhai P, Oka SI, Mizushima W, Nakamura M*, et al.* Mitophagy Is Essential for Maintaining Cardiac Function During High Fat Diet-Induced Diabetic Cardiomyopathy. Circ Res **2019**;124(9):1360-71 doi 10.1161/CIRCRESAHA.118.314607.
38. Jia G, Hill MA, Sowers JR. Diabetic Cardiomyopathy: An Update of Mechanisms Contributing to This Clinical Entity. Circ Res **2018**;122(4):624-38 doi 10.1161/CIRCRESAHA.117.311586.
39. Billia F, Hauck L, Konecny F, Rao V, Shen J, Mak TW. PTEN-inducible kinase 1 (PINK1)/Park6 is indispensable for normal heart function. Proc Natl Acad Sci U S A **2011**;108(23):9572-7 doi 10.1073/pnas.1106291108.
40. Donati B, Lorenzini E, Ciarrocchi A. BRD4 and Cancer: going beyond transcriptional regulation. Mol Cancer **2018**;17(1):164 doi 10.1186/s12943-018-0915-9.

3.8 Tables and Figures

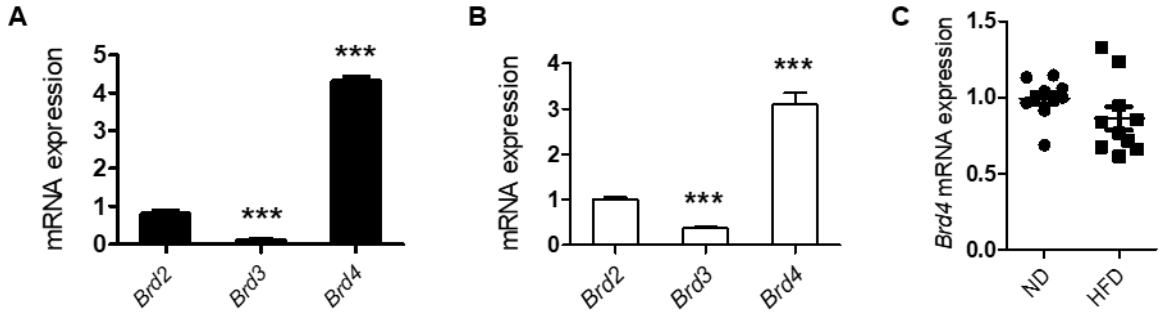

Figure 3.1 mRNA levels of BET family proteins in neonatal cardiomyocytes and adult mouse heart.

A, Quantification of the mRNA levels of *Brd2*, *Brd3*, and *Brd4* in adult mouse cardiac tissues, normalized to *Brd2* (n = 4, ***$P < 0.001$ vs. *Brd2*). B, Quantification of the mRNA levels of *Brd2*, *Brd3*, and *Brd4* in mouse neonatal cardiomyocytes, normalized to *Brd2* (n = 4, ***$P < 0.001$ vs. *Brd2*). C, 2-month-old WT mice were fed ND or HFD for 6 months. mRNA level of *Brd4* in mouse cardiac tissues from mice fed ND or HFD (n = 10/group).

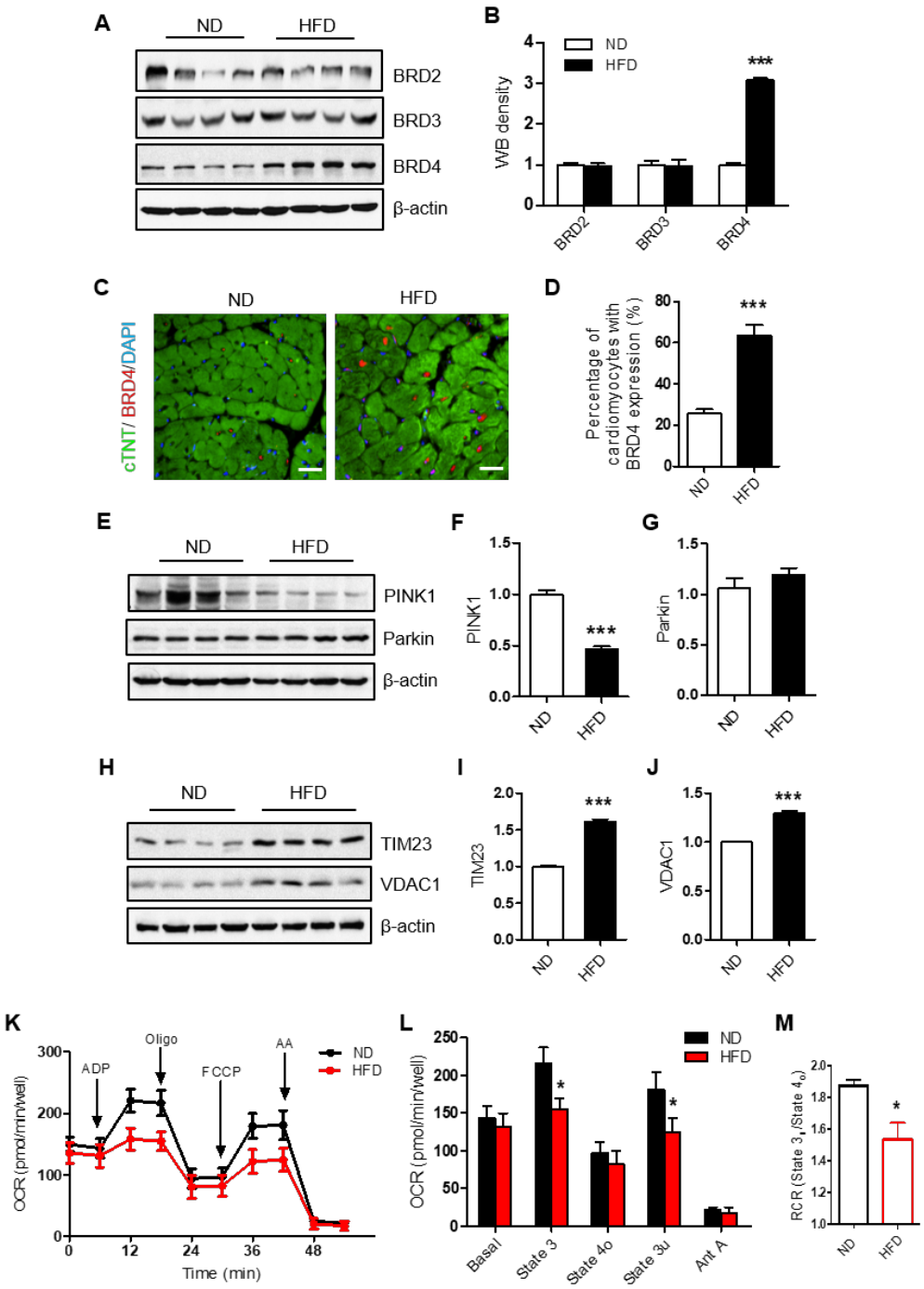

Figure 3.2 Upregulation of BRD4 is associated with inhibition of PINK1-mediated mitophagy. 2-month-old WT mice were fed ND or HFD for 6 months. A, Western blot analysis of BET family proteins, including BRD2, BRD3, and BRD4 in heart tissues from mice fed ND or HFD. B, Densitometric analysis of the indicated proteins (n = 8/group; ***$P < 0.001$ vs. ND). C, Representative

images of BRD4 immunofluorescent staining in hearts from ND- or HFD-fed mice. Nuclei were stained with DAPI and cardiomyocytes were stained with cardiac troponin T (cTNT). Scale bar, 50 μm. D, Percentage of cardiomyocytes with BRD4 staining (n = 8/group; ***$P < 0.001$ vs. ND). E, Western blot analysis of PINK1 and Parkin protein levels in heart tissues from mice fed ND or HFD. F, Densitometric analysis of PINK1 expression (n = 8/group; ***$P < 0.001$ vs. ND). G, Densitometric analysis of Parkin expression. H, Western blot analysis of mitochondrial marker proteins, including TIM23 and VDAC1 in mouse cardiac tissues. I, Densitometric analysis of TIM23 expression (n = 8/group; ***$P < 0.001$ vs. ND). J, Densitometric analysis of VDAC1 expression (n = 8/group; ***$P < 0.001$ vs. ND). K, Mitochondrial coupling of isolated mouse cardiac mitochondria was measured using a Seahorse XF96 metabolic flux analyzer. L, Graph of respirations of different states (n = 3; *$P < 0.05$ vs. ND). M, Mitochondrial respiratory control ratio (RCR) (n = 4; *$P < 0.05$).

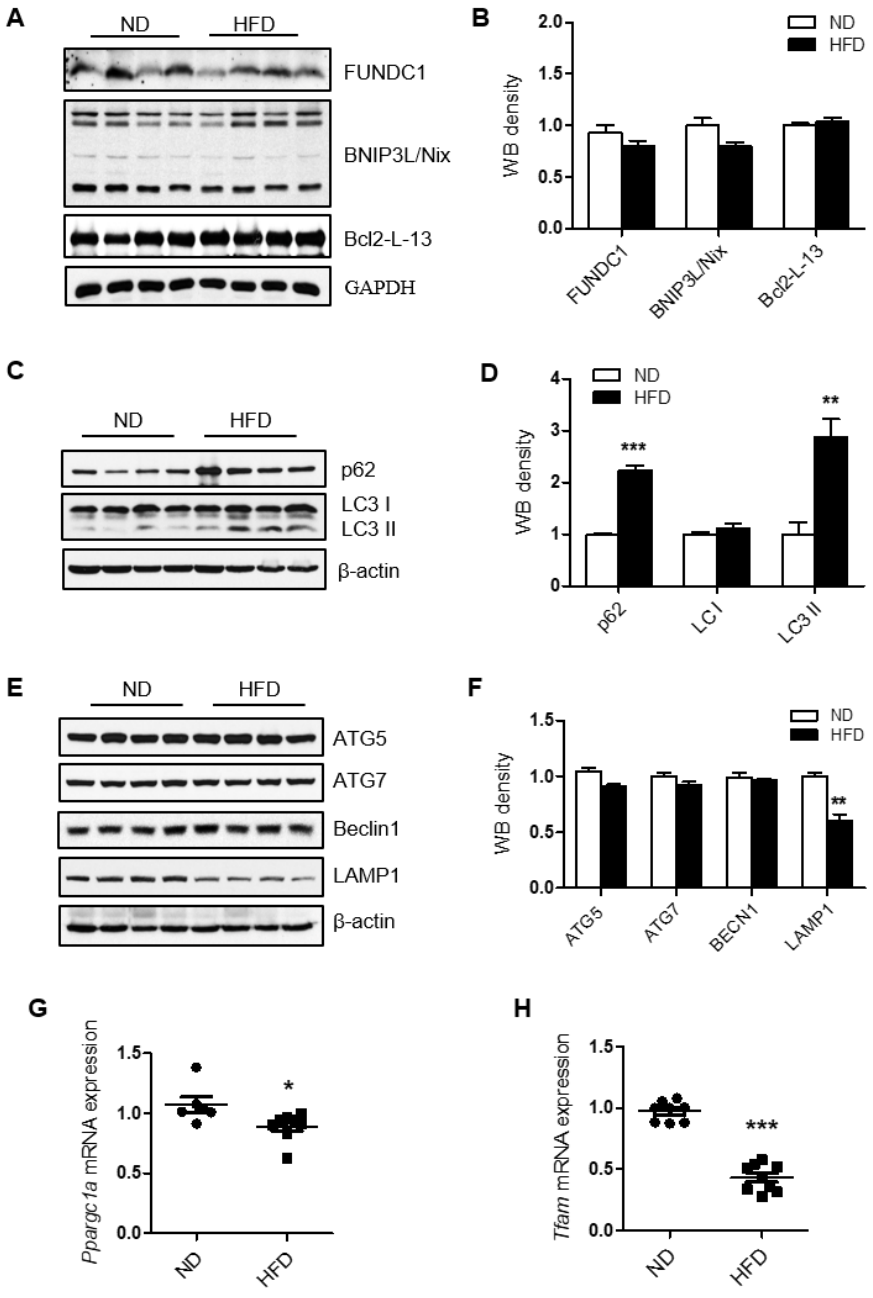

Figure 3.3 HFD feeding inhibits autophagic flux and mitochondrial biogenesis.

2-month-old WT mice were fed ND or HFD for 6 months. A, Western blot analysis of mitophagy-related proteins, including FUN14 domain containing 1, BCL2 Interacting Protein 3 like, and BCL2-like protein 13 in mouse cardiac tissues. B, Densitometric analysis of the indicated proteins. C, Western blot analysis of p62, LC3 I, and LC3 II protein levels of heart tissues from ND- or HFD-fed mice. D, Densitometric

analysis of the indicated proteins (n = 8/group; $^{**}P < 0.01$, $^{***}P < 0.001$ vs. ND). E, Western blot analysis of ATG5, ATG7, Beclin1, and LAMP1 protein levels of heart tissues from mice fed ND or HFD. F, Densitometric analysis of the indicated proteins (n = 8/group; $^{**}P < 0.01$ vs. ND). G, mRNA level of *Ppargc1a* in cardiac tissues of mice fed HFD or ND for 6 months (n = 6-8, $^{*}P < 0.05$ vs. ND). H, mRNA level of *Tfam* in cardiac tissues of mice fed HFD or ND for 6 months (n = 8-10, $^{***}P < 0.001$ vs. ND).

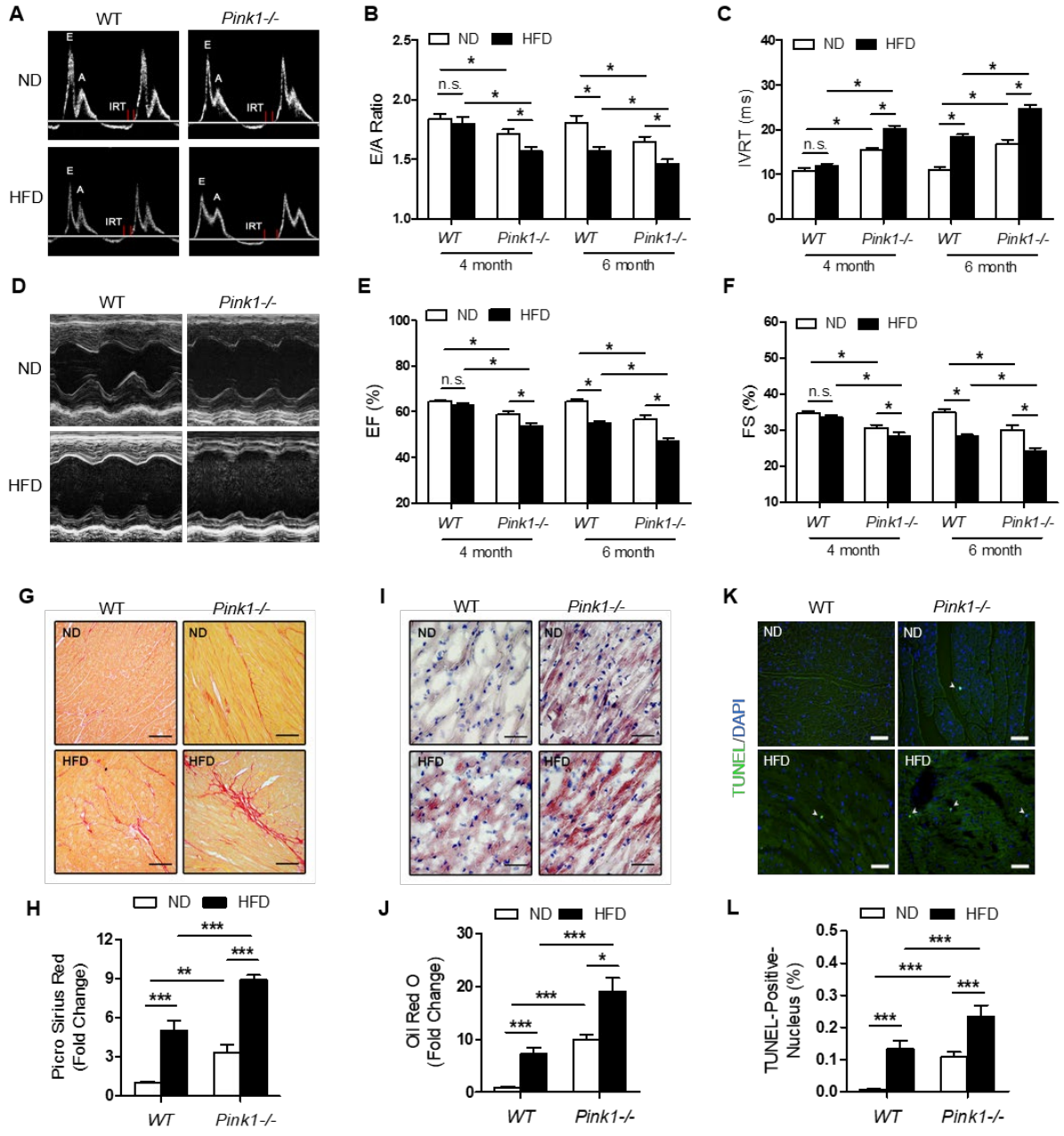

Figure 3.4 Pink1 deletion accelerates and aggravates cardiomyopathy in HFD-fed mice.

2-month-old WT and *Pink1-/-* mice were fed ND or HFD for 4 or 6 months. A, Representative Doppler flow measurements of mitral inflow. B, Ratios of the early (E) to late (A) ventricular filling velocities (n = 8-13/group; **P* < 0.05). C, Left ventricular isovolumic relaxation time (IVRT) (n = 8-13/group; **P* < 0.05). D, Representative images of M-mode echocardiography. E, Ejection fraction (EF) (n = 8-13/group;

*P < 0.05). F, Fractional shortening (FS) (n = 8-13/group; *P < 0.05). 2-month-old WT and *Pink1-/-* mice were fed ND or HFD for 6 months. G, Representative Picro Sirius Red staining images of cardiac tissues. Scale bar, 50 µm. H, Quantitative analysis of Picro Sirius Red staining (n = 8/group; **P < 0.01, ***P < 0.001). I, Representative Oil Red O staining images of cardiac tissues. Scale bar, 50 µm. J, Quantitative analysis of Oil Red O staining (n = 8/group; *P < 0.05, ***P < 0.001). K, Representative TUNEL staining images of cardiac tissues; nuclei were stained with DAPI. Scale bar, 50 µm. L, Quantitative analysis of TUNEL staining (n = 6/group, ***P < 0.001).

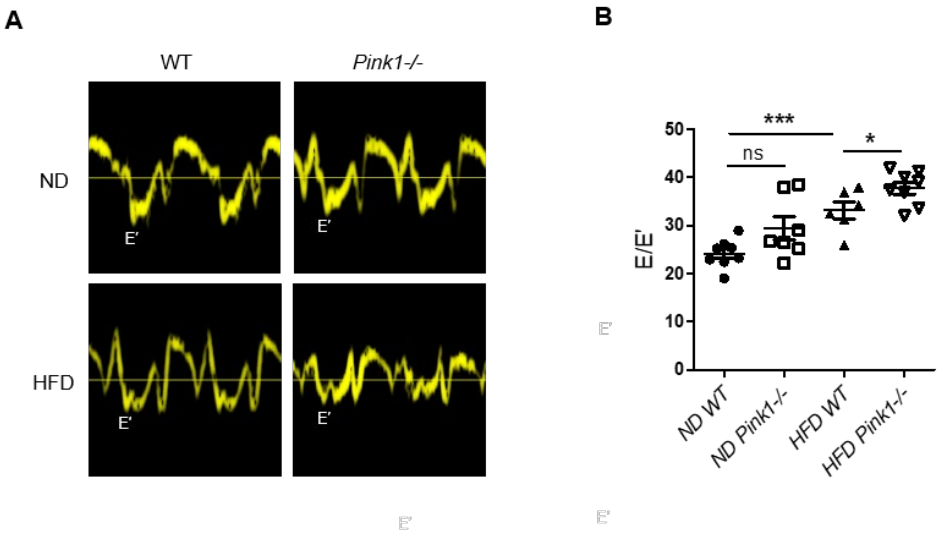

Figure 3.5 E/E' of Pink1-/- mice fed a ND or HFD.

2-month-old WT and *Pink1-/-* mice were fed ND or HFD for 4 months. A, Representative tissue Doppler images. B, Ratio between early mitral inflow velocity wave (E) and mitral annular early diastolic velocity (E′) wave (E/E′), n = 6-8/group; *P < 0.05, ***P < 0.001.

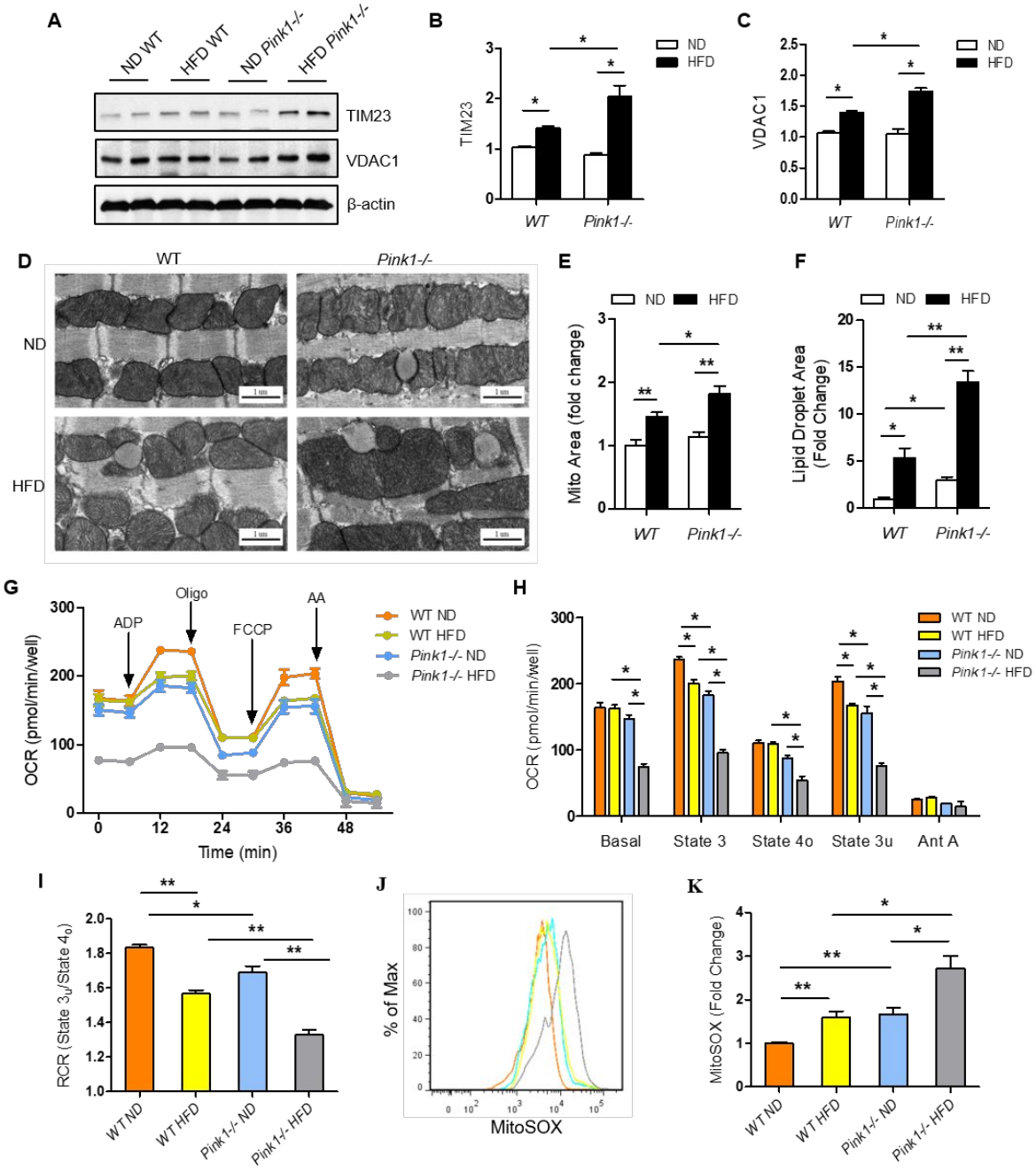

Figure 3.6 Pink1 deletion worsens mitochondrial dysfunction in HFD-fed mice.

2-month-old WT and *Pink1-/-* mice were fed ND or HFD for 6 months. A, Western blot analysis of mitochondrial marker proteins, including TIM23 and VDAC1, in the hearts of WT or *Pink1-/-* mice fed with ND or HFD. B, Densitometric analysis of TIM23 (n = 6/group; **P* < 0.05). C, Densitometric

analysis of VDAC1 (n = 6/group; *$P < 0.05$). D, Representative TEM images of cardiac mitochondria in WT or *Pink1-/-* mice fed ND or HFD for 6 months. Scale bar 1 μm. E, Quantification of mitochondrial area (n = 4/group; *$P < 0.05$, **$P < 0.01$). F, Quantification of lipid droplets (n = 4/group; *$P < 0.05$, **$P < 0.01$). G, Mitochondrial coupling of isolated mouse cardiac mitochondria was measured using a Seahorse XF96 metabolic flux analyzer. H, Graph of respirations of different states (n = 3; *$P < 0.05$). I, Mitochondrial respiratory control ratio (RCR) (n = 3; *$P < 0.05$, **$P < 0.01$). J, Flow cytometric analysis of mitochondrial ROS in isolated mitochondria from WT and *Pink1-/-* mice hearts by MitoSOX. K, Mean fluorescence intensity quantification (n = 4; *$P < 0.05$, **$P < 0.01$).

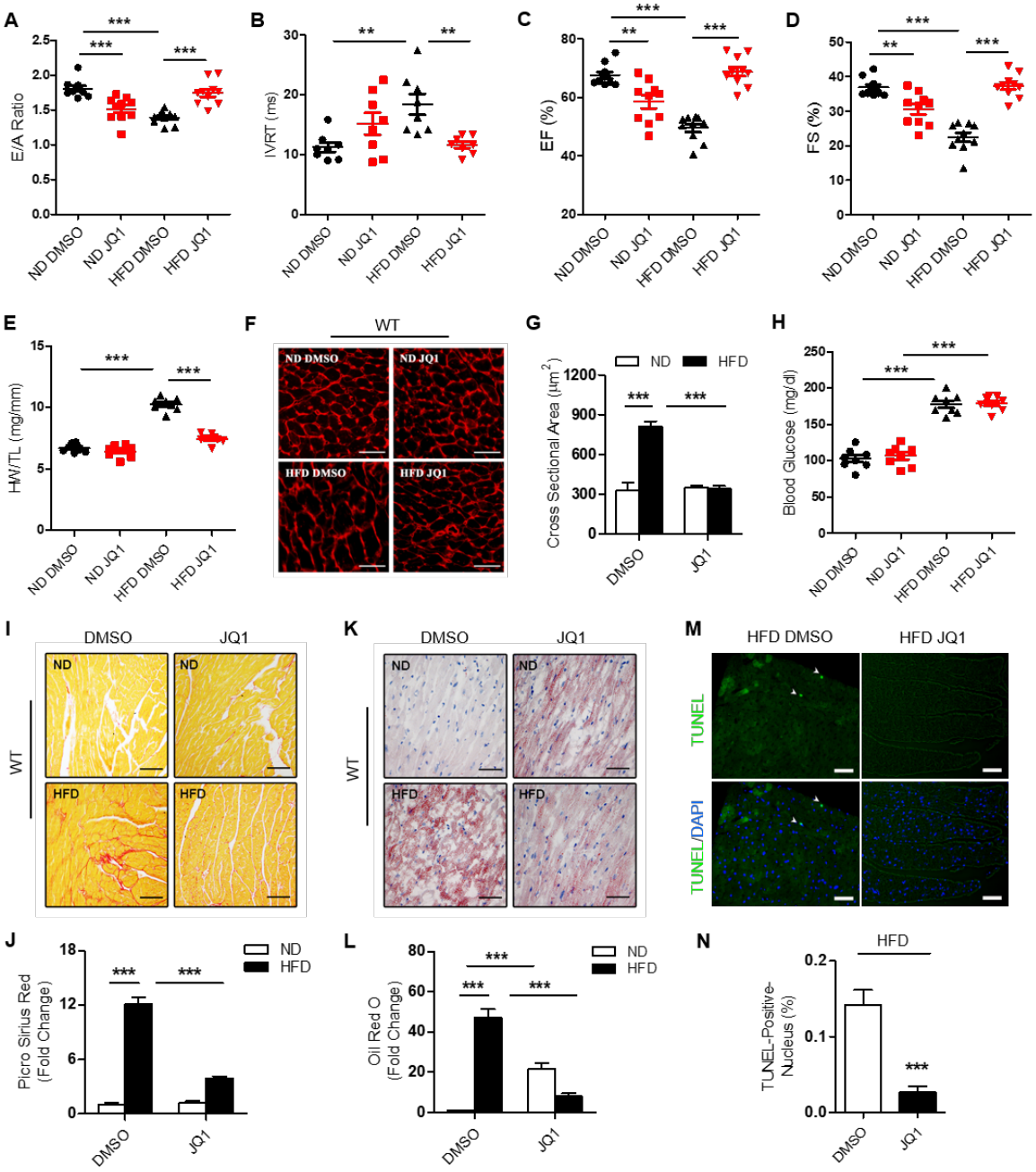

Figure 3.7 BRD4 inhibition with JQ1 potently alleviates cardiac dysfunction and cardiac remodeling in HFD-fed mice.

2-month-old WT mice were fed ND or HFD for 7 months and treated with JQ1 during the last month of feeding. A, Ratios of the early (E) to late (A) ventricular filling velocities (n = 10/group; ***$P < 0.001$). B, Left ventricular isovolumic relaxation time (IVRT) (n = 10/group; **$P < 0.01$). C, Ejection fraction (EF) (n = 10/group; **$P < 0.01$, ***$P < 0.001$). D, Fractional shortening (FS) (n = 10/group; **$P < 0.01$,

***P < 0.001). E, Ratio of heart weight/tibia length (HW/TL) (n = 8/group; ***P < 0.001). F, Representative wheat germ agglutinin staining images of cardiac tissues. Scale bar, 50 µm. G, Quantitative analysis of cardiomyocyte cross-sectional area (n = 4/group; ***P < 0001). H, Fasting blood glucose (n = 8/group; ***P < 0.001). I, Representative Oil Red O staining images of cardiac tissues in indicated groups. Scale bar, 50 µm. J, Quantitative analysis of Oil Red O staining (n = 8/group; ***P < 0.001). K, Representative Picro Sirius Red staining images of cardiac tissues in indicated groups. Scale bar, 50 µm. L, Quantitative analysis of Picro Sirius Red staining (n = 8/group; ***P < 0.001). M, Representative TUNEL staining images of cardiac tissues; nuclei were stained with DAPI. Scale bar, 50 µm. N, Quantitative analysis of TUNEL staining (n = 6/group; ***P < 0.001 vs. DMSO HFD).

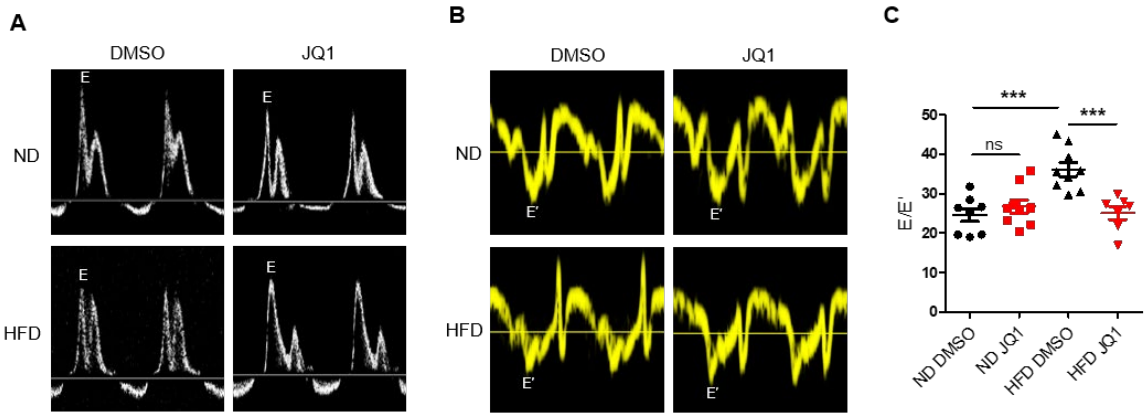

Figure 3.8 E/E' of ND or HFD-fed WT mice treated with JQ1.

2-month-old WT mice were fed ND or HFD for 7 months and treated with JQ1 during the last month of feeding. A, Representative Doppler flow measurements of mitral inflow. B, Representative tissue Doppler images. C, Ratio between early mitral inflow velocity wave (E) and mitral annular early diastolic velocity (E′) wave (E/E′), n = 7-9/group; ***P < 0.001.

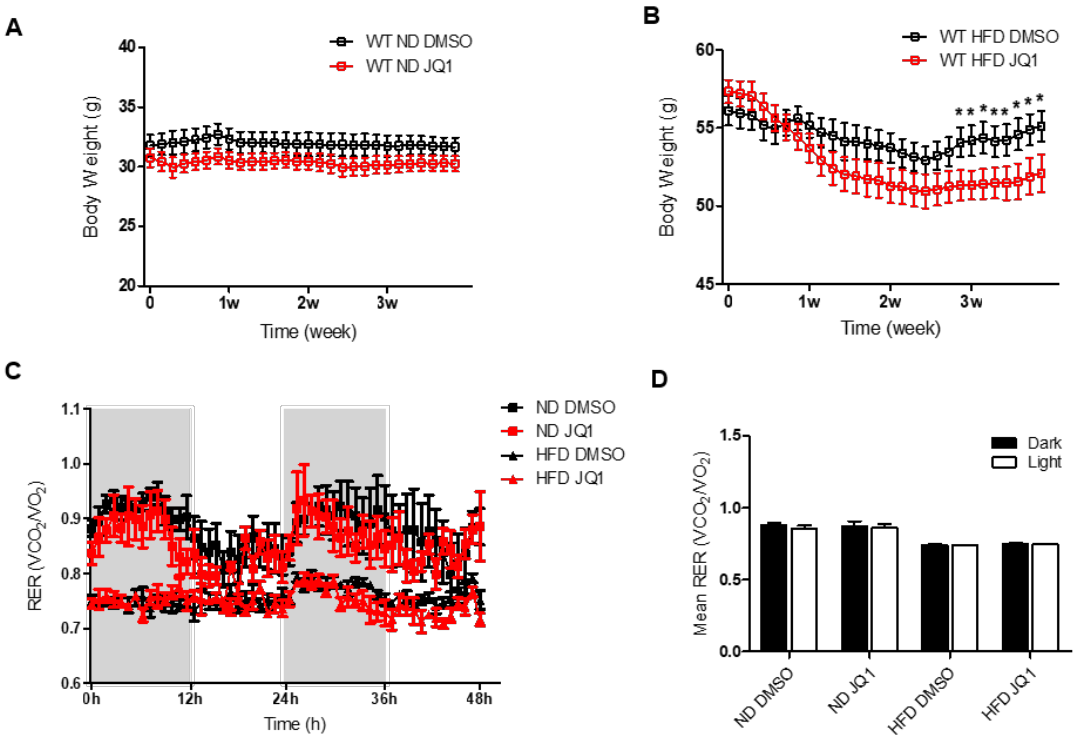

Figure 3.9 Comprehensive metabolic monitoring for ND or HFD-fed WT mice treated with JQ1.

2-month-old WT mice were fed ND or HFD for 7 months and treated with JQ1 for the last month of feeding. A, Body weight of ND-fed mice based on a daily record of the 30 days of JQ1 administration. B, Body weight of HFD-fed mice based on a daily record for the 30 days of JQ1 administration (n = 8/group; $*P < 0.05$). C, Mice were individually placed in metabolic cages (PhenoMaster) and allowed to acclimatize for 3 days before RER (VCO2/VO2) readings were taken (n = 4 mice per group). D, Mean RER.

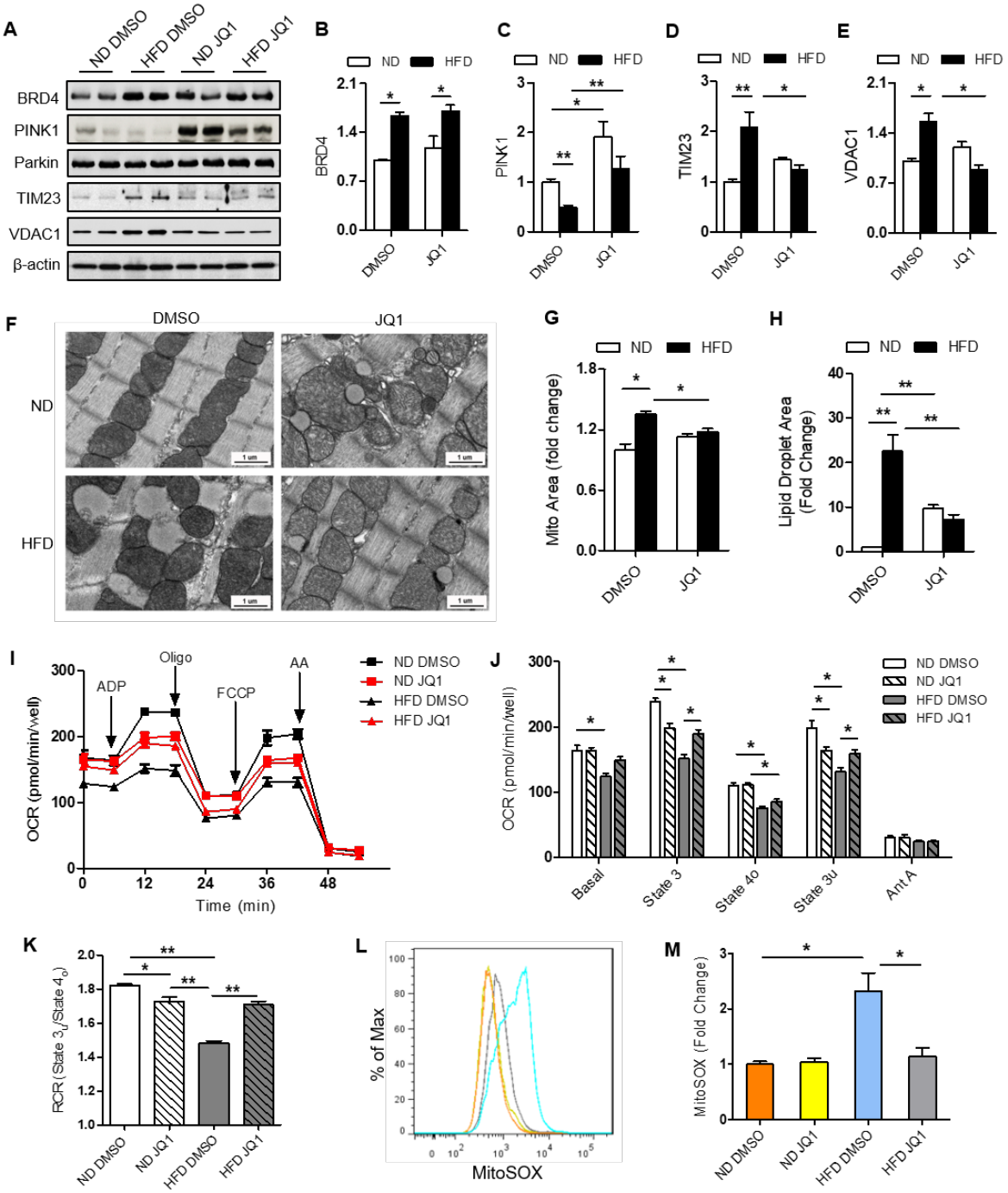

Figure 3.10 BRD4 inhibition with JQ1 promotes mitophagy and improves mitochondrial function in HFD-fed mice.

2-month-old WT mice were fed ND or HFD for 7 months and treated with JQ1 during the last month of feeding. A, Western blot analysis of indicated proteins in heart tissues from DMSO- or JQ1-treated mice

fed a ND or HFD. B, Densitometric analysis of BRD4 (n = 6/group; *$P < 0.05$). C, Densitometric analysis of PINK1 (n = 6/group; *$P < 0.05$; **$P < 0.01$). D, Densitometric analysis of TIM23 (n = 6/group; *$P < 0.05$; **$P < 0.01$). E, Densitometric analysis of VDAC1 (n = 6/group; *$P < 0.05$). F, Representative TEM images of cardiac mitochondria in DMSO- or JQ1-treated mice fed ND or HFD. Scale bar 1 μm. G, Quantification of the mitochondrial area ratio (n = 4/group; *$P < 0.05$). H, Quantification of lipid droplets (n = 4/group; **$P < 0.01$). I, Mitochondria coupling of isolated mouse cardiac mitochondria was measured using a Seahorse XF96 metabolic flux analyzer. J, Graph of respirations of different states (n = 3; *$P < 0.05$). K, Mitochondrial respiratory control ratio (RCR) (n = 3; *$P < 0.05$; **$P < 0.01$). L, Flow cytometric analysis of mitochondrial ROS in isolated mitochondria from heart tissues of DMSO- or JQ1-treated mice fed ND or HFD by MitoSOX. M, Mean fluorescence intensity quantification (n = 3; *$P < 0.05$).

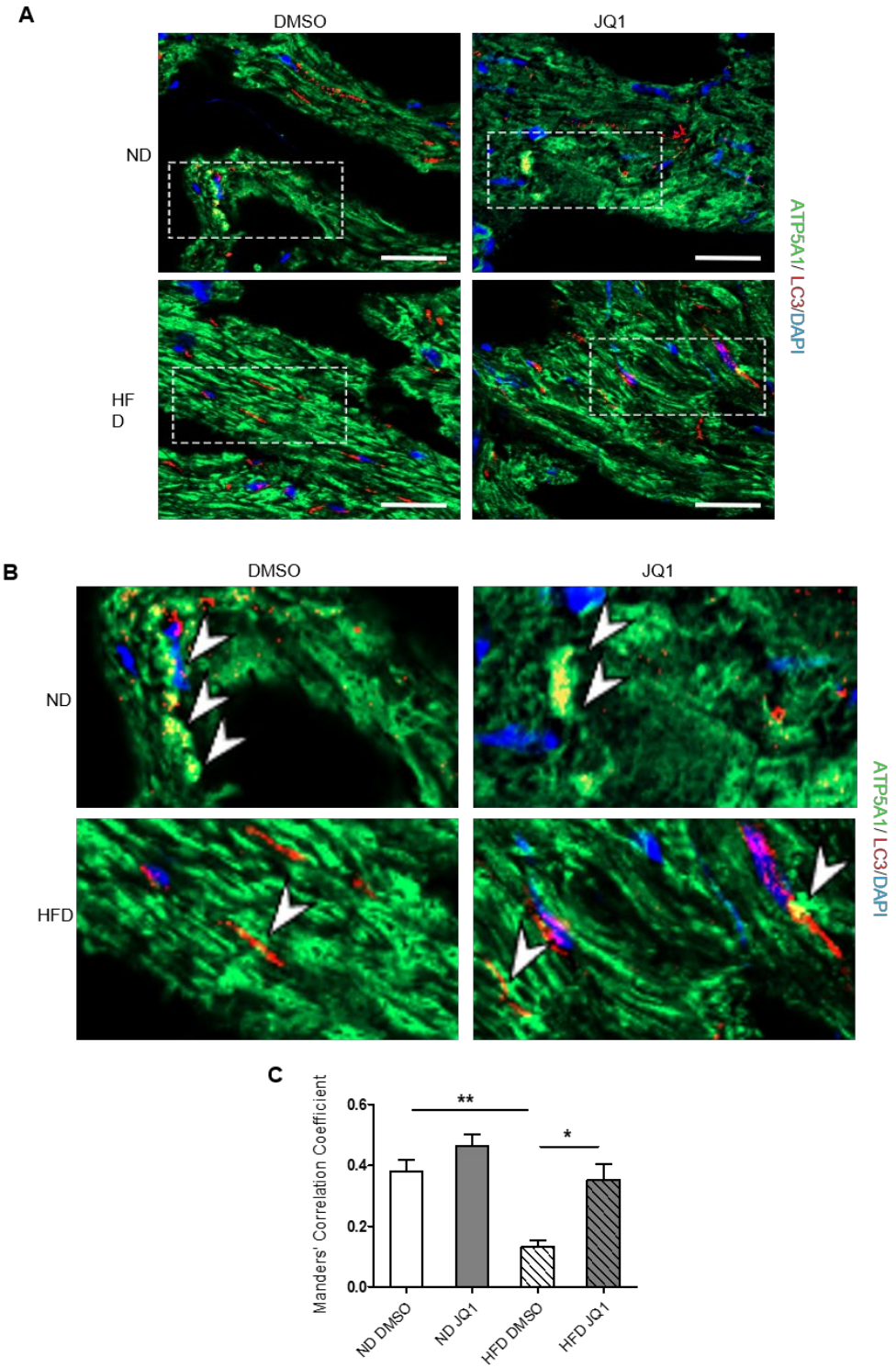
A
DMSO
JQ1
ND
HF
D
ATP5A1/ LC3/DAPI
B
DMSO
JQ1
ND
HFD
ATP5A1/ LC3/DAPI
C
Manders' Correlation Coefficient
0.6
0.4
0.2
0.0
**
*
ND DMSO
ND JQ1
HFD DMSO
HFD JQ1

Figure 3.11 Colocalization of LC3 and ATP5A1 in the hearts of ND or HFD-fed WT mice treated with JQ1.

2-month-old WT mice were fed ND or HFD for 7 months and treated with JQ1 during the last month of feeding. A, Representative images of ATP5A1 and LC3 immunofluorescent staining in hearts from ND- or HFD-fed mice treated with DMSO or JQ1. Nuclei were stained with DAPI. Scale bar, 20 μm. B, Enlarged images of selected area in penal A. C, Colocalization analysis of ATP5A1 and LC3 (n = 5/group; **P* < 0.05, ***P* < 0.01).

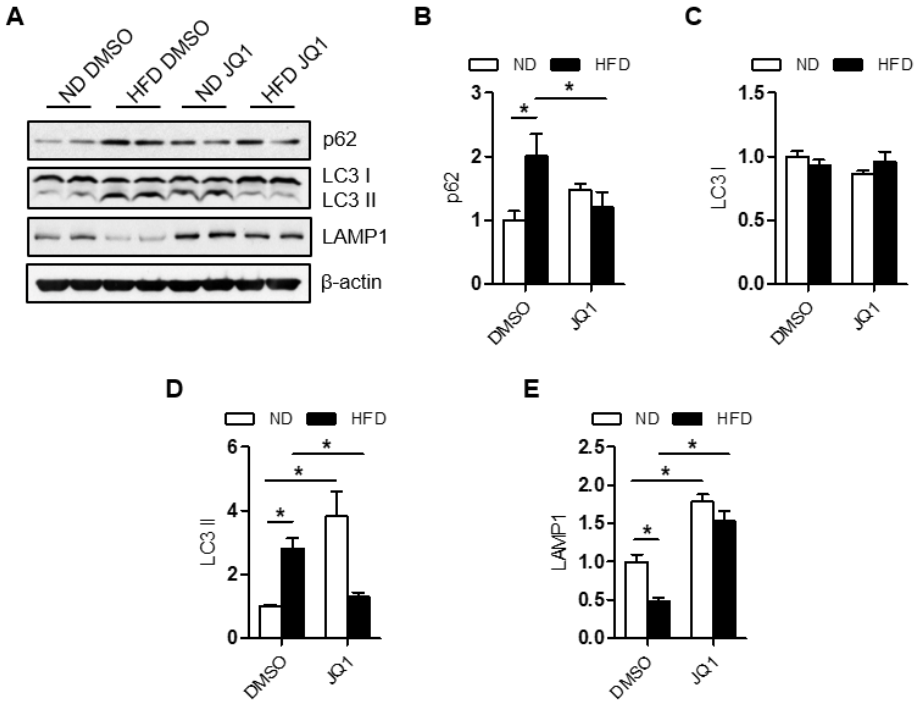

Figure 3.12 BRD4 inhibition with JQ1 promotes autophagy in HFD-fed mice.

2-month-old WT mice were fed ND or HFD for 7 months and treated with JQ1 during the last month of feeding. A, Western blot analysis of indicated proteins in heart tissues from DMSO- or JQ1-treated mice fed a ND or HFD. B, Densitometric analysis of p62 (n = 6/group; **P* < 0.05). C, Densitometric analysis of LC3 I. D, Densitometric analysis of LC3 II (n = 6/group; **P* < 0.05). E, Densitometric analysis of LAMP1 (n = 6/group; **P* < 0.05).

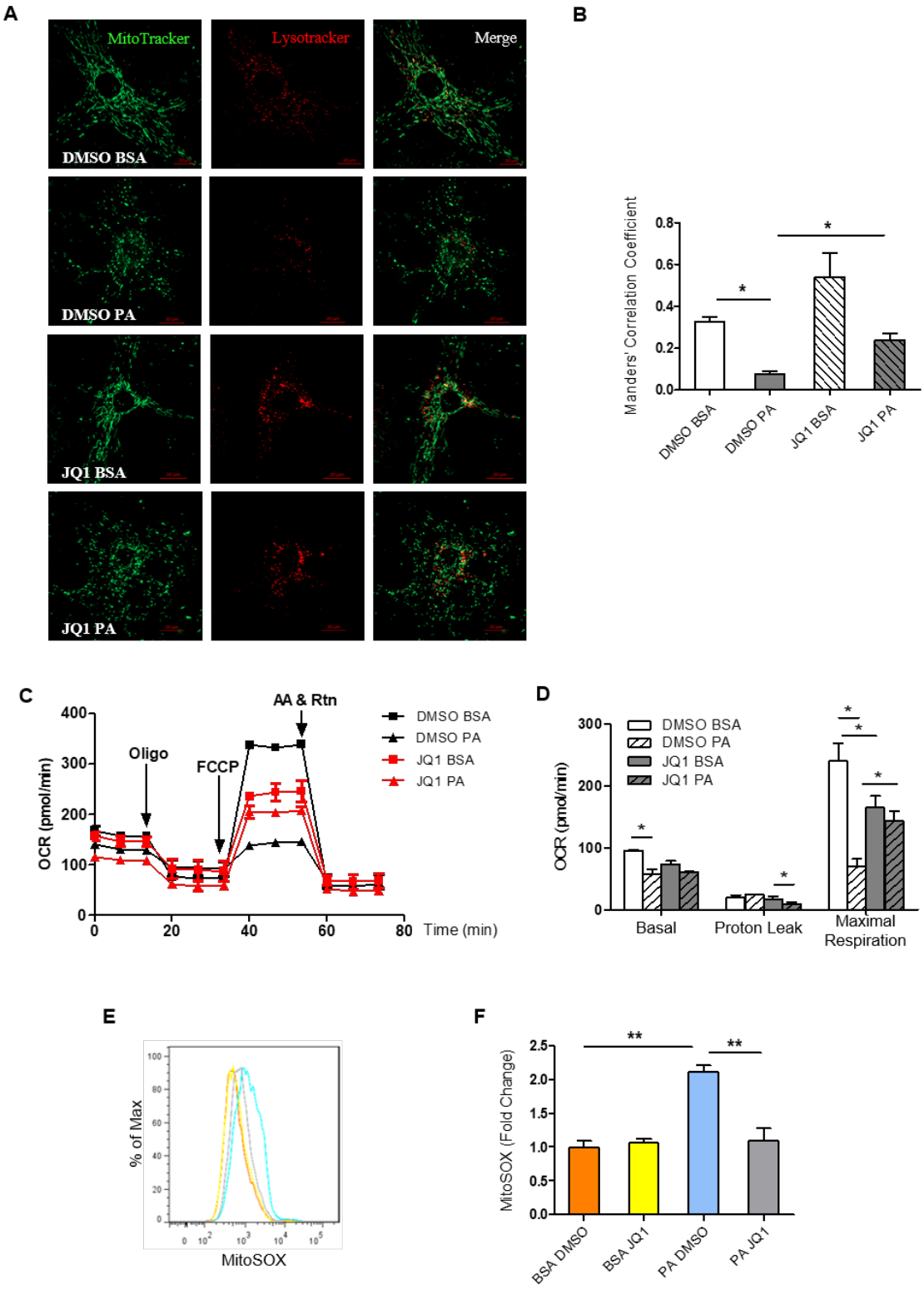
A
MitoTracker
Lysotracker
Merge
DMSO BSA
DMSO PA
JQ1 BSA
JQ1 PA
B
Manders' Correlation Coefficient
0.8
0.6
0.4
0.2
0.0
*
*
DMSO BSA
DMSO PA
JQ1 BSA
JQ1 PA
C
AA & Rtn
Oligo
FCCP
DMSO BSA
DMSO PA
JQ1 BSA
JQ1 PA
OCR (pmol/min)
400
300
200
100
0
0
20
40
60
80
Time (min)
D
DMSO BSA
DMSO PA
JQ1 BSA
JQ1 PA
OCR (pmol/min)
300
200
100
0
*
*
*
*
*
Basal
Proton Leak
Maximal Respiration
E
% of Max
100
80
60
40
20
0
MitoSOX
F
MitoSOX (Fold Change)
2.5
2.0
1.5
1.0
0.5
0.0
**
**
BSA DMSO
BSA JQ1
PA DMSO
PA JQ1

Figure 3.13 BRD4 inhibition with JQ1 promotes mitophagy and improves mitochondrial function in cultured neonatal cardiomyocytes.

Mouse neonatal cardiomyocytes were treated with DMSO or JQ1 in the presence of BSA or PA. A, Representative confocal images of mouse neonatal cardiomyocytes labeled with MitoTracker and LysoTracker. Scale bar, 20 μm. B, Colocalization analysis of MitoTracker and LysoTracker (n = 3; $*P < 0.05$). C, Mitochondria OCR was measured using a Seahorse XF96 metabolic flux analyzer. D, Graph of basal respiration, proton leak, and maximal respiration (n = 3; $*P < 0.05$). E, Flow cytometric analysis of mitochondrial ROS production in mouse neonatal cardiomyocytes by MitoSOX staining. F, Mean fluorescence intensity calculation (n = 3; $**P < 0.01$).

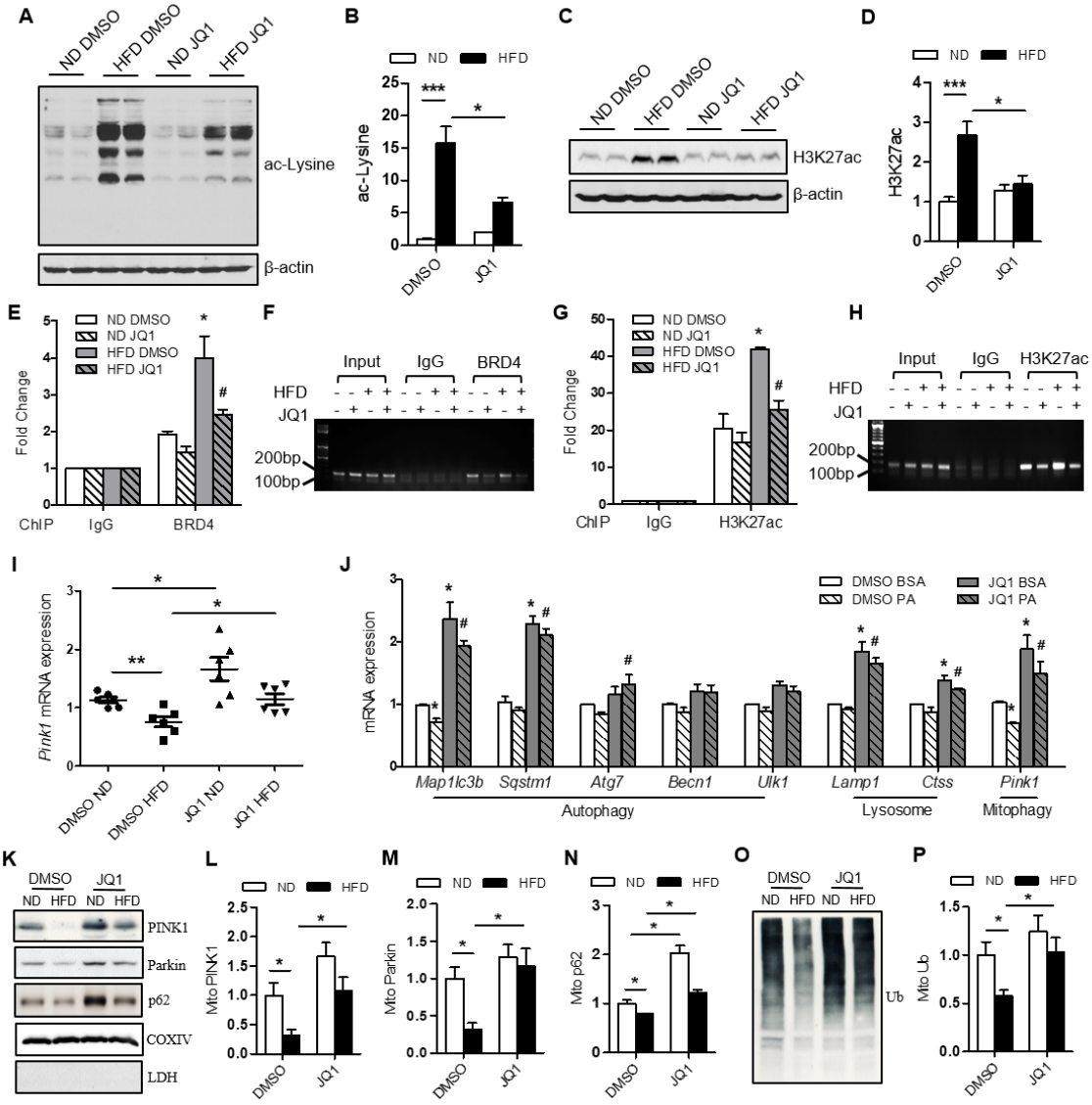

Figure 3.14 Molecular basis for JQ1 activation of PINK1/Parkin-mediated mitophagy.

2-month-old WT mice were fed ND or HFD for 7 months and treated with JQ1 for the last month of feeding. A, Western blot analysis of total protein lysine acetylation (ac-Lysine) in heart tissues from DMSO- or JQ1-treated mice fed ND or HFD. B, Densitometric analysis of ac-Lysine levels (n = 4/group; *$P < 0.05$, ***$P < 0.001$). C, Western blot analysis of H3K27ac levels in heart tissues from ND- or HFD-treated mice. D, Densitometric analysis of H3K27ac level (n = 6/group; *$P < 0.05$, ***$P < 0.001$). E, Results of ChIP-qPCR assay for BRD4 binding to the *Pink1* gene promoter in mouse heart tissues (n =

4/group; *$P < 0.05$ [DMSO ND vs. DMSO HFD], $^{\#}P < 0.05$ [JQ1 HFD vs. DMSO HFD]). F, Image of BRD4 ChIP at the *Pink1* gene promoter. G, Results of the ChIP-qPCR assay for H3K27ac binding to the *Pink1* gene promoter in heart tissues (n = 4/group; *$P < 0.05$ [DMSO ND vs. DMSO HFD], $^{\#}P < 0.05$ [JQ1 HFD vs. DMSO HFD]). H, Image of H3K27ac ChIP at the *Pink1* gene promoter. I, *Pink1* mRNA level in mouse heart tissues in indicated groups (n = 6/group; *$P < 0.05$, **$P < 0.01$). J, mRNA level of Atgs in mouse neonatal cardiomyocytes treated with DMSO or JQ1 in the presence of BSA or PA. (n = 3; *$P < 0.05$ vs. DMSO BSA, $^{\#}P < 0.05$ vs. DMSO PA). K, Mitochondrial fraction (Mito) was prepared using mouse heart samples. Western blot analysis of PINK1, Parkin, and p62 in the Mito fraction were shown. Lactate dehydrogenase (LDH) was used as a marker for the cytosol. Mitochondrial cytochrome c oxidase subunit IV (COXIV) was used as a marker for mitochondria. L, Densitometric analysis of PINK1 expression (n = 3; *$P < 0.05$). M, Densitometric analysis of Parkin expression (n = 3; *$P < 0.05$). N, Densitometric analysis of p62 expression (n = 3; *$P < 0.05$). O, Western blot analysis of the total ubiquitinated protein level in the Mito fraction of mouse heart samples. P, Densitometric analysis of ubiquitinated protein expression in the Mito fraction (n = 3; *$P < 0.05$).

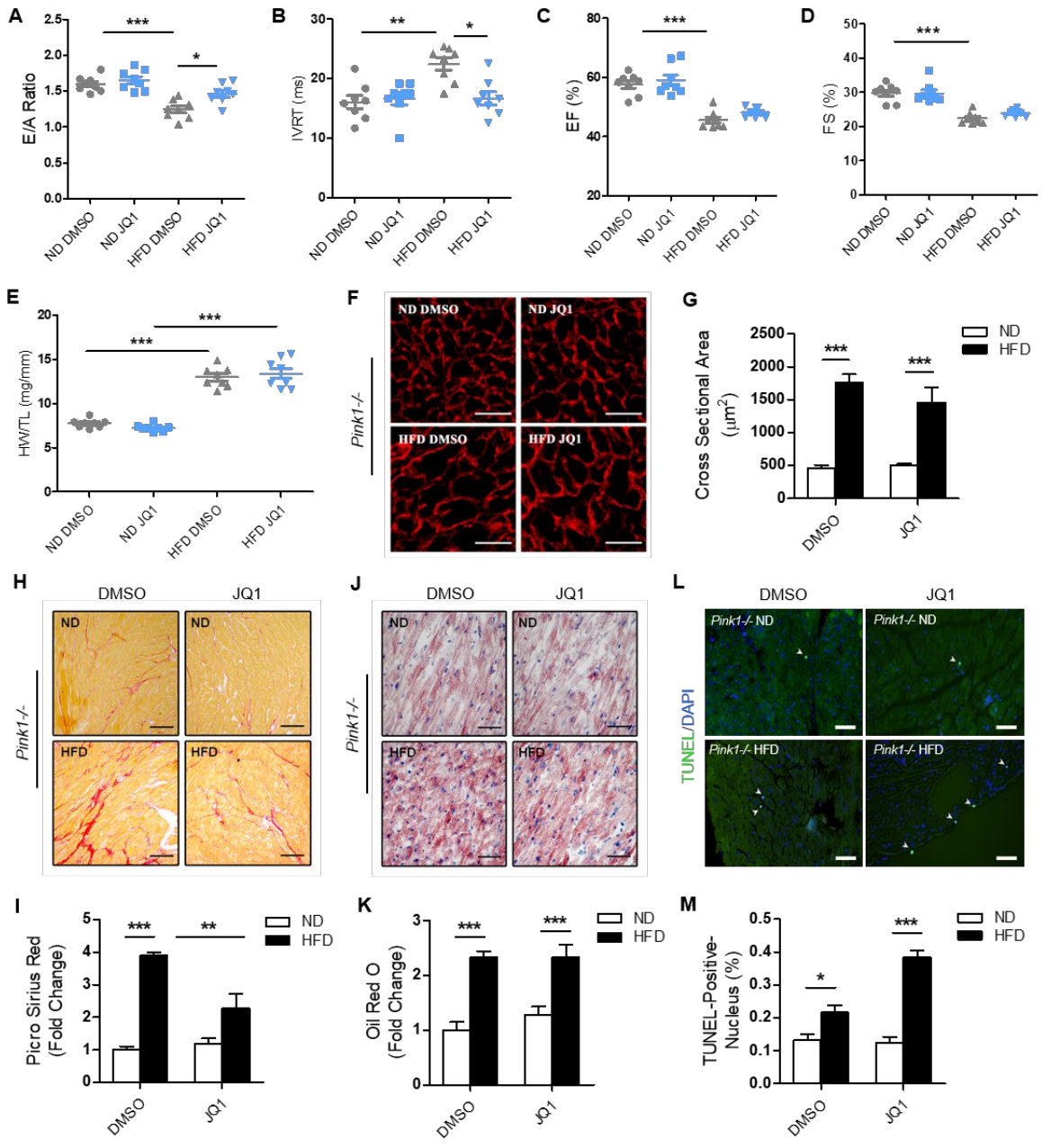

Figure 3.15 Pink1 deletion abrogates the therapeutic effect of JQ1 on cardiac dysfunction, lipid accumulation, and apoptosis in HFD-fed mice.

2-month-old *Pink1-/-* mice were fed ND or HFD for 7 months and treated with JQ1 for the last month of feeding. A, Ratios of the early (E) to late (A) ventricular filling velocities (n = 8/group; **P* < 0.05, ****P* < 0.001). B, Left ventricular isovolumic relaxation time (IVRT) (n = 8/group; **P* < 0.05, ***P* < 0.01). C, Ejection fraction (EF) (n = 8/group; ****P* < 0.001). D, Fractional shortening (FS) (n = 8/group; ****P* <

0.001). E, Ratio of heart weight/tibia length (HW/TL) (n = 8/group; ***$P < 0.001$). F, Representative wheat germ agglutinin staining images in cardiac tissues. Scale bar, 50 µm. G, Quantitative analysis of cardiomyocyte cross-sectional area (n = 4/group; ***$P < 0.001$). H, Representative Oil Red O staining images of cardiac tissues. Scale bar, 50 µm. I, Quantitative analysis of Oil Red O staining (n = 5/group; **$P < 0.01$, ***$P < 0.001$). J, Representative Picro Sirius Red staining images of cardiac tissues. Scale bar, 50 µm. K, Quantitative analysis of Picro Sirius Red staining (n = 5/group; ***$P < 0.001$). L, Representative TUNEL staining images of cardiac tissues; nuclei were stained with DAPI. Scale bar, 50 µm. M, Quantitative analysis of TUNEL staining (n = 5/group; *$P < 0.05$, ***$P < 0.001$).

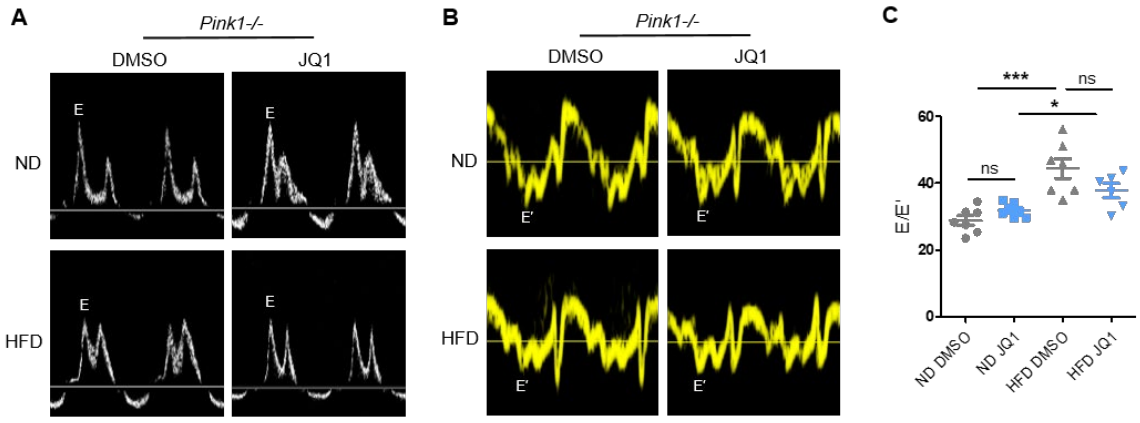

Figure 3.16 E/E' of ND or HFD-fed Pink1-/- mice treated with JQ1.

2-month-old *Pink1-/-* mice were fed ND or HFD for 7 months and treated with JQ1 for the last month of feeding. A, Representative Doppler flow measurements of mitral inflow. B, Representative tissue Doppler images. C, Ratio between early mitral inflow velocity wave (E) and mitral annular early diastolic velocity (E′) wave (E/E′), n = 6-8/group; *$P < 0.05$, ***$P < 0.001$.

Table 3.1 Primary Antibody Information

Antibody	Application	Supplier	Catalog number	Dilution
β-Actin	WB	Santa Cruz	sc-47778	1 : 2000
ATG5	WB	abcam	ab108327	1 : 1000
ATG7	WB	Cell Signaling	8558s	1 : 1000
ATP5A1	IFC	proteintech	66037-1-Ig	1:200
Bcl2-L-13	WB	proteintech	16612-1-AP	1 : 1000
Beclin1	WB	Cell Signaling	3738s	1 : 1000
BNIP3L/Nix	WB	Cell Signaling	9089s	1 : 1000
BRD2	WB	Cell Signaling	5848s	1 : 1000
BRD3	WB	Santa Cruz	sc-81202	1 : 1000
BRD4	WB, IFC	abcam	ab128874	1 : 1000, 1 : 100
COXIV	WB	Cell Signaling	4850s	1 : 2000
FUNDC1	WB	Aviva Systems Biology	ARP53281-P050	1 : 500
GAPDH	WB	Santa Cruz	sc-137179	1 : 2000
H3K27ac	WB	Cell Signaling	8173s	1 : 1000
LAMP1	WB	Santa Cruz	sc-17768	1 : 500
LC3A/B	WB, IFC	Cell Signaling	4108s	1 : 1000, 1:100
LDH	WB	Santa Cruz	sc-33781	1 : 1000
ac-Lysine	WB	Cell Signaling	9441s	1 : 500
PINK1	WB	Santa Cruz	sc-517353	1 : 500
Parkin	WB	abcam	ab15954	1 : 1000
p62	WB	abcam	Ab56416	1 : 5000
TIM23	WB	Aviva Systems Biology	ARP65617-P050	1 : 1000
Ub	WB	Santa Cruz	sc-8017	1 : 500
VDAC1	WB	Cell Signaling	4661s	1 : 1000

Table 3.2 Primers Information

Name	Sequence (5'-3')
Actb	F: GGCTGTATTCCCCTCCATCG
	R: CCAGTTGGTAACAATGCCATGT
Atg7	F: ATGCCAGGACACCCTGTGAACTTC
	R: ACATCATTGCAGAAGTAGCAGCCA
Becn1	F: GAGGCATGGAGGGGTCTAAG
	R: GTCTCTCCTGGTTTCGCCTG
Brd2	F: ATGAGTGGTGCGGCTTTAGG
	R: TTGTCGTACTGACATCCAGCG
Brd3	F: GGACTCAAACCCAGACGAGATT
	R: TGTTGACAATGGTTTCCTCTGC
Brd4	F: CCATGGACATGAGCACAATC
	R: TGGAGAACATCAATCGGACA
Ctss	F: ATGCCCCTGGTGTGCTCTG
	R: CTTCTTCTTCATTCTTATC
Lamp1	F: CAGCACTCTTTGAGGTGAAAAAC
	R: CCATTCGCAGTCTCGTAGGTG
Map1lc3b	F: TTATAGAGCGATACAAGGGGGAG
	R: CGCCGTCTGATTATCTTGATGAG
Pink1	F: CACACTGTTCCTCGTTATGAAGA
	R: CTTGAGATCCCGATGGGCAAT
Ppargc1a	F: AGCCGTGACCACTGACAACGAG
	R: GCTCATGGTTCTGAGTGCTAAG
Sqstm1	F: AGGATGGGGACTTGGTTGC
	R: TCACAGATCACATTGGGGTGC
Tfam	F: GAAGGGAATGGGAAAGGTAGA
	R: AACAGGACATGGAAAGCAGAT
Ulk1	F: CGTCGAGACCGTGGGCAAG
	R: CCTCCAGGTCGTGCTTCTC

4 Conclusions

4.1 General discussion and significance

Atherosclerosis is a chronic inflammatory disease with plaque builds up inside the arteries. Atherosclerosis can affect any artery in the body, including arteries in the heart, brain, kidneys etc., and it can lead to serious problems including heart attack, stroke, or even death. The plaques contain lipids, inflammatory cells, VSMCs, and connective tissues. Plaque destabilization and rupture are key mechanisms that contribute to end-stage clinical events such as acute coronary syndromes and symptomatic carotid artery disease (1). Research studies indicate that proliferation and migration of VSMCs play an important role in maintaining plaque stability through the maintenance of a protective fibrous cap overlying the thrombotic lipid core of advanced lesions (2,3). Thus understanding key regulators of VSMCs proliferation and migration will facilitate future strategies to modulate the disease process.

In this dissertation, we demonstrated that KAT2A/GCN5 is the enzyme that mediates acetylation of TUBA and is degraded specifically through autophagy in VSMCs. However, KAT2A/GCN5 is firstly identified as a histone acetyl transferase to be involved in a broad range of cellular processes including gene transcription, differentiation, DNA repair, nucleosome assembly, and cell cycle regulation. In this work, we cannot exclude an indirect regulation of TUBA acetylation via other molecules. In addition, either increasing of acetylation or decreasing of deacetylation may increase the acetylation of TUBA under autophagy-deficient conditions. Although alternation of autophagy doesn't change the expression of HDAC6 or SIRT2, which are known TUBA deacetylase (4), we cannot rule out the effects of other unknown TUBA deacetylase. While we showed that upregulation of microtubule acetylation leads to enhancement of microtubule stability, role of TUBA acetylation on microtubule stability has been controversial. Some studies indicated that TUBA acetylation had no effect on microtubule

polymerization, while some other studies reported that increased acetylation of TUBA by HDAC6 inhibition increases microtubule stability and inhibits cell motility.

Recent studies have revealed that activities of microtubule-based motors regulate the biogenesis and trafficking of autophagosomes (5). In this dissertation, we demonstrated that autophagy can, in turn, regulate microtubule dynamics and cell motility through modulating TUBA acetylation. While we showed that suppression of autophagy upregulates microtubule acetylation which results in enhancement of microtubule stability, the role of autophagy on microtubule stability seems to be different in different cell type. In cultured central nervous system neurons, activating autophagy stabilizes microtubules by degrading stathmin 2, a membrane-associated neuron-specific protein that destabilizes microtubule, which leads to promotion of axon growth after spinal cord injury (6). The role of autophagy in regulating VSMCs migration also remains debatable. Thus, further investigation of the role of autophagy in regulating VSMCs migration is an interesting topic of study. Typically, a mouse model with VSMC-specific deletion of autophagy-related genes, such as ULK1, may be useful for these investigations.

Diabetes mellitus (DM) which characterized by high blood glucose levels and dyslipidemia, is one of the most prevalent diseases worldwide. In parallel with the increase in diabetes mellitus, the prevalence of diabetic cardiomyopathy is increased to 12% in diabetic patients (7). Despite the rapid increase in the number of preclinical and clinical studies on diabetic cardiomyopathy in the past decades, the pathogenesis of this disease still remains unclear. As a consequence, no consensus has been reached regarding the effective approaches to treat diabetic cardiomyopathy or diabetes- related heart failure. Therefore, it is necessary and significant to reveal the mechanisms of diabetic cardiomyopathy.

In this dissertation, we found that *Pink1* genetic deletion accelerates and exacerbates cardiac dysfunction in HFD-fed mice. However, Billia *et al*. showed that *Pink1* global knockout mice exhibited pathological cardiac phenotype at basal conditions due to an impairment of mitochondrial function and redox homeostasis (8). Further, multiple factors may collectively contribute to the development of diabetic cardiomyopathy, such as hyperglycaemia, hyperlipidemia, increasing cardiac oxidative stress, inflammation, myocardial fibrosis, as well as mitochondrial dysfunction. Thus, in addition to inhibition of PINK1/Parkin-mediated mitophagy, HFD feeding worsened cardiomyopathy in *Pink1* knockout mice may be the combined effects of accumulation of oxidative stress and obesity.

The first stage of diabetic cardiomyopathy is usually clinically asymptomatic, but is evidenced by cardiac diastolic dysfunction (reduction of early diastolic filling and an increase in atrial filling), increased ventricular stiffness, enlarged atrial, and elevated LV end-diastolic pressure. The second stage of diabetic cardiomyopathy is characterized by cardiac remodeling, LV hypertrophy, cardiac diastolic dysfunction, and the emergence of clinical indications of HF (9). In the second part of this dissertation, we generated diabetic cardiomyopathy mouse model by feeding two-month-old *C57BL/6J* mice with ND or HFD for six months. Profound cardiac diastolic dysfunction and systolic dysfunction were found, which indicate second state of diabetic cardiomyopathy. Our results showed that PINK1/Parkin-mediated mitophagy is reduced in the heart of second-stage diabetic cardiomyopathy, which is crucial for maintaining normal cardiac function in the settings of diabetes. However, mitophagy activity is precisely regulated by different pathways and may change during the pathological development of diabetic cardiomyopathy. Thus, further investigation of the role of mitophagy in the different stages of diabetic cardiomyopathy is an interesting topic of study.

Type 2 diabetes is often associated with insulin resistance, which is a condition that all the cells in the body become less sensitive to the effects of insulin, so a higher level of insulin is required to maintain its physiological functions. Although our studies demonstrate that JQ1 administration can rescue cardiac abnormities in diabetes complications through elevating general autophagy and PINK1/Parkin-mediated mitochondrial quality control, an important question still need to be answered is whether the beneficial effect of JQ1 on cardiac function is due to its influence on the whole body insulin resistance condition. It is noteworthy that we used a dose of 10 mg/kg/day for the JQ1 treatment, which is four-times less than that used by other groups. We found that 50 mg/kg/day caused a dramatic body weight loss and death of HFD-fed mice within one week. The discrepancy may be due to difference of mice aged and diabetic condition, which inhibits drug metabolism and excretion by inducing multi-organ dysfunction, including hepatic and renal dysfunction. Thus, it is of great importance to optimize the dosage of JQ1 based on age, disease, disease stage, and disease severity. In this dissertation, we demonstrated that the specific BET bromodomain inhibitor JQ1 injection restores HFD-induced diabetic cardiomyopathy in WT mice. However, the mammalian BET family comprises BRD2, BRD3, BRD4, and testis-specific BRDT. Studying the effect of the specific protein on the pathogenesis of the disease has proven to be a challenging problem. Further investigation using BET proteins cardiac specific knockout mice are helpful means to study the molecular mechanism underlying therapeutic effect of JQ1 on HFD-induced diabetic cardiomyopathy.

4.2 Conclusions and perspectives

This dissertation systemically studied the regulation of cardiovascular homeostasis by autophagy. Firstly, we discovered a novel autophagy-dependent degradation pathway for an acetyltransferase that regulates VSMCs migration at physiology condition. Secondly, we

expanded our work to disease condition, which includes novel insights into the underlying molecular mechanisms of diabetic cardiomyopathy. Finally, we identified JQ1, a BET inhibitor, as a therapeutic intervention in the diabetic cardiomyopathy.

The complete pathophysiology of cardiovascular diseases, which are the leading cause of death globally, are still being elucidated. Autophagy and mitophagy play an important role in the modulation of cellular homeostasis. It is likely that dysfunctional autophagy contributes to the morbidity and mortality associated with cardiovascular diseases. Further studies are certainly required to clarify many aspects of molecular mechanisms underlying autophagy regulation of cardiovascular homeostasis, which are essential for identifying effective preventive strategies and treatments.

4.3 References

1. Zaman AG, Helft G, Worthley SG, Badimon JJ. The role of plaque rupture and thrombosis in coronary artery disease. Atherosclerosis **2000**;149(2):251-66.
2. Gomez D, Owens GK. Smooth muscle cell phenotypic switching in atherosclerosis. Cardiovasc Res **2012**;95(2):156-64 doi 10.1093/cvr/cvs115.
3. Johnson JL. Emerging regulators of vascular smooth muscle cell function in the development and progression of atherosclerosis. Cardiovasc Res **2014**;103(4):452-60 doi 10.1093/cvr/cvu171.
4. Zhang F, Su B, Wang C, Siedlak SL, Mondragon-Rodriguez S, Lee HG*, et al.* Posttranslational modifications of alpha-tubulin in alzheimer disease. Transl Neurodegener **2015**;4:9 doi 10.1186/s40035-015-0030-4.
5. Kast DJ, Dominguez R. The Cytoskeleton-Autophagy Connection. Curr Biol **2017**;27(8):R318-R26 doi 10.1016/j.cub.2017.02.061.
6. He M, Ding Y, Chu C, Tang J, Xiao Q, Luo ZG. Autophagy induction stabilizes microtubules and promotes axon regeneration after spinal cord injury. Proc Natl Acad Sci U S A **2016**;113(40):11324-9 doi 10.1073/pnas.1611282113.
7. Bertoni AG, Hundley WG, Massing MW, Bonds DE, Burke GL, Goff DC, Jr. Heart failure prevalence, incidence, and mortality in the elderly with diabetes. Diabetes Care **2004**;27(3):699-703 doi 10.2337/diacare.27.3.699.
8. Billia F, Hauck L, Konecny F, Rao V, Shen J, Mak TW. PTEN-inducible kinase 1 (PINK1)/Park6 is indispensable for normal heart function. Proc Natl Acad Sci U S A **2011**;108(23):9572-7 doi 10.1073/pnas.1106291108.
9. Jia G, Hill MA, Sowers JR. Diabetic Cardiomyopathy: An Update of Mechanisms Contributing to This Clinical Entity. Circ Res **2018**;122(4):624-38 doi 10.1161/CIRCRESAHA.117.311586.